# Supplementary Information

# A synthetic cationic helical polypeptide as a multipotent innate immune activator for cancer immunotherapy

DaeYong Lee,[1,2*] Kristin Huntoon,[1,2*] Yifan Wang,[3*] Minjeong Kang,[3] Yifei Lu,[1,2] Seong Dong Jeong,[1,2] Todd M. Link,[4] Thomas D. Gallup[1,2], Yaqing Qie,[1,2] Xuefeng Li,[3] Yifan Ma,[3] Shiyan Dong,[3] Benjamin R. Schrank,[3] Adam Grippin,[3] Abin Antony,[3] Jonghoon Ha,[3] Mengyu Chang,[3] Yi An,[5] Liang Wang,[3] Dadi Jiang,[3] Jing Li,[3] Albert C. Koong,[3] John A. Tainer,[4] Wen Jiang,[3,#] Betty Y.S. Kim[1,2,#]

[1] Department of Neurosurgery, The University of Texas MD Anderson Cancer Center, Houston, TX, USA
[2] Brain Tumor Center, The University of Texas MD Anderson Cancer Center, Houston, TX, USA
[3] Department of Radiation Oncology, The University of Texas MD Anderson Cancer Center, Houston, TX, USA
[4] Department of Molecular and Cellular Oncology, The University of Texas MD Anderson Cancer Center, TX, USA
[5] Department of Therapeutic Radiology, Yale School of Medicine, CT, USA

*These authors contributed equally

[#]Corresponding authors: Dr. Wen Jiang (wjiang4@mdanderson.org) and Dr. Betty Y S Kim (bykim@mdanderson.org)

**Contents** | **Page numbers**

## Supplementary methods

### Physical characterization

All NMR spectra were measured with a Bruker 500 MHz DXR NMR Spectrometer. Deuterated dimethylsulfoxide (DMSO-$d_6$, Sigma Aldrich, USA) and water ($D_2O$, Sigma Aldrich, USA) were used as NMR solvents. Molecular weights were determined by gel permeation chromatography (YL9100 HPLC system, Younglin, Korea). 0.1 M LiBr *N*,*N*'-dimethylformamide solution was used as a mobile phase with a 0.5 mL/min flow rate. A circular dichroism spectrometer (J-815 spectropolarimeter 150 L type, JASCO, Japan) was used to determine the secondary protein conformation using a quartz cell with a 0.02 mm path length in the rage of 200 to 260 nm at 25˚C. The CD spectra were measured with 100 nm/min scanning, 1 nm bandwidth, 4 s response time, 1.0 nm data pitch, and 10 accumulations. The polypeptide concentrations were adjusted to 1 mg/mL. For pH titration curves, the polypeptide solution (1 mg/mL in deionized water) was adjusted to approximately pH 3.5, and then titrated with 0.1 N NaOH solution.

### Transmission electron microscopy

The polypeptides (1 mg/mL in deionized water) were incubated with fetal bovine serum (FBS) (10% in deionized water), and then the nanocomplexes were negatively stained with 1% uranyl acetate solution. Stain was blotted dry from the grids with filter paper and samples were allowed to dry. Samples were then examined in a JEM 1010 transmission electron microscope (JEOL, USA, Inc., Peabody, MA) at an accelerating voltage of 80 kV. Digital images were obtained using the AMT Imaging System (Advanced Microscopy Techniques Corp., Danvers, MA).

### Degradability

P1, P2, and P3 (10 mg/mL in PBS) were incubated with mouse serum (10% in FBS) at 37°C for 24 h, and the serum protein was then removed by ethanol precipitation. Size exclusion

chromatography was done with untreated or serum-treated polypeptides to evaluate degradability of polypeptides.

**Apoptosis assay**

4T1, EO771 ($2\times 10^5$ cells/12 well plate), bone-marrow–derived macrophages (BMDMs), or bone marrow–derived dendritic cells (BMDCs) ($5 \times 10^5$ cells/12-well plate) were treated with P1, P2, P3 (4 μg/mL) and lipopolysaccharide (LPS) (100 ng/mL) and valinomycin (5 μM) for 24 h. The cells were stained with fluorescein isothiocynate (FITC)-annexin V and PI according to the manufacture's protocol (Dead Cell Apoptosis Kits with Annexin V for Flow Cytometry, ThermoFisher Scientific, USA). Apoptotic events were measured by flow cytometry.

**Confocal laser scanning microscopy (CLSM) for staining organelles**

M2 BMDMs seeded on confocal dishes were dyed with Mitotracker Deep Red (400 nM, ThermoFisher Scientific, USA), ER tracker Red (100 nM, ThermoFisher Scientific, USA), or Lysotracker Deep Red (50 nM, ThermoFisher Scientific, USA) for 30 min before being treated with FITC-P1 for 3 h (mitochondria) and for 30 min, 1 h, and 3 h (lysosomes). The cells were washed with PBS three times and then fixed with a 4% paraformaldehyde solution to visualize the cells by CLSM.

**Immunofluorescence**

M2 BMDMs seeded on confocal dishes were treated with P1, LPS, or cGAMP for 1 day or with FITC-P1 for 3 h for STING (Stimulator of interferon genes) immunofluorescence. The cells were washed with PBS three times, fixed and permeabilized to stain intracellular proteins before the cells were treated with the primary antibody overnight at 4˚C and then with the fluorophore-tagged secondary antibody for 1 h. Cells were imaged by CLSM.

**Cell membrane destabilization**

M2 BMDMs ($5 \times 10^5$ cells/12-well plate) were treated with calcein (1 μg/mL) and then incubated with P1, LPS, or cGAMP for 3 h. The cells were rinsed with PBS three times, stained with cell viability dye, and then fixed with a 4% paraformaldehyde solution before being stained with antibodies. The fluorescence intensity of calcein was quantified by flow cytometry. For lysosome activity, M2 BMDMs ($5 \times 10^5$ cells/12-well plate) were treated with P1 for 24 h and cytochalasin D (positive control) for 2 h. Lysosomal intracellular activity was measured according to the manufacturer's protocol (Lysosomal Intracellular Activity Assay Kit, abcam, UK)

**Serum stability**

P1, P2, and P3 were dissolved in PBS, 5%, 10%, 20% FBS-containing phosphate buffered saline (PBS). The final concentration of each polypeptide was adjusted to 1 mg/mL. The hydrodynamic diameter and polydispersity index were measured by a dynamic light scattering method (Zetasizer Nano, Malvern, UK). Transmission electron microscopy was used to visualize the morphology of nanocomplexes between the polypeptide and serum proteins. The polypeptides (1 mg/mL in PBS) were incubated with FBS (5% in PBS), and then the nanocomplexes were negatively stained with 2% uranyl acetate solution.

**Hemolysis assay**

Red blood cells were obtained by centrifuging blood samples from C57BL6 mice, and then treated with PBS, P1, P2, P3, PLL, PLG, or 10% Triton X-100 for 2 h at 37˚C. The red blood cells were then spun down to collect supernatant. The absorbance ($A$) at 540 nm of each sample was detected with a multi-reader. Hemolysis was calculated as:

Hemolysis (%) = $(A_{sample}-A_{PBS})/(A_{triton\ X\text{-}100}-A_{PBS}) \times 100$ (%).

**Relative cell viability**

BMDMs ($3 \times 10^4$ cells/well in 96-well plates), BMDCs ($3 \times 10^4$ cells/well in 96-well plates) or breast cancer cells ($1 \times 10^4$ cells/well in 96-well plates) were treated with polypeptides (200, 100, 20, 10, 2, 1, 0.2, and 0.1 μg/mL), cGAMP, CpG, lipid nanoparticle-formulating cGAMP, or CpG (200, 10, and 1 μg/mL) for 1 day, after which 3-(4,5-dimethylthiazol-2-yl)-2,5-diphenyltetrazolium bromide solution (20 μL, 2.5 mg/mL in PBS, Sigma Aldrich, USA) was added to the cells, and the cells were then incubated for 2 h to form formazan. cGAMP or CpG-loaded lipid nanoparticles were prepared by following the manufacturer's procedure [Lipid Nanoparticle (LNP-102) Exploration Kit, Cayman Chemical, USA]. To solubilize the formazan formed in cells, dimethylsulfoxide (100 μL) was added to each well after the supernatant was discarded. Each UV-Vis absorbance ($A$) was detected by an UV-Vis multi-reader (CLARIOstar, BMG Labtech, USA) at 590 nm. The relative cell viability was obtained by the ratio of $A_{\text{sample}}$ to $A_{\text{untreated}}$.

**Evaluation of systemic toxicity**

Six-week-old female C57BL/6J mice were intravenously injected with (4-(2-hydroxyethyl)-1-piperazineethanesulfonic acid) (HEPES), P1, or cGAMP on day 0, 2, and 4. The body weights of the mice in each group were measured every other day. On day 16, blood samples were collected from each mouse via cardiac puncture, and alanine aminotransferase (ALT), aspartate aminotransferase (AST), blood urea nitrogen (BUN), and creatinine levels were evaluated from blood plasma, and blood cells were used to assess the population of leukocytes ($CD45^+$ cells). To verify acute toxic effects after the polypeptide treatment, six-week-old female C57BL/6J mice were intravenously administrated with HEPES or P1 on day 0, 2, and 4. Blood samples and organs were obtained on day 5 (24 h after the last treatment) for long-term toxicity, or at 6 h and 24 after the treatment for short-term toxicity. Organs including heart, liver, spleen, kidney, and

lungs were stained with hematoxylin and eosin to determine toxicity via histologic analysis. To evaluate inflammation, RNAs or proteins were extracted from hepatocytes, liver-resident macrophages, and peripheral blood mononuclear cells to conduct western blotting of the markers for cGAS-STING and TLR9 (Toll Like Receptor 9) axes or RT-qPCR of gene encoding inflammation. For assessment of organ and blood toxicities, blood tests were conducted to measure AST, ALT, BUN, and creatinine for organ toxicity, and absolute blood counts for systemic toxicity.

## Supplementary Figures

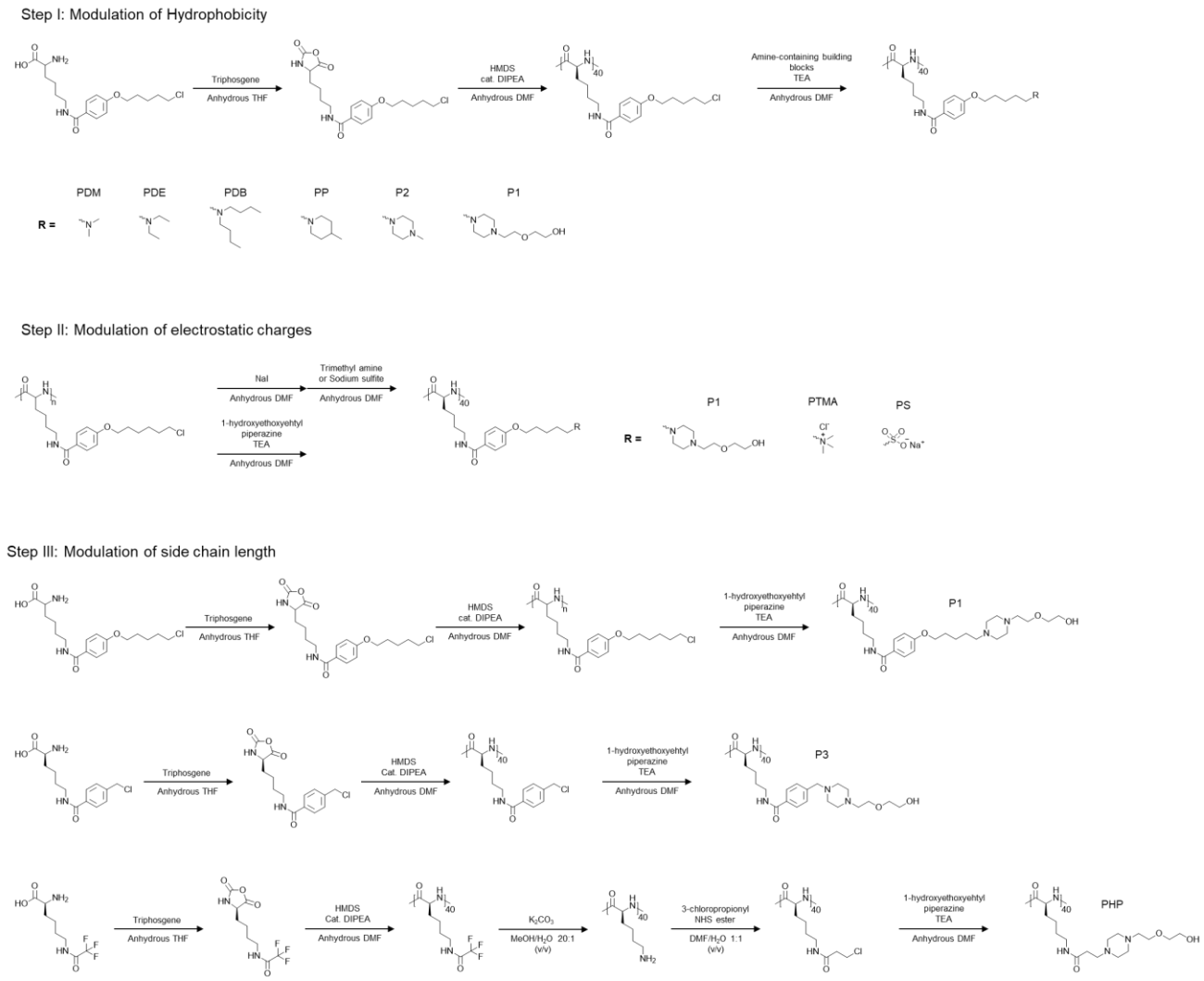


**Supplementary Fig. 1. Schema for synthesizing polypeptides by varying their hydrophobicity, electrostatic charges, and side-chain length.** A 3-step optimization process was used to find the optimal polypeptide for generating pro-inflammatory responses in innate immune cells, DMF, *N*,*N*'-dimethylformamide; DIPEA, diisopropylethyl amine; THF, tetrahydrofuran; TEA, trimethyl amine.

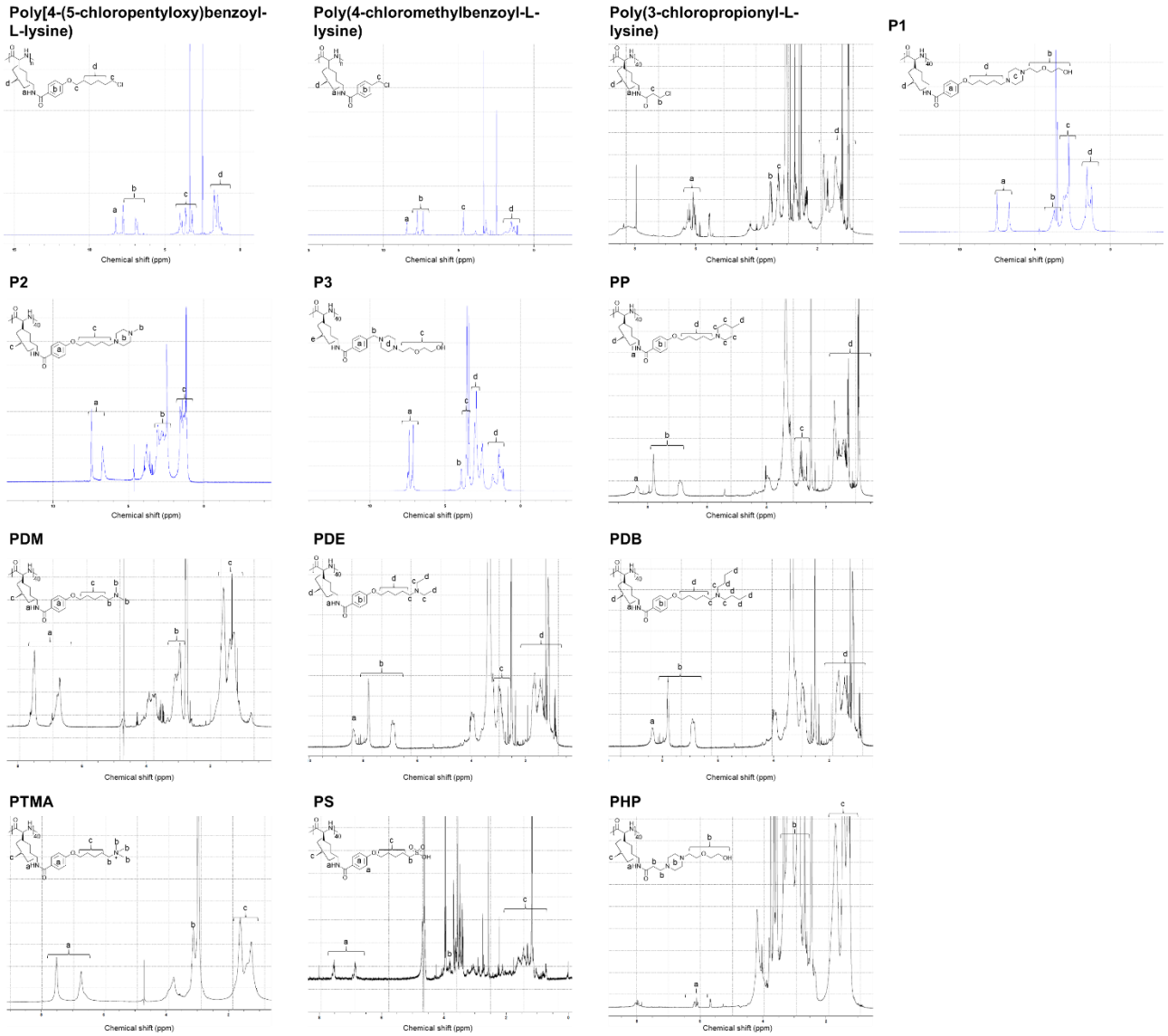


**Supplementary Fig. 2 NMR characterization of polypeptides.** Poly [4-(5-chloropentyloxy)benzoyl-L-lysine], poly(4-chloromethylbenzoyl-L-lysine), poly(3-chloropropionyl-L-lysine), PDE, PDB, and PP dissolved in DMSO-$d_6$. P1, P2, P3, PDM, PTMA, PS, and PHP solubilized in $D_2O$.

| Polypeptide entry | Number of mers | Polydisersity index | Degree of modification (%) | Calculated MW (g/mol) | Electrostatic charge density at pH 7.4 (mEq/g) |
|---|---|---|---|---|---|
| PDM | 40 | 1.31 | >90 | 14900 | +2.73 |
| PDE | 40 | 1.31 | >90 | 16000 | +2.45 |
| PDB | 40 | 1.31 | 80 | 17500 | +1.73 |
| P1 | 40 | 1.31 | >90 | 19600 | +1.99 |
| P2 | 40 | 1.31 | >90 | 18500 | +2.24 |
| PP | 40 | 1.31 | >90 | 17000 | +2.34 |
| PTMA | 40 | 1.31 | >90 | 15500 | +2.58 |
| PS | 40 | 1.28 | 75 | 16400 | -1.83 |
| P3 | 36 | 1.28 | >90 | 11000 | +2.33 |
| PHP | 41 | 1.09 | >90 | 9000 | +2.78 |

**Supplementary Fig. 3. Physical characterization of the polypeptides.** The number of mers and polydispersity index of all the polypeptides were determined by gel permeation chromatography of poly [4-(5-chloropentyl)oxybenzoyl-L-lysine] for PDM, PDE, PDB, P1, P2, PP, PTMA and PS, poly (4-chloromethylbenzoyl-l-lysine) for P3, and poly($N^{\varepsilon}$-trifluotoacetyl-L-lysine) for PHP. Degree of modification was calculated by $^{1}$H-NMR spectroscopy. Electrostatic charge density at pH 7.4 was obtained by (number of electrolytes in each polypeptide)/(molecular weight of each polypeptide). The number of electrolytes was determined by MarvinSketch 23.8 Software.

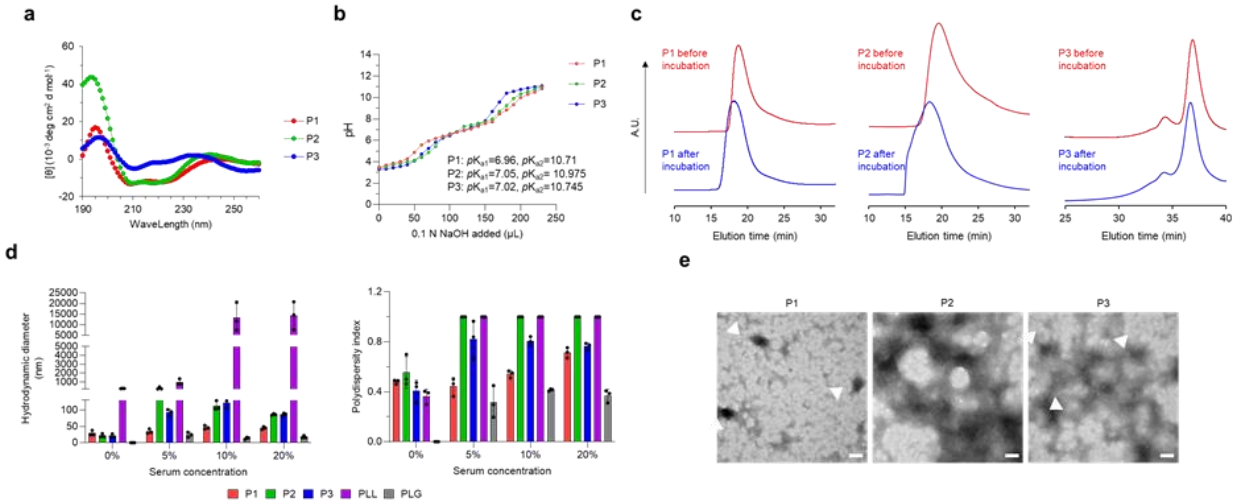


**Supplementary Fig. 4. Physical characterization of P1, P2 and P3** (a) Circular dichroism spectrometry of P1 (with high helicity), P2 (with low helicity) and P3 (with low helicity). (b) pH titration of P1, P2, and P3 shows that all polypeptides had similar $pK_a$ values. (c) P1, P2, and P3 were not degraded upon 24 h incubation with serum at 37°C; A.U., arbitrary unit. (d) Bar graphs of hydrodynamic diameter and polydispersity index show that P1 and P3 (endowed with an ethylene glycol moiety) showed higher serum stability than the other polypeptides, as characterized by dynamic laser scattering (n=3, mean±SD). Poly-L-lysine (PLL) and poly-L-glutamate (PLG) were used as a positive and a negative control, respectively, for polypeptide aggregation.I) Transmission electron microscopy images show the morphology of nanocomplexes formed between the polypeptide and serum proteins, white arrow indicates nanocomplexes between serum proteins and polypeptide, scale bar, 100 nm.

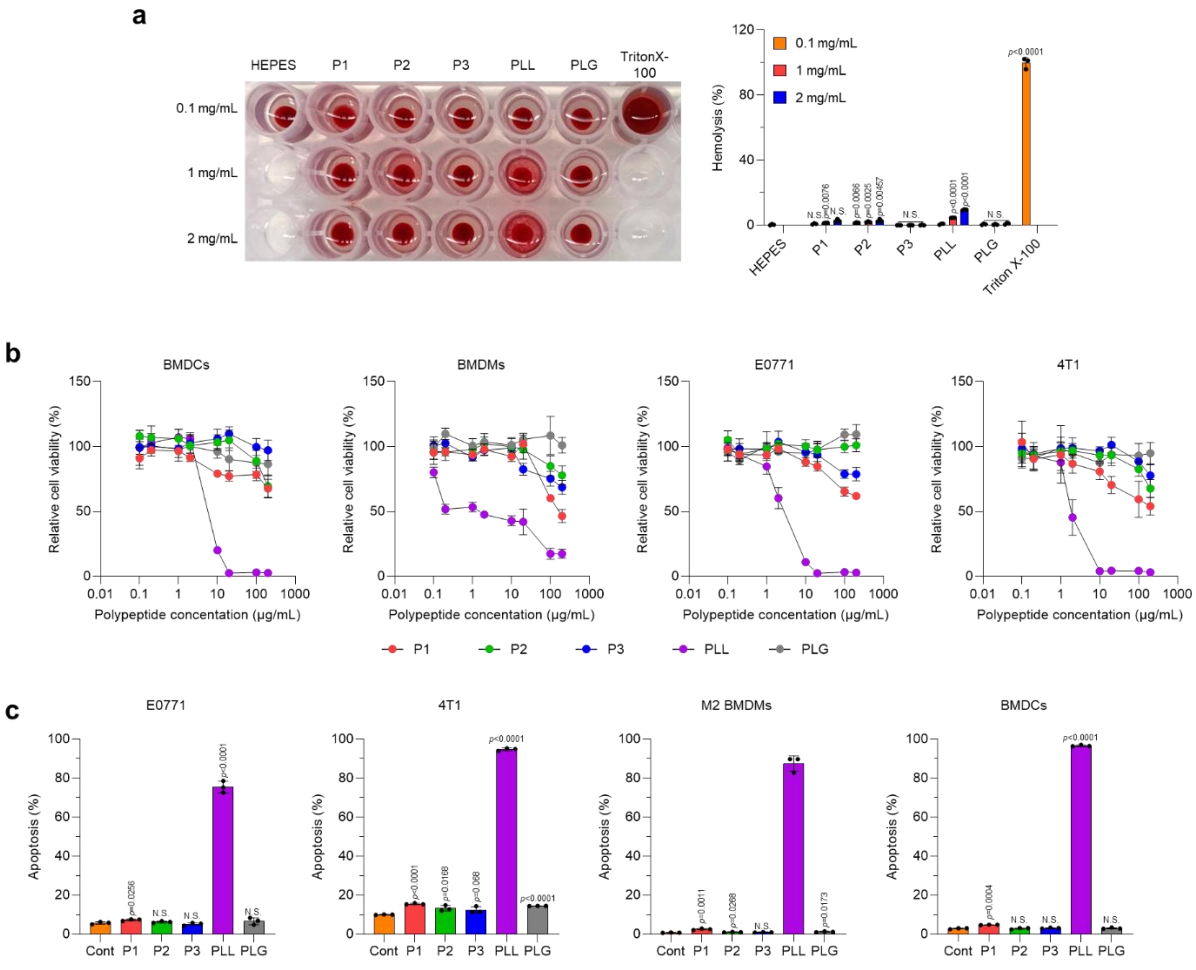


**Supplementary Fig. 5. Toxicity evaluation of polypeptides *in vitro*.** (a) Hemolytic activity of various concentrations of P1, P2, P3, poly-L-lysine (PLL) and poly-L-glutamate (PLG) in red blood cells (n=3, mean±SD) relative to controls. (c) Relative viability of different cells treated with P1, P2, P3, PLL, or PLG, as evaluated by MTT assay (n=6, mean±SD). (d) Apoptosis was determined by staining cells with FITC-Annexin V and PI, and evaluated by flow cytometry (n=3, mean±SD), unpaired Student's *t* test in comparison with Cont. PLL was used as a positive control and PLG as a negative control.

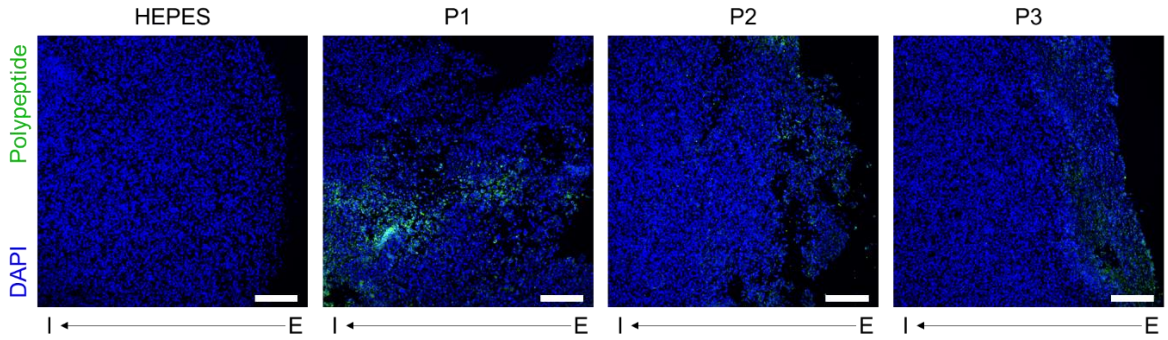


**Supplementary Fig. 6. P1 penetrates EO771 breast tumors more deeply than P2 or P3**. The tumor was harvested 12 h after the final treatment with FITC-tagged P1, P2, or P3 (10 mg/kg); scale bar, 250 μm; I, intratumoral; E, extratumoral.

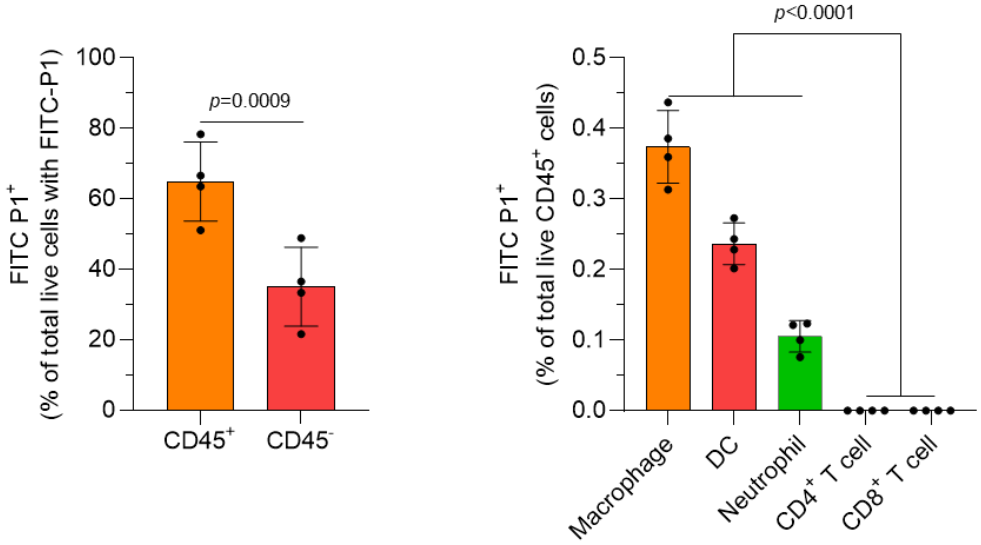


**Supplementary Fig. 7. P1 has specificity for myeloid cells within the tumor microenvironment**. FITC-tagged P1 was given intravenously to EO771 tumor-bearing mice and tumors were harvested 12 h afterward. (a) P1 was more favorably taken up in $CD45^+$ cells (n=4, mean±SD), Student's *t* test in comparison with the indicated conditions. (b) P1 accumulated in macrophages, DCs (dendritic cells), and neutrophils within the tumor microenvironment to a much greater extent than in tumor-infiltrating T cells (n=4, mean±SD), Student's *t* test in comparison with the indicated conditions.

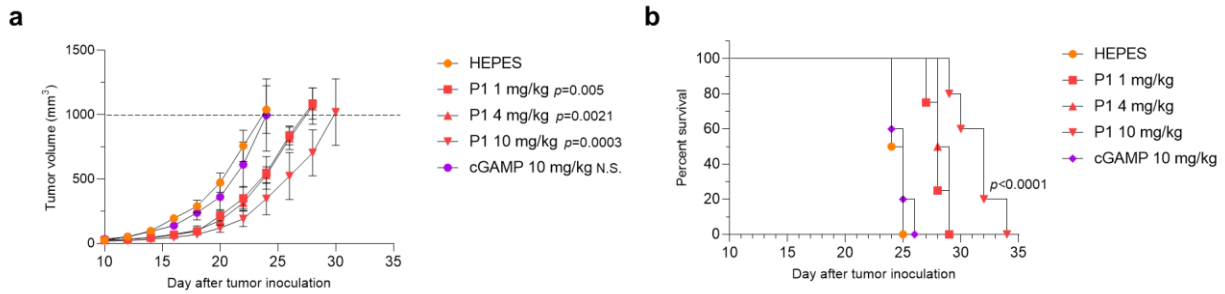


**Supplementary Fig. 8. Tumor growth and mouse survival curves after treatment with different concentrations of P1 or cGAMP**. (a) EO771 tumor-bearing C57BL/6J mice were intravenously injected with HEPES, P1, or cGAMP on days 10, 12, and 14. (n=4 for HEPES; P1, 1 mg/kg; P1, 4 mg/kg; n=5 for P1 10 mg/kg, cGAMP 10 mg/kg, mean±SD), unpaired Student's *t* test relative to HEPES on day 24; N.S., not significant. (b). Kaplan-Meier survival curves for tumor-bearing mice treated with HEPES, P1, or cGAMP, log-rank (Mantel-Cox) test.

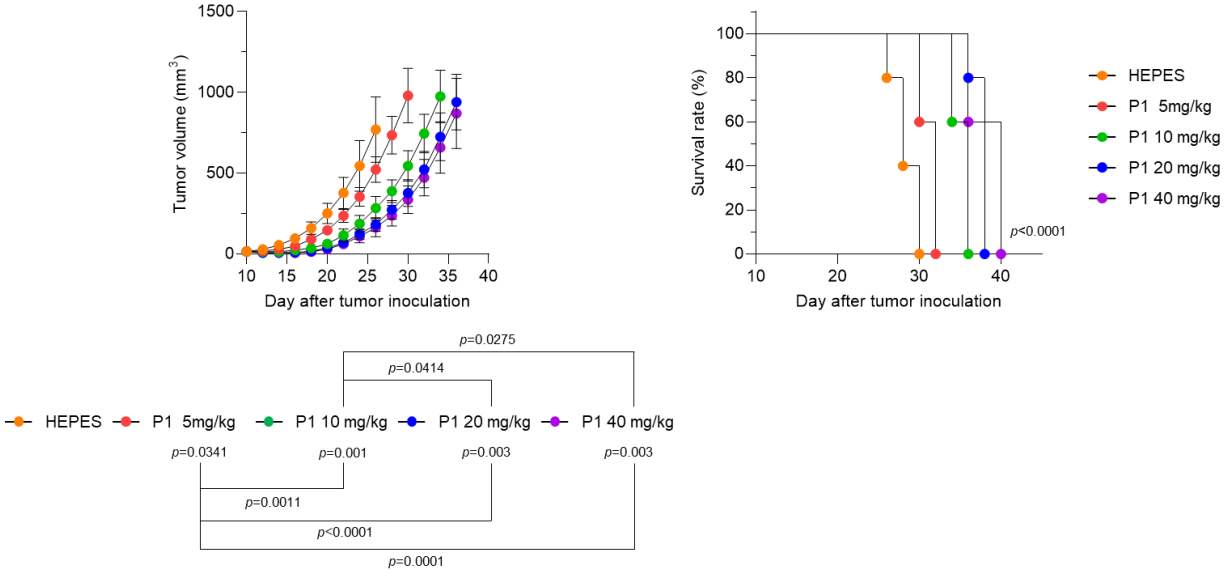


**Supplementary Fig. 9. Tumor growth and mouse survival curves after different doses of P1**. (a) EO771 tumor-bearing C57BL/6J mice were intravenously injected with HEPES, or P1 (5, 10, 20, and 40 mg/kg) on days 10, 12, and 14. (n=5, mean±SD), unpaired Student's *t* test relative to HEPES or the indicated conditions at day 24; N.S., not significant. (b). Kaplan-Meier survival curves for tumor-bearing mice treated with HEPES or P1; log-rank (Mantel-Cox) test.

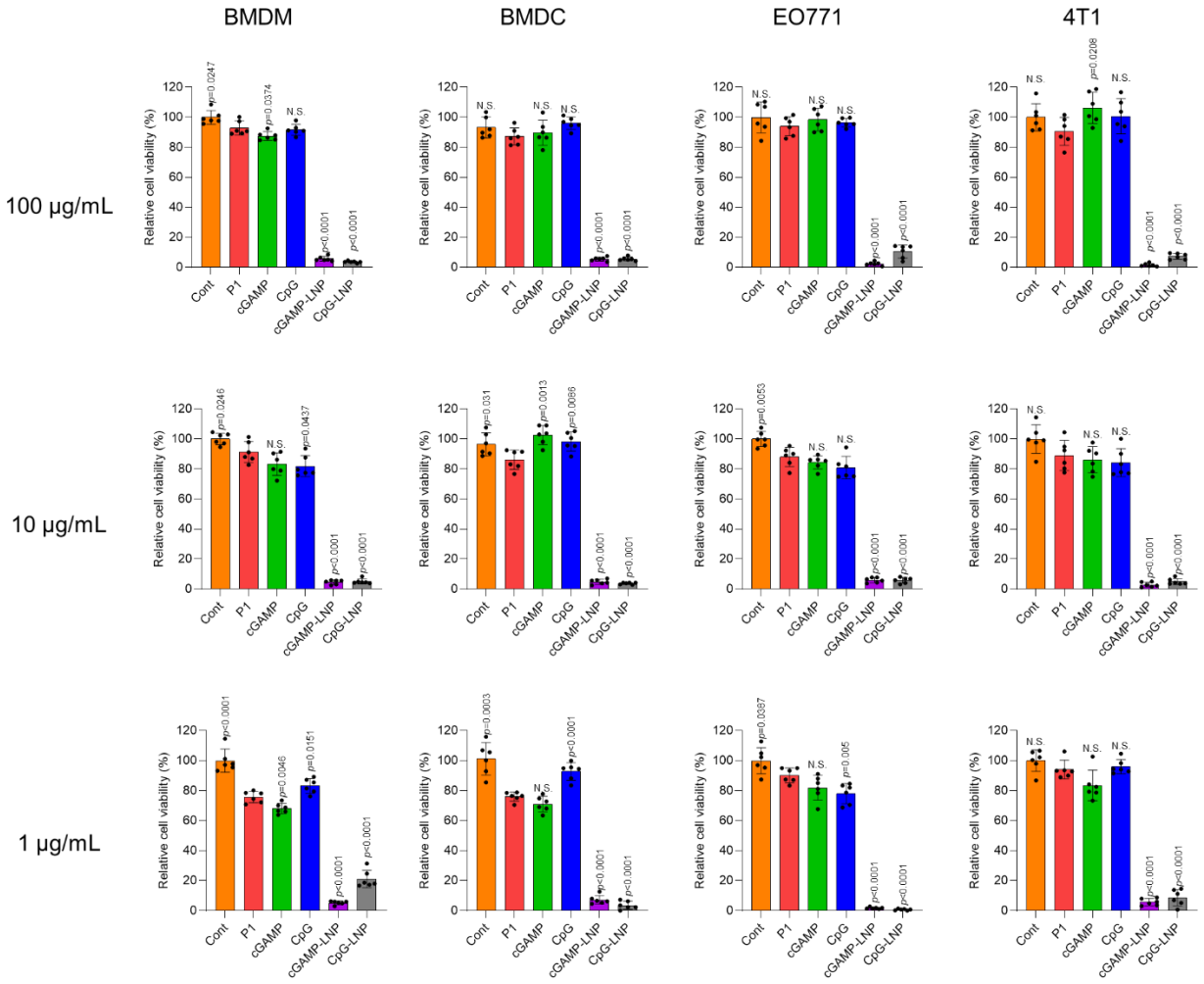


**Supplementary Fig. 10. P1 does not induce cytotoxic effects in tumor cells and APCs relative to nanoformulated cGAMP or CpG.** BMDMs, BMDCs, and EO771 and 4T1 tumor cells were treated with the indicated concentrations of P1, cGAMP, CpG, cGAMP-loaded lipid nanoparticle (cGAMP-LNP), or CpG-loaded lipid nanoparticle (CpG-LNP) for 24 h at the indicated concentrations (n=6, mean±SD), unpaired Student's *t* test in comparison with P1; N.S., not significant.

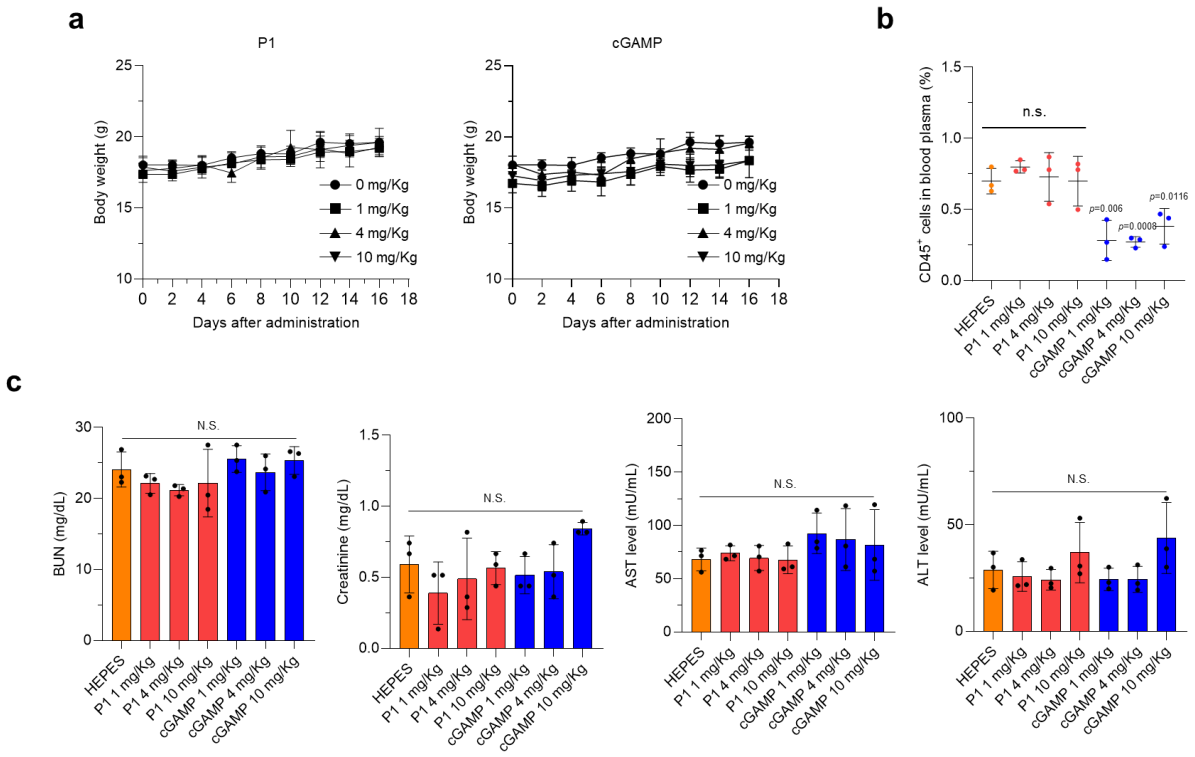


**Supplementary Fig. 11. P1 shows outstanding biocompatibility *in vivo*.** C57BL/6J mice were given P1, or cGAMP intravenously three times every other day. (a) Body weights of P1- and cGAMP-treated mice (n=3, mean±SD). (b) Proportions of $CD45^+$ cells in blood plasma after treatment with P1 or cGAMP as evaluated by flow cytometry (n=3, mean±SD), unpaired Student's *t* test; n.s., not significant. (c) Levels of blood urea nitrogen (BUN), creatinine, alanine aminotransferase (ALT), and aspartate aminotransferase (AST) in blood plasma of treated mice (n=3, mean±SD), ordinary one-way analysis (ANOVA); N.S., not significant.

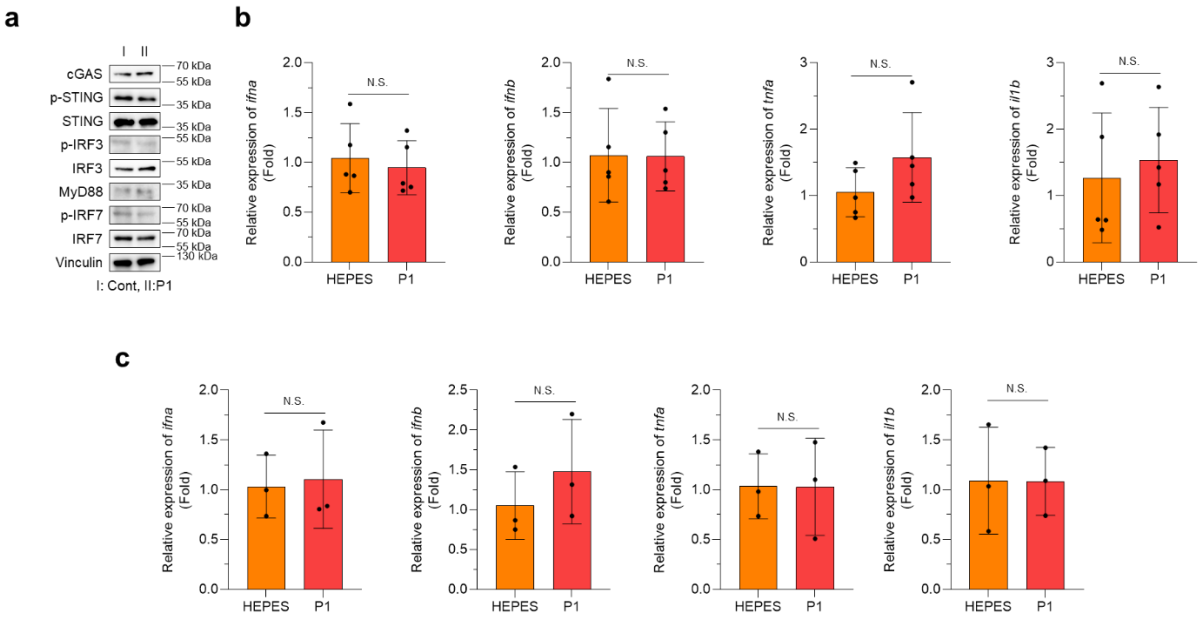


**Supplementary Fig. 12. P1 does not induce inflammation in liver and peripheral blood mononuclear cells.** C57BL/6J mice were given HEPES or P1 (10 mg/kg) intravenously three times every other day; liver and blood samples were obtained 24 h after the final treatment. (a) Western blot images show that P1 did not activate cGAS-STING-IRF3 or TLR-MyD88-IRF7 signaling in hepatocytes. (b,c) P1 treatment did not upregulate the expression of genes encoding *ifna*, *ifnb*, *tnfa*, or *il1b* in hepatocytes (n=5, mean±SD) or peripheral blood mononuclear cells (n=3, mean±SD); N.S., not significant.

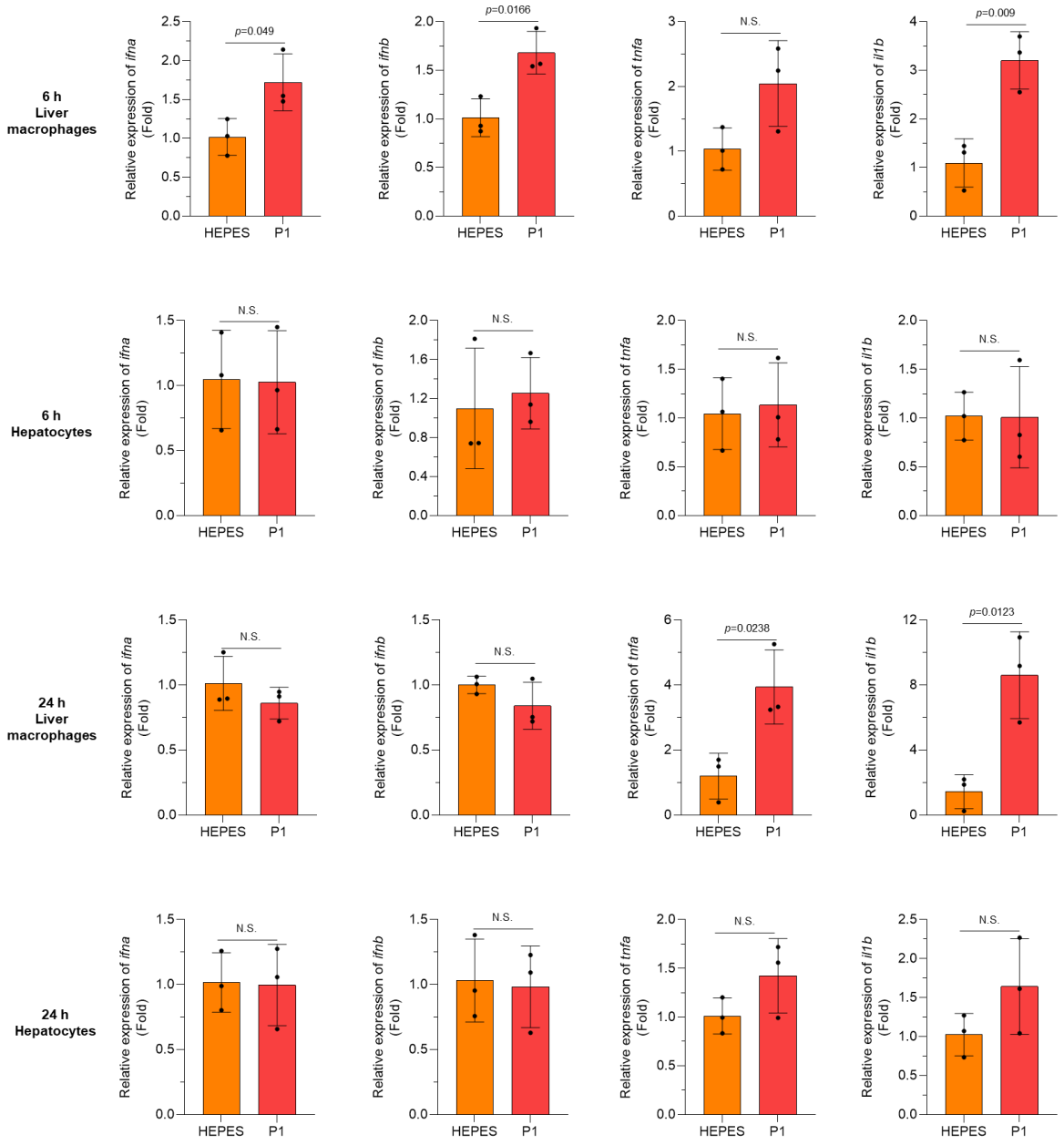


**Supplementary Fig. 13. P1 induces transient inflammation in liver macrophages but not in whole hepatocytes both at 6 and 24 h after the treatment.** C57BL/6J mice were intravenously given HEPES or P1 (10 mg/kg) once. Liver was obtained 6 and 24 h after the treatment. P1 treatments upregulated expression of genes encoding *ifna*, *ifnb*, *tnfa*, and *il1b* in hepatocytes but not in liver macrophages (n=3, mean±S.D); N.S., not significant.

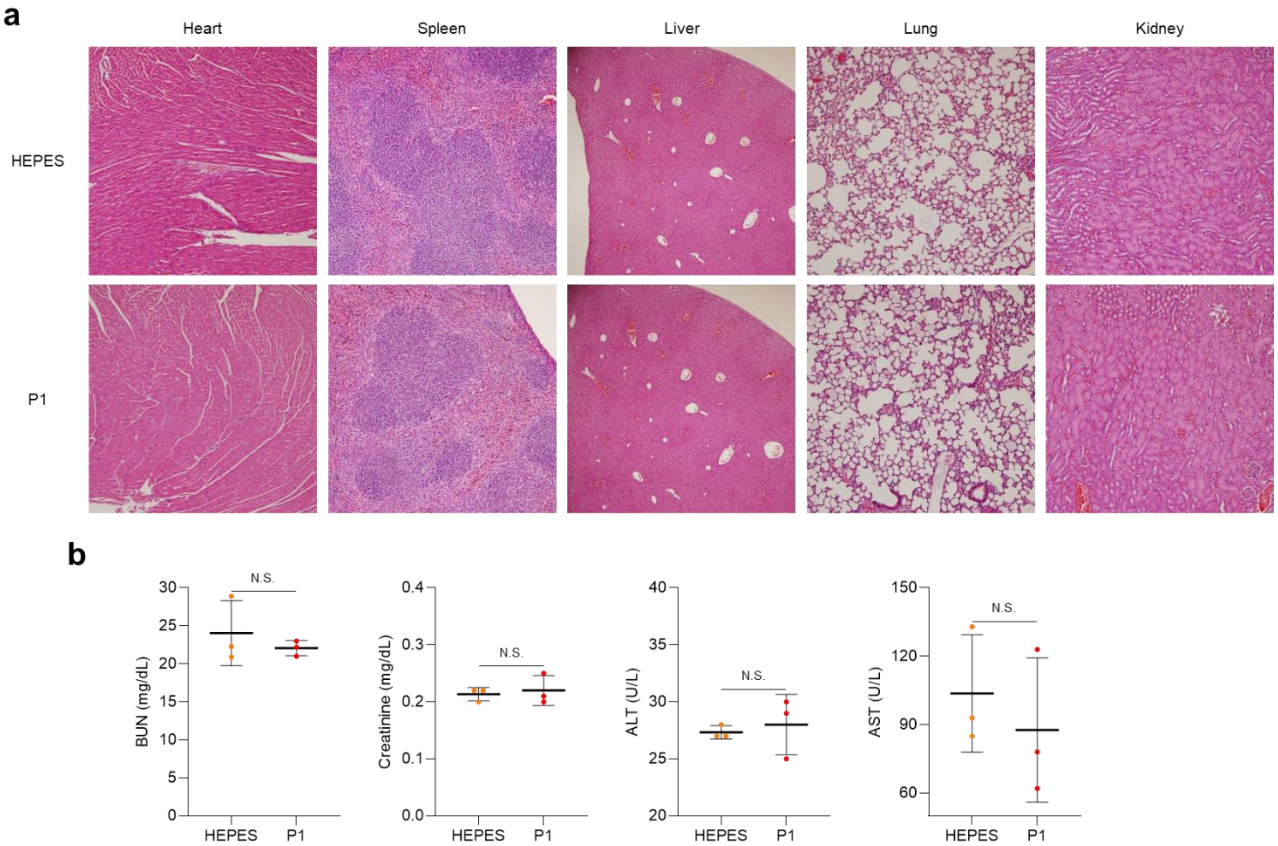


**Supplementary Fig. 14. P1 does not induce organ toxicity.** C57BL/6J mice were given HEPES or P1 (10 mg/kg) intravenously three times every other day, and organs and blood samples were obtained 24 h after the final treatment. (a) Histologic images of heart, spleen, liver, lung, and kidney show that P1 did not induce toxicity in these organs (10X magnification). (b) Levels of blood urea nitrogen (BUN), creatinine, alanine aminotransferase (ALT), and aspartate aminotransferase (AST) in blood plasma of treated mice (n=3, mean±SD), unpaired Student's *t* test in comparison with HEPES, N.S.: not significant.

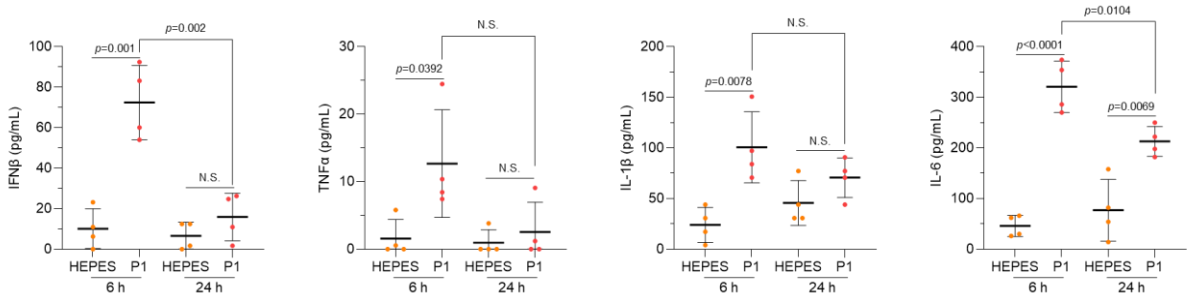


**Supplementary Fig. 15. P1 treatment induces systemic inflammation in an acute manner *in vivo*.** HEPES or P1 (10 mg/kg) was given intravenously to EO771 tumor-bearing mice. Serum plasma was collected at 6 h and 24 h via intracardiac bleeding. P1 treatment increased levels of IFNβ, TNFα, IL-1β or IL-6 in serum at 6 h but at 24 h (n=4, mean±S.D.); unpaired Student's *t* test compared with the indicated conditions.

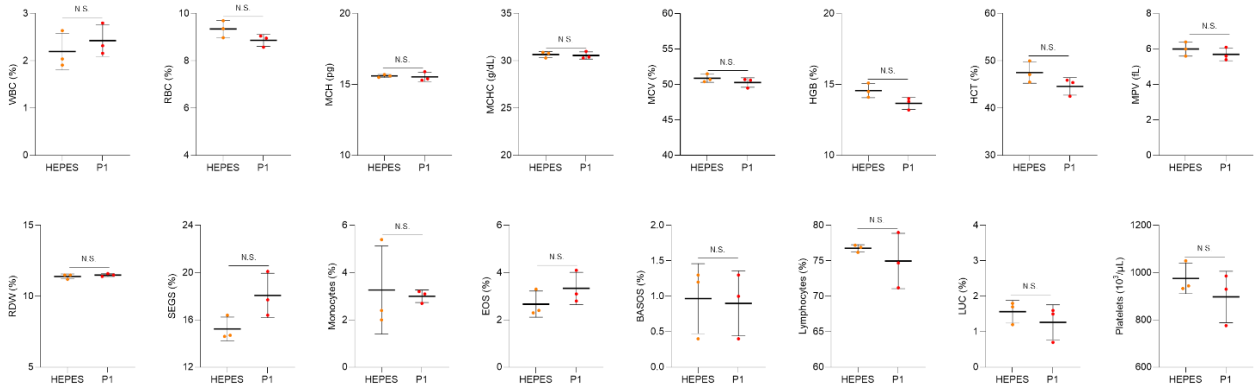


**Supplementary Fig. 16. P1 does not generate systemic inflammation.** C57BL/6J mice were given HEPES or P1 (10 mg/kg) intravenously three times every other day. Blood samples were collected 24 h after the final treatment. No appreciable differences were seen in complete blood counts from mice 24 h after the final treatment (n=3, mean±SD), unpaired Student's *t* test in comparison with HEPES. WBC (White Blood Cell), white blood cell; RBC (Red Blood Cell), red blood cell; MCH, mean corpuscular hemoglobin; MCV, mean corpuscular volume; MCHC, mean corpuscular hemoglobin concentration; HGB, hemoglobin; HCT, hematocrit; MPV, mean platelet volume; RDW; red cell distribution width; SEGS, segmental neutrophils; EOS, eosinophils; BASOS, basophils; LUC, large unstained cells; N.S., not significant.

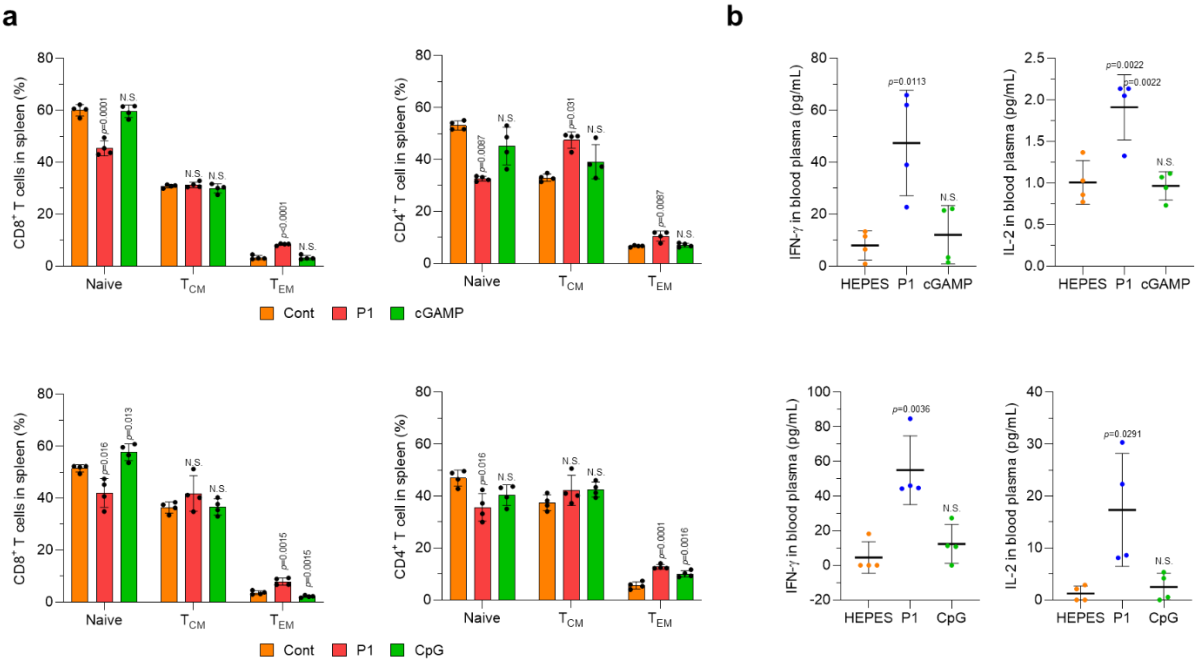


**Supplementary Fig. 17. P1 activates systemic antitumor immunity in EO771 tumor-bearing mice more strongly than cGAMP or CpG oligodeoxynucleotide.** (a) Flow cytometry of splenic T cells isolated from spleens of EO771 tumor-bearing mice on day 17 (n=4, mean±SD). (b) IFN-γ and IL-2 levels in blood plasma, quantified by enzyme-linked immunosorbent assay (n=4, mean±SD); unpaired Student's *t* test in comparison with cGAMP treatment; N.S., not significant.

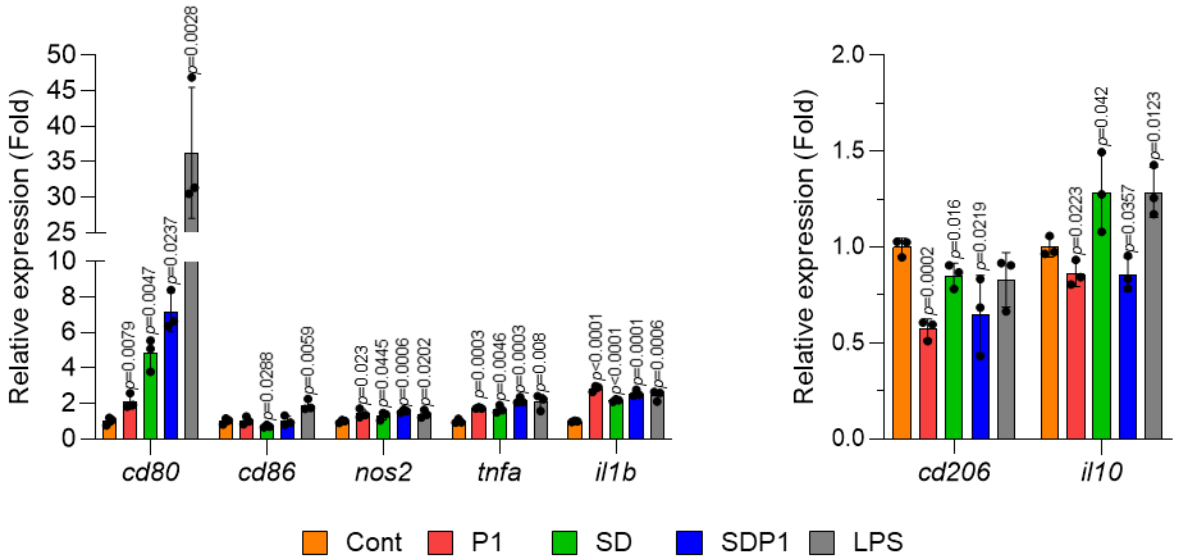


**Supplementary Fig. 18. P1 triggers pro-inflammatory signaling in THP1-derived macrophages.** P1 increased the expression of M1-associated markers but decreased expression of M2-associated markers in THP1-derived M2 macrophages (n=3, SD); unpaired Student's *t* test in comparison with control.

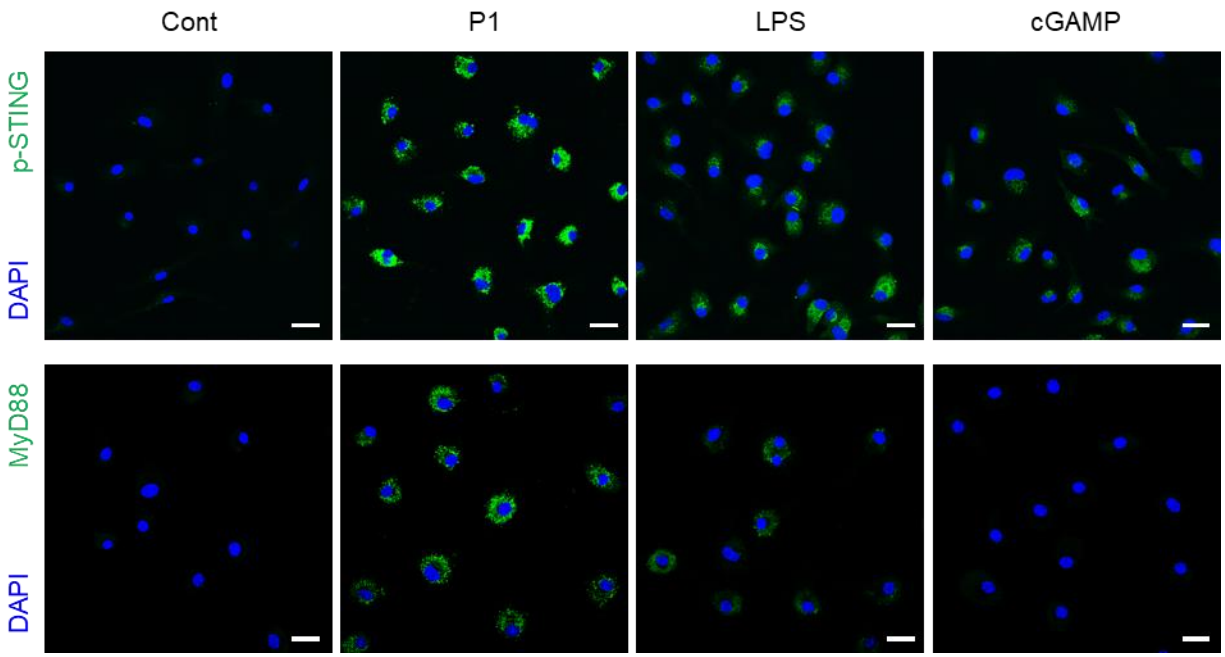


**Supplementary Fig. 19. P1 activates phosphorylation of STING and upregulates expression of MyD88.** Immunofluorescence image of p-STING and MyD88 in M2 bone marrow-derived macrophages (BMDMs) at 24 h after treatment. Scale bar, 30 μm.

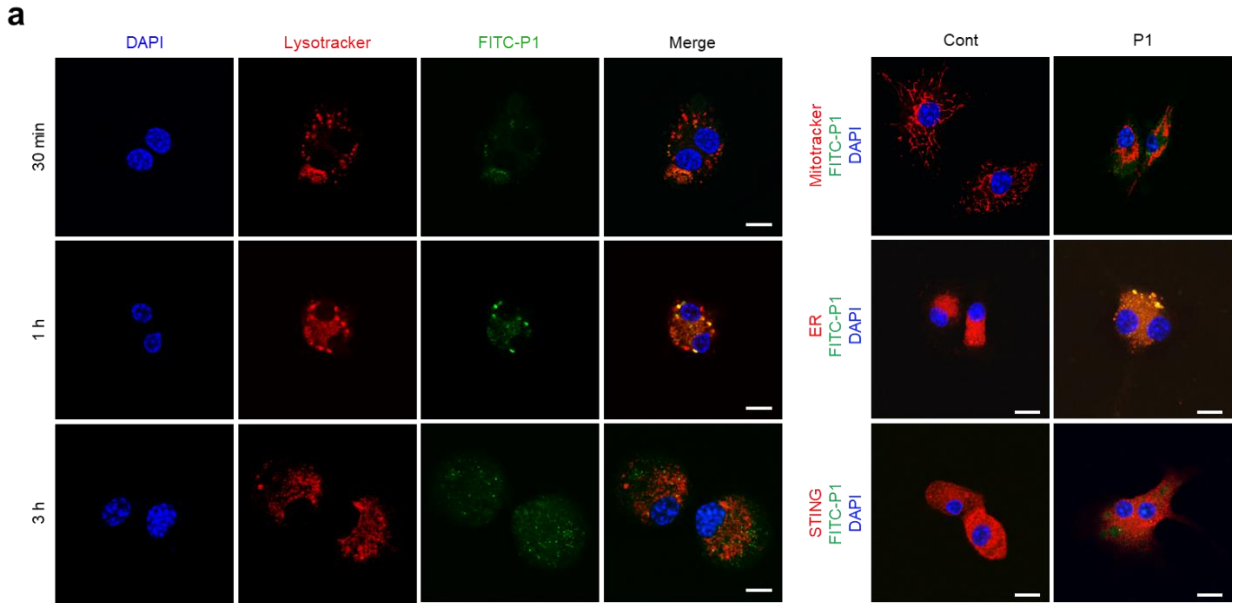


**Supplementary Fig. 20. Trafficking of P1 in M2 BMDMs.** (a) P1 escaped from lysosomes at 3 h (scale bar 10 μm). (b) P1 was localized in the endoplasmic reticulum (ER) but not in mitochondria. P1 was labeled with fluorescein isothiocyanate (FITC).

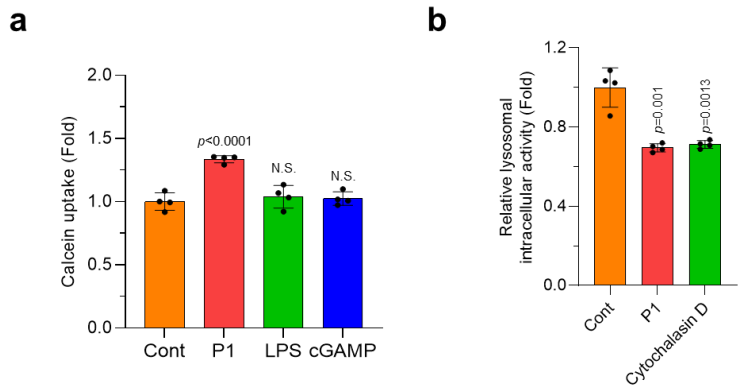


**Supplementary Fig. 21. P1 physically disrupts lipid plasma membranes.** (a) P1 destabilized lipid plasma membranes but did not influence STING activation (n=4 SD). (b) P1 disrupted lysosome integrity in BMDMs. (n=4, SD), unpaired Student's *t* test in comparison with Cont. Cytochalasin D used as a positive control; N.S., not significant.

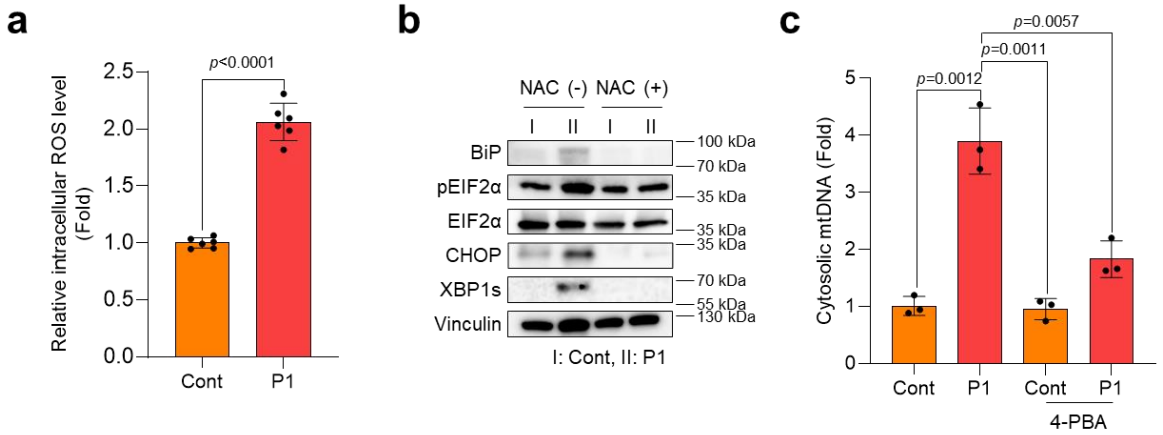


**Supplementary Fig. 22. P1 triggers mtDNA release via ROS-mediated ER stress.** (a) P1 treatment of BMDMs led to increased intracellular ROS levels (n=6, mean±SD); unpaired Student's *t* test in comparison with Cont. (b) Western blots of ER stress-related markers show that P1 treatments did not induce ER stress in *N*-acetylcysteine (NAC, 10 mM)-exposed BMDMs. (c) P1 treatments inhibited mtDNA release in BMDMs under ER stress-inhibiting conditions; sodium 4-phenylbutyric acid (4-PBA, 5 mM) was used as an ER stress inhibitor (n=6, mean±SD); unpaired Student's *t* test in comparison with the indicated conditions.

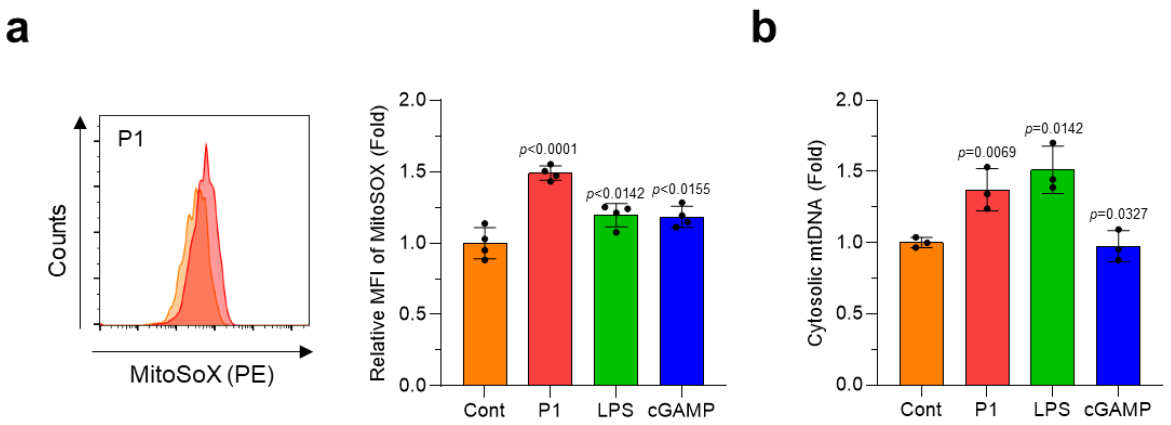


**Supplementary Fig. 23. P1 damages mitochondria to promote the release of mtDNA in THP1-derived human macrophage-like cells.** (a) Increased mitochondrial reactive oxygen species (ROS) levels, as evaluated by flow cytometry (n=4). (b) P1 triggered mtDNA release in THP1-derived M2 macrophages (n=3, mean±SD), unpaired Student's *t* test in comparison with Cont.

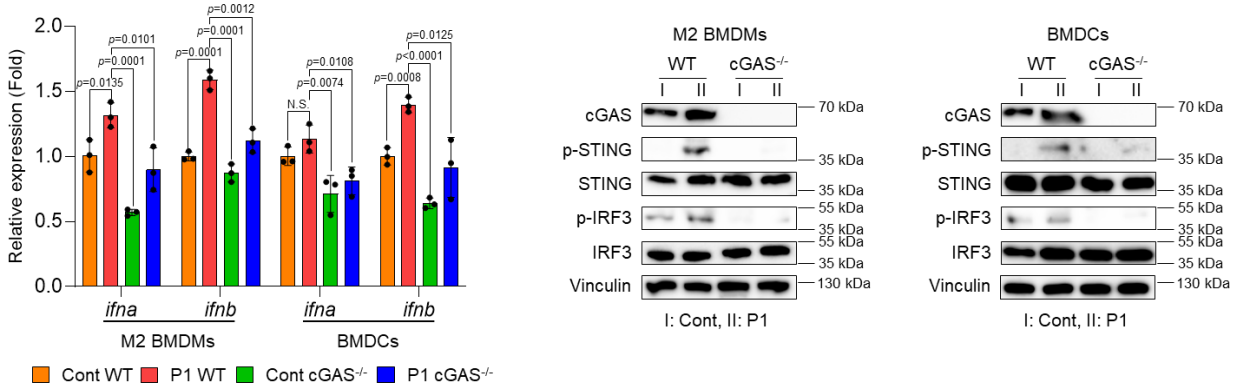


**Supplementary Fig. 24. P1-mediated generation of type I IFN responses requires cGAS stimulation in antigen-presenting cells.** (a) cGAS deficiency inhibited the expression of *ifna* and *ifnb* in M2 BMDMs or BMDCs, as determined by quantitative reverse transcription-polymerase chain reaction (n=3, mean±SD); unpaired Student's *t* test in comparison with the indicated conditions, N.S., not significant. (b) Western blots of cGAS-STING-IRF3 axis show that cGAS knockout de-activated the cGAS-STING cascade.

## Autophagy required for TLR9 activation

We measured extracellular mtDNA contents upon treatment with cationic helical polypeptide. P1-exposed M2 BMDMs and BMDCs emitted mtDNAs from the cytosol, which were likely taken up by the neighboring APCs (Supplementary Fig. 25a). Next, to demonstrate the mechanism by which P1-induced mtDNA facilitates TLR (Toll like receptors) activation, western blotting of proteins related to TLR pathways was carried out under autophagy-inhibiting conditions[1,2]. Inhibition of autophagy by silencing autophagy-related gene 5 (ATG) was found to deactivate the MyD88 and canonical NF-κB pathways, implying that P1-induced mtDNA were trapped in the neighboring APCs' lysosome and promoted subsequent TLR activation (Supplementary Fig. 25b).

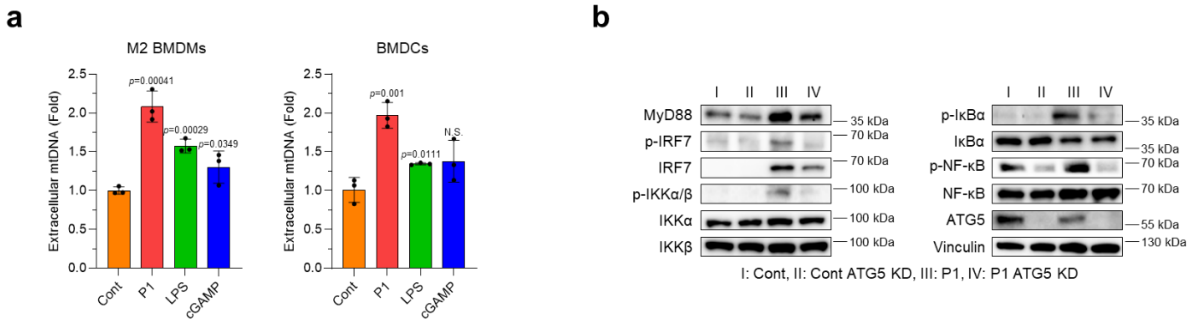


**Supplementary Fig. 25. TLR9 stimulation is essential for P1-mediated innate immune activation.** (a) Extracellular mtDNA levels in M2 BMDMs or BMDCs treated with P1 (n=3, mean±SD); unpaired Student's *t* test in comparison to Cont; N.S., not significant. (b) Autophagy related 5 (ATG5) knockdown (KD) in M2 BMDMs de-activated MyD88-IRF7 and canonical NF-κB pathways.

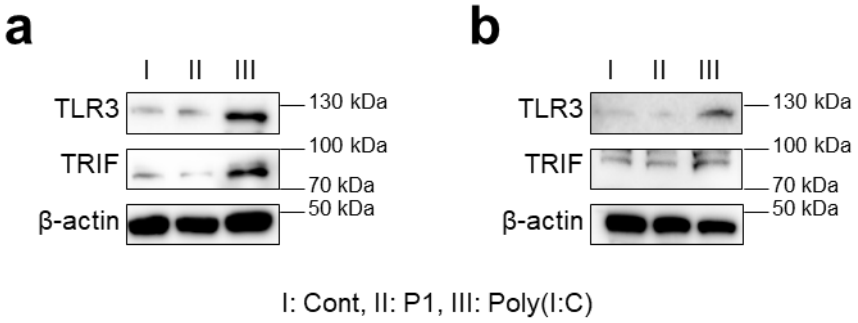


**Supplementary Fig. 26. P1 does not stimulate TLR3-TIR-domain-containing adapter-inducing interferon-β (TRIF) in bone marrow-derived (a) macrophages or (b) dendritic cells.** Western blots show that treating these antigen-presenting cells with P1 did not upregulate expression of TLR3 or TRIF protein compared with poly(I:C), a TLR3 agonist.

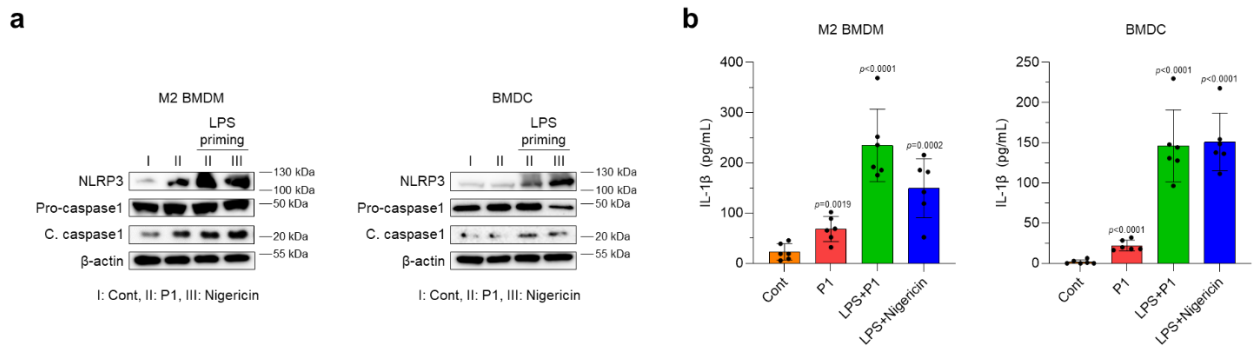


**Supplementary Fig. 27. P1 stimulates the NLRP3 inflammasome axis in BMDMs and BMDCs primed with LPS.** (a) Western blot images show that P1 upregulated NLRP3 expression and promoted cleavage of caspase-1 in BMDMs and BMDCs. (b) P1 treatment triggered interleukin (IL)-1β secretion in BMDMs and BMDCs, as evaluated by enzyme-linked immunosorbent assay (n=6, mean±SD). Unpaired Student's *t* test in comparison with control (Cont).

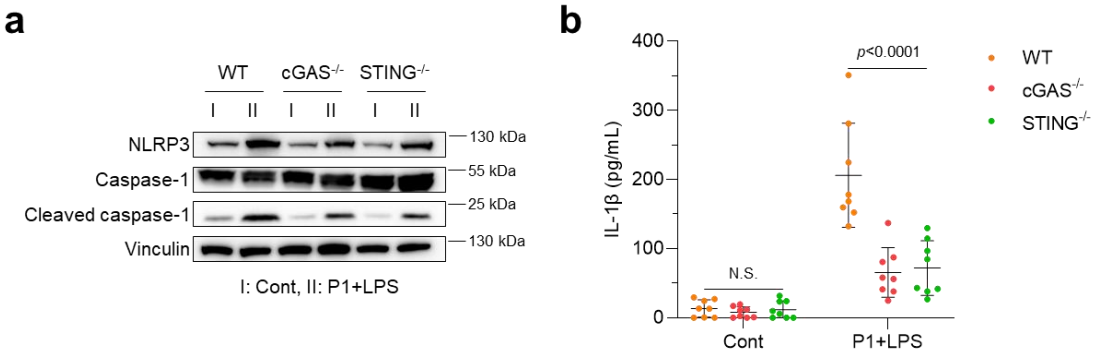


**Supplementary Fig. 28. P1 with LPS priming activates NLRP3 inflammasome pathway in BMDMs in a cGAS- or STING-dependent fashion.** (a) Western blot images showing that knockout of cGAS or STING downregulated NLRP3 inflammasome axis in BMDMs. (b) Deficiency of cGAS or STING suppressed secretion of IL-1β in BMDMs (n=8, mean±SD), ordinary ANOVA; N.S., not significant.

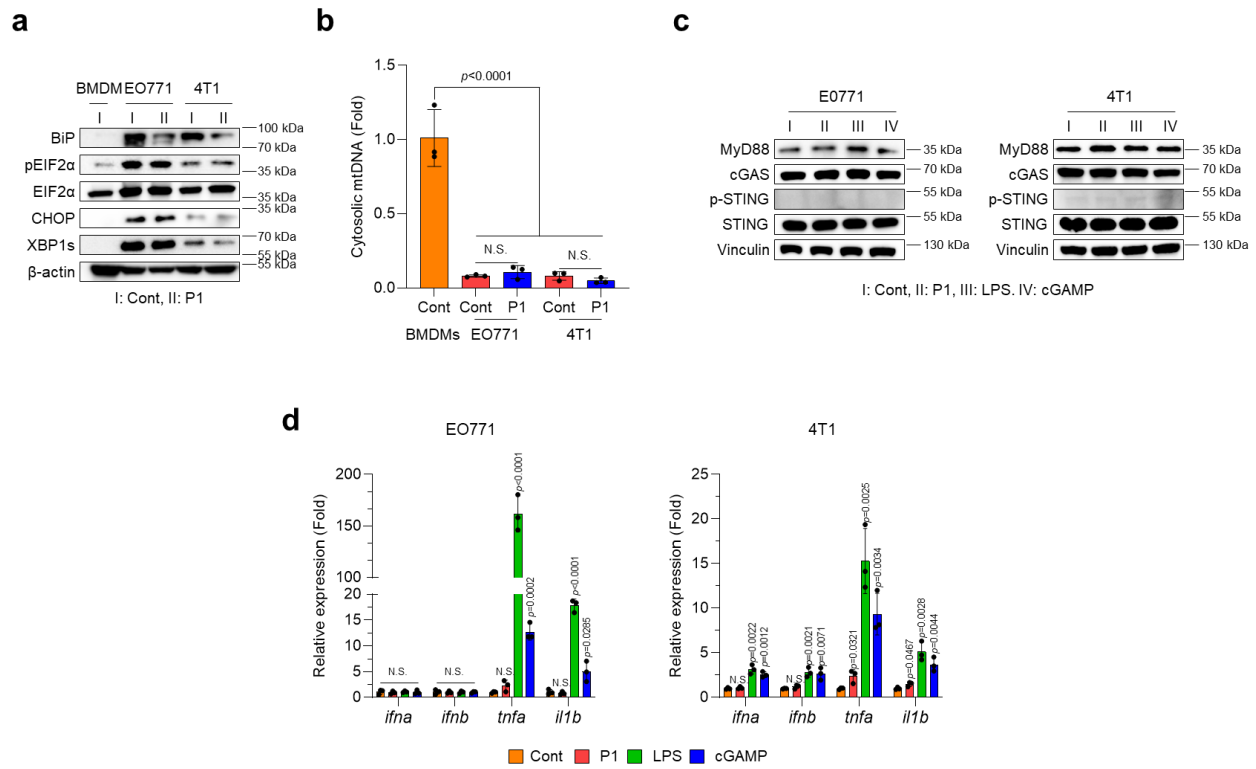


**Supplementary Fig. 29. P1 does not affect activation of MyD88 and cGAS-STING pathways in cancer cells via ER stress-mediated mtDNA release.** (a) Immunoblotting of ER stress-related proteins shows that P1 did not induce ER stress in EO771 or 4T1 breast cancer cell lines. (b) P1 did not promote mtDNA release in EO771 or 4T1 breast cancer cell lines (n=3, mean±SD), unpaired Student's *t* test in comparison with Cont. (c) Western blotting of proteins related to MyD88 and cGAS-STING pathways in EO771 and 4T1 breast cancer cells. (d) P1 did not generate pro-inflammatory responses in EO771 or 4T1 breast cancer cell lines compared with LPS (n=3, mean±SD), unpaired Student's *t* test in comparison with Cont; N.S., not significant.

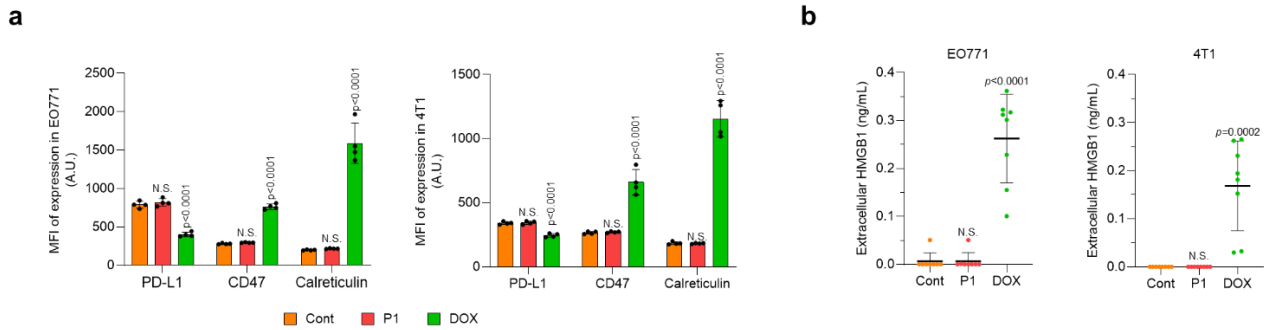


**Supplementary Fig. 30. P1 treatment does not induce immunogenic cell death or upregulate immune checkpoints in breast tumor cells.** (a) P1 treatment did not increase the expression of PDL1 (Programmed cell Death Ligand 1), CD47, or calreticulin on the surface of EO771 or 4T1 breast cancer cells; doxorubicin (DOX) was used as a positive control (n=4, mean±SD), unpaired Student's *t* test in comparison with Cont. (c) P1 did not promote release of high mobility group box 1 protein (HMGB1) from EO771 or 4T1 breast cancer cells (n=8, mean±SD), unpaired Student's *t* test in comparison with Cont; N.S., not significant.

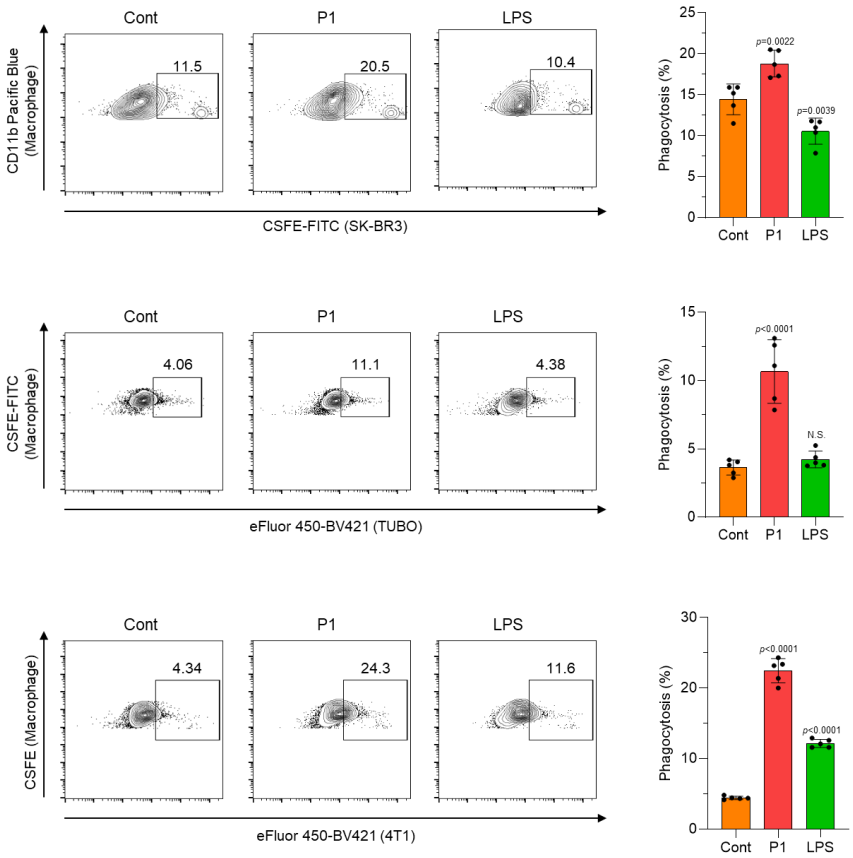


**Supplementary Fig. 31. M2 macrophages exposed to P1 show enhanced phagocytosis of breast cancer cell lines SK-BR3, TUBO, and 4t1.** n=5, mean±SD; unpaired Student's *t* test in comparison with control (Cont).

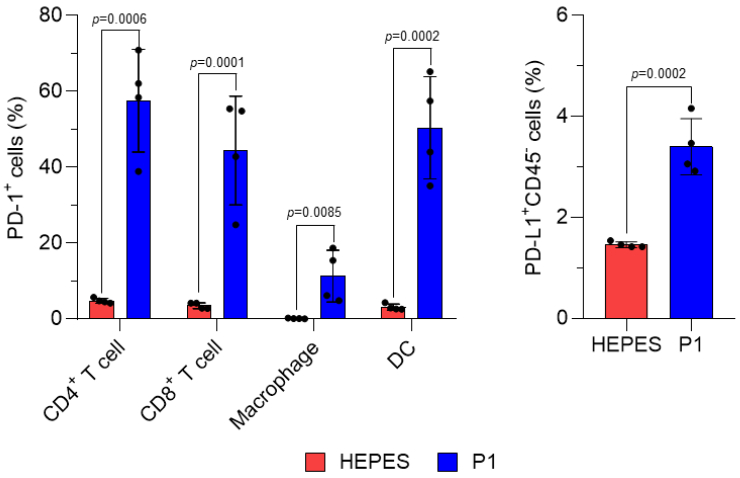


**Supplementary Fig. 32. P1 upregulates PD1 (Programmed cell Death 1) on tumor-infiltrating immune cells and PDL1 expression on EO771 tumor cells.** Flow cytometry of tumor-infiltrating immune cells and CD45⁻ cells from EO771 tumors at 1 day after the last treatment (n=4, mean±SD); unpaired Student's *t* test in comparison with HEPES treatment.

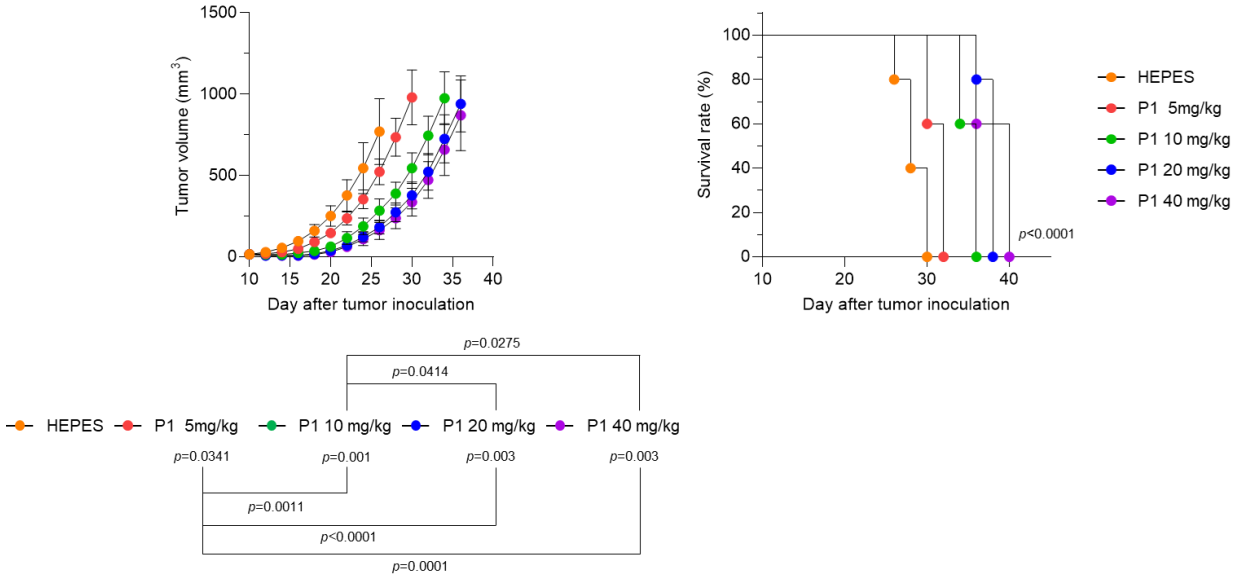


**Supplementary Fig. 33. P1 alone and in combination with αPD1 has antitumor effects on large (>100 mm³) EO771 tumors.** (a,b) P1 and P1+αPD1 retarded tumor growth (n=5, mean±SD); unpaired Student's *t* test in comparison with HEPES or the indicated conditions at day 12 after the first treatment; and extended the survival of tumor-bearing mice with large EO771 tumors to a greater extent than did the other treatments; log-rank (Mantel-Cox) test for Kaplan-Meier survival curves.

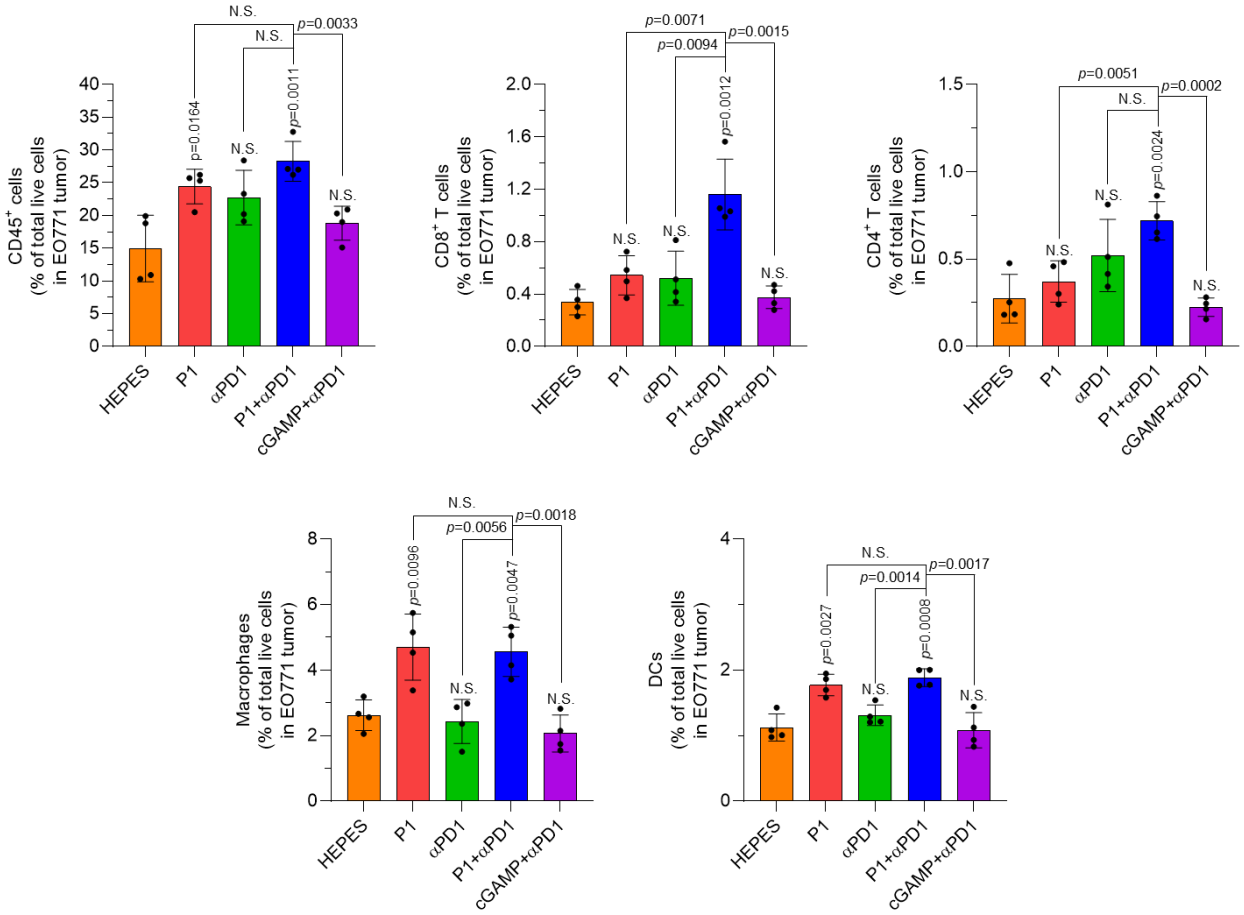


**Supplementary Fig. 34. P1+αPD1 treatment increases the populations of tumor-infiltrating lymphocytes within EO771 tumors.** Immune profiling of CD45$^+$ cells, CD8+ T cell, CD4+ T cells, macrophages, and DCs without CD45$^+$ cell enrichment, as evaluated by flow cytometry (n=4, mean±SD), unpaired Student's *t* test in comparison with HEPES or the indicated conditions, N.S.: not significant.

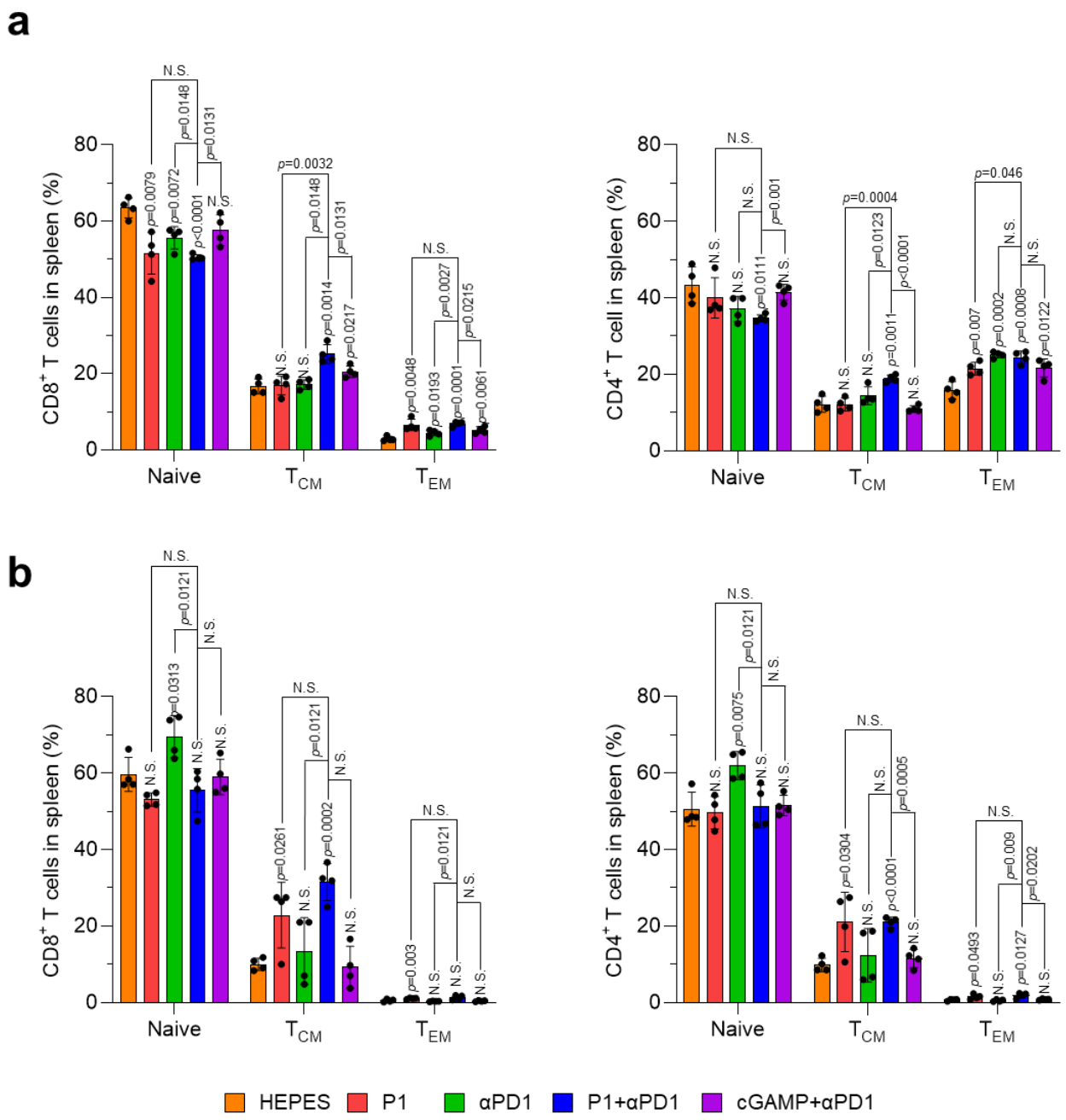


**Supplementary Fig. 35. Systemic treatment with P1+αPD1 shifts splenic T cells toward memory subtypes.** Flow cytometry of T cells isolated from the spleens (harvested on day 17) of mice bearing (a) EO771 tumors or (b) 4T1 tumors (n=4, mean±SD); unpaired Student's *t* test in comparison with HEPES or the indicated conditions, N.S., not significant.

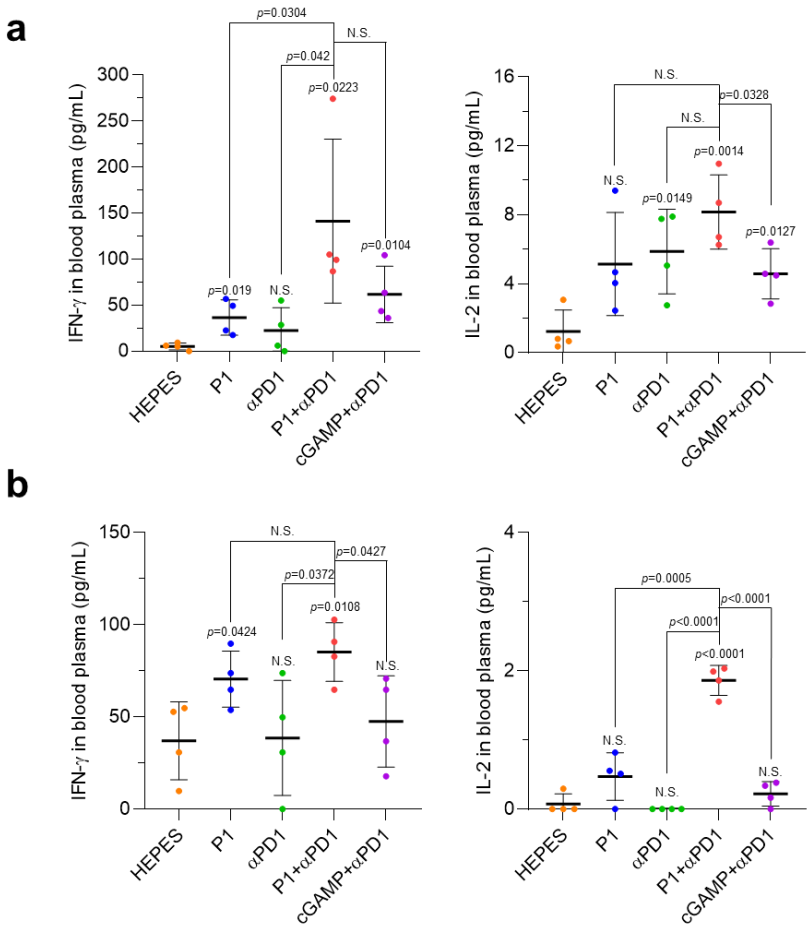


**Supplementary Fig. 36. Systemic treatment with P1 plus αPD1 upregulates pro-inflammatory cytokines.** Interferon (IFN)-γ and interleukin (IL)-2 levels in blood plasma (collected on day 17) of mice bearing (a) EO771 tumors and (b) 4T1 tumors, as quantified by enzyme-linked immunosorbent assay (n=4, mean±SD); unpaired Student's *t* test in comparison with HEPES or the indicated conditions, N.S., not significant.

## References


1 De Leo, M. G. *et al.* Autophagosome–lysosome fusion triggers a lysosomal response mediated by TLR9 and controlled by OCRL. *Nature Cell Biology* **18**, 839-850, doi:10.1038/ncb3386 (2016).

2 Liu, Y. *et al.* TLR9 and beclin 1 crosstalk regulates muscle AMPK activation in exercise. *Nature* **578**, 605-609, doi:10.1038/s41586-020-1992-7 (2020).

**Flow Gating strategies**

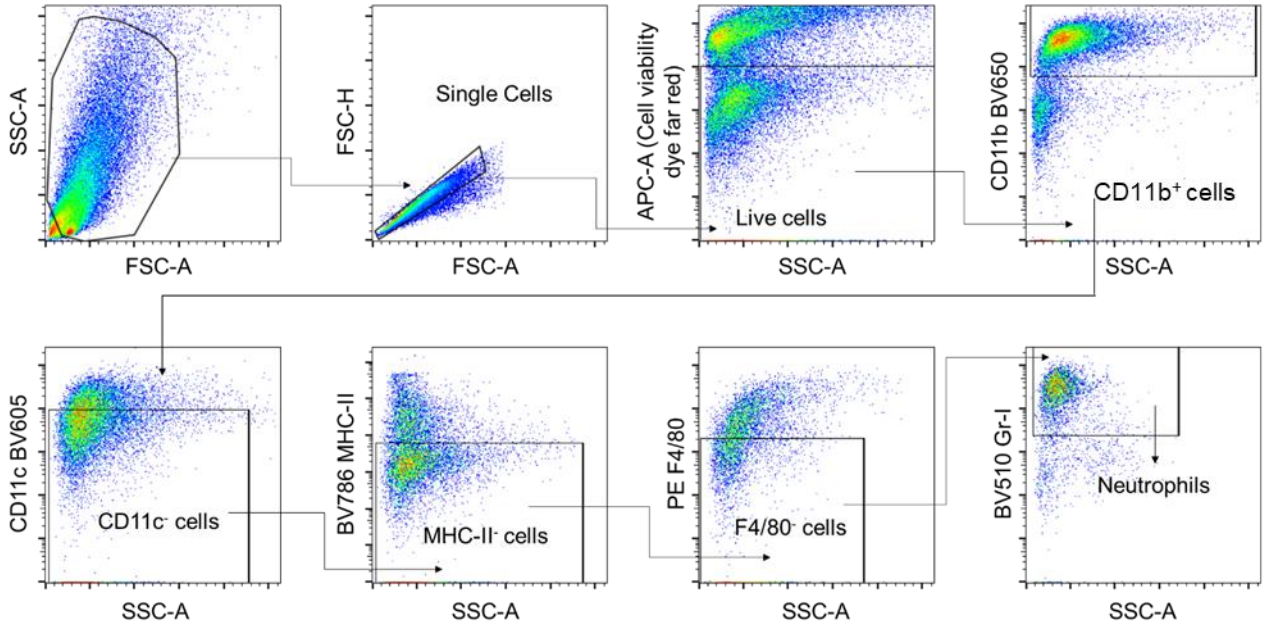


Neutrophil gating strategy, Fig. 1g and Supplementary Fig. 9.

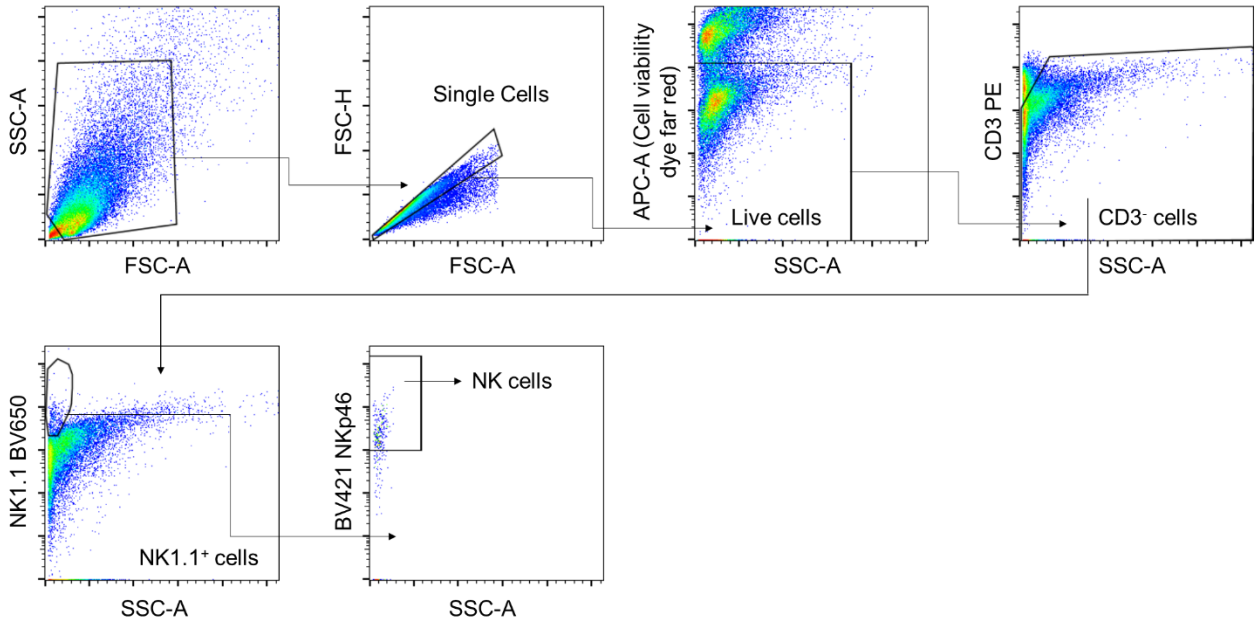


NK (Natural Killer) cell gating strategy, Fig. 1g

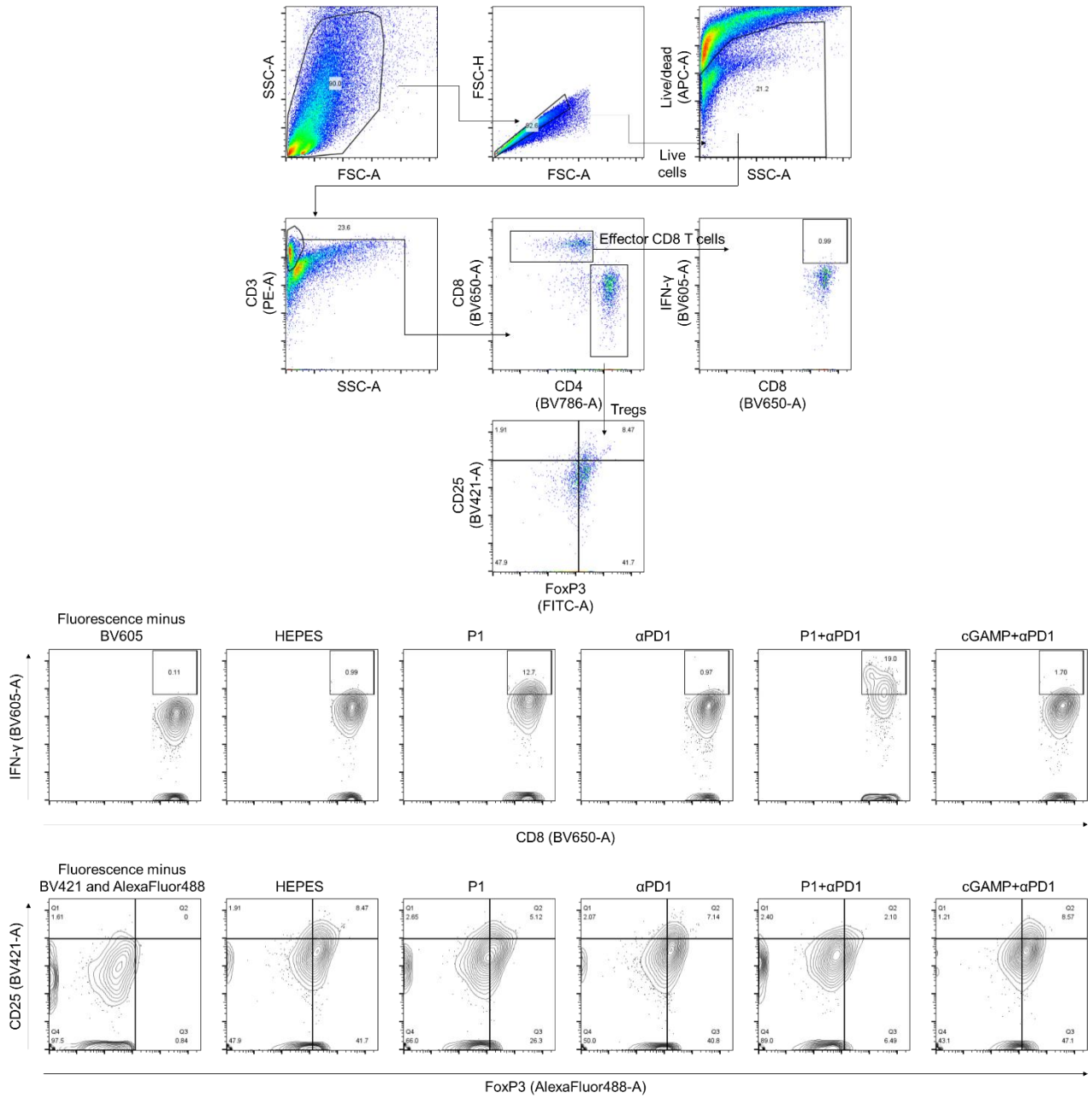


Tumor-infiltrating T lymphocytes, Fig. 1e, 2e, 5e, 7b,d, Extended Fig. 1, 2e, 7f, Supplementary Fig. 9, 31, 33

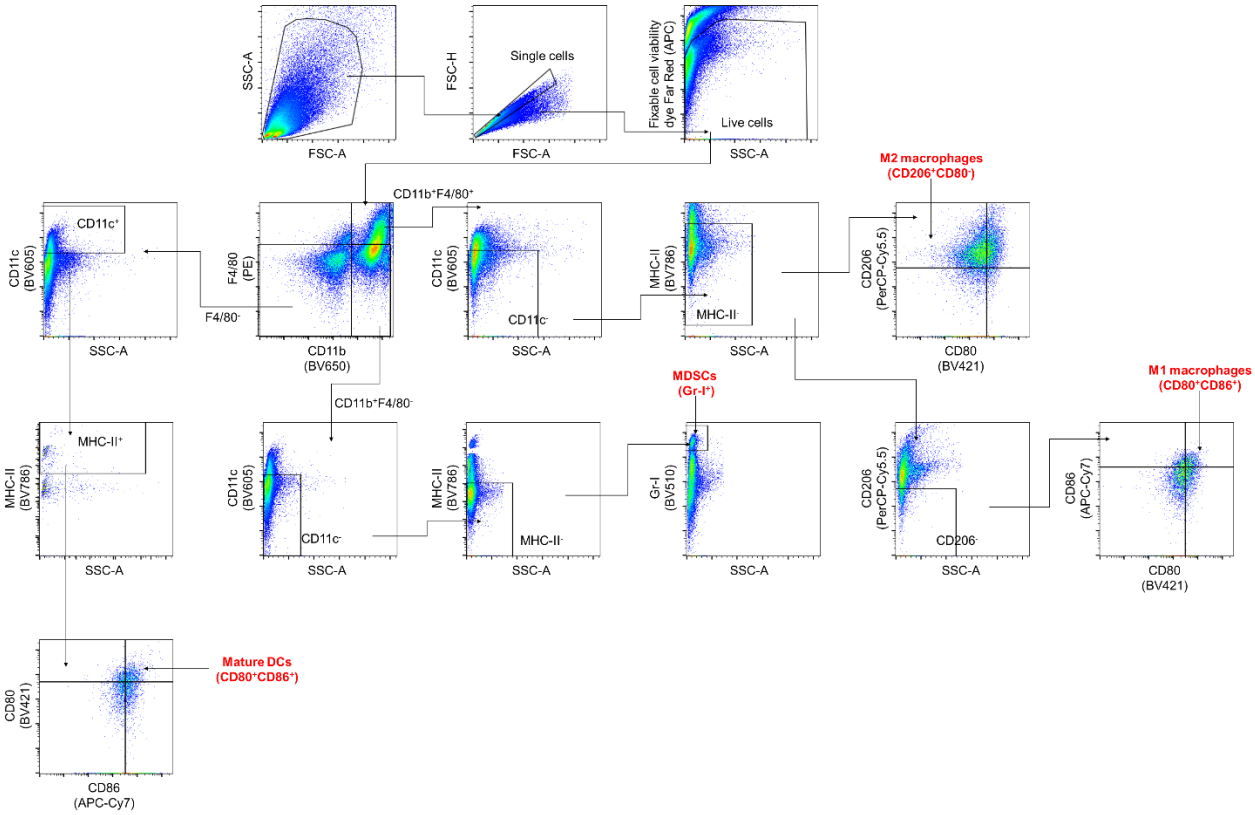


Tumor-infiltrating myeloid cells, Fig. 1e, 2f, 5g, 7b,d, Extended Fig. 1, 2g, Supplementary Fig. 9, 31, 33.

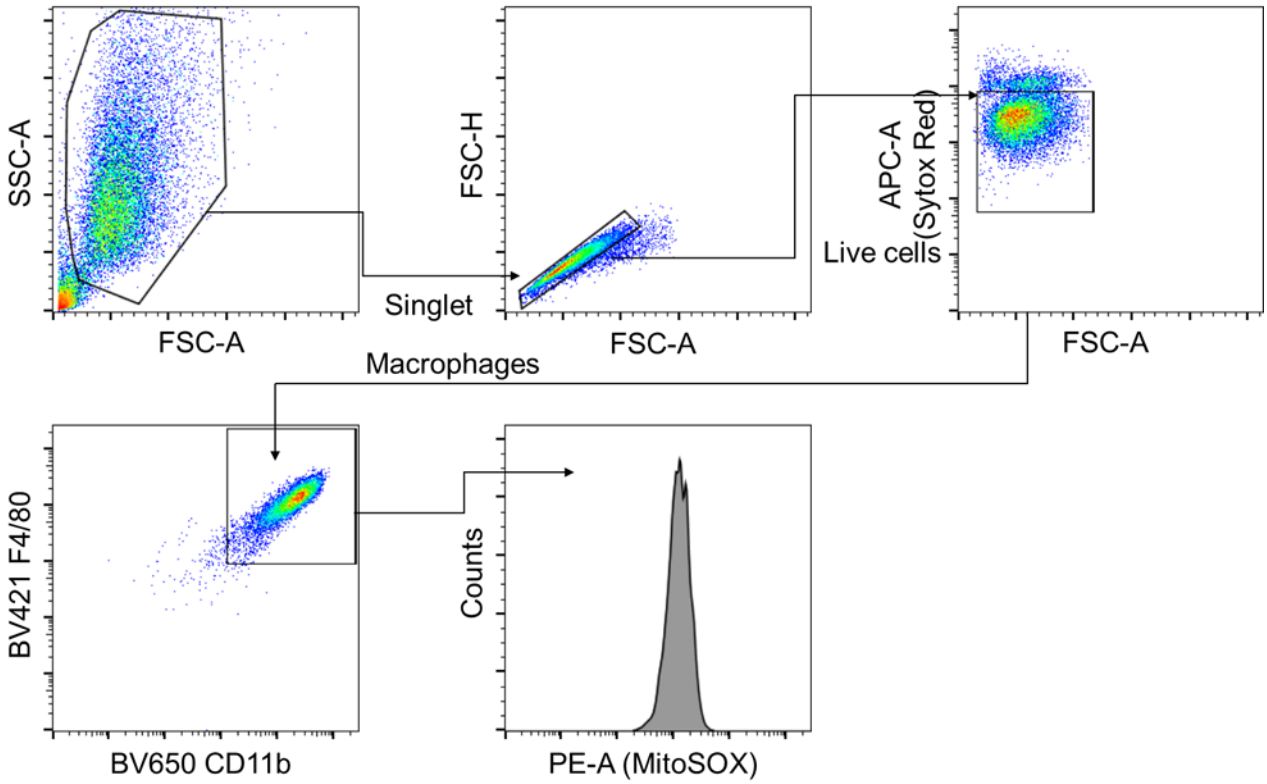


Macrophage MitoSOX measurement, Fig. 3e

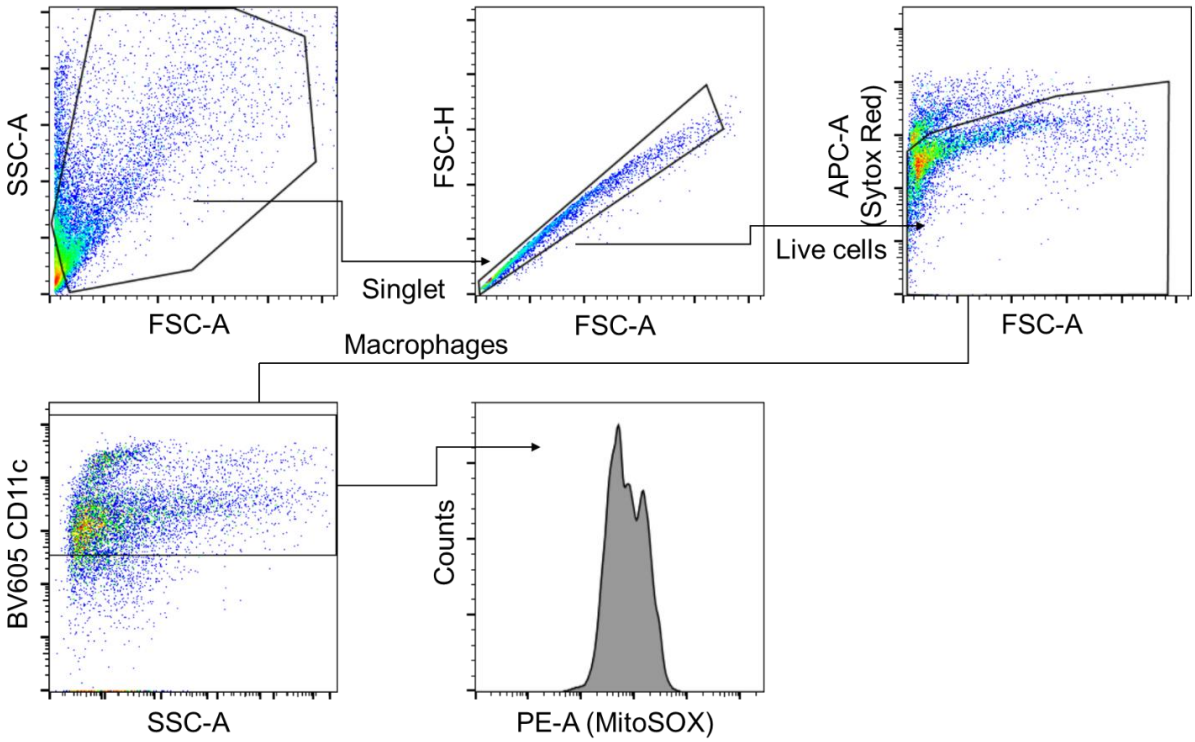


BMDC (bone marrow derived DCs) MitoSOX measurement, Fig. 3e.

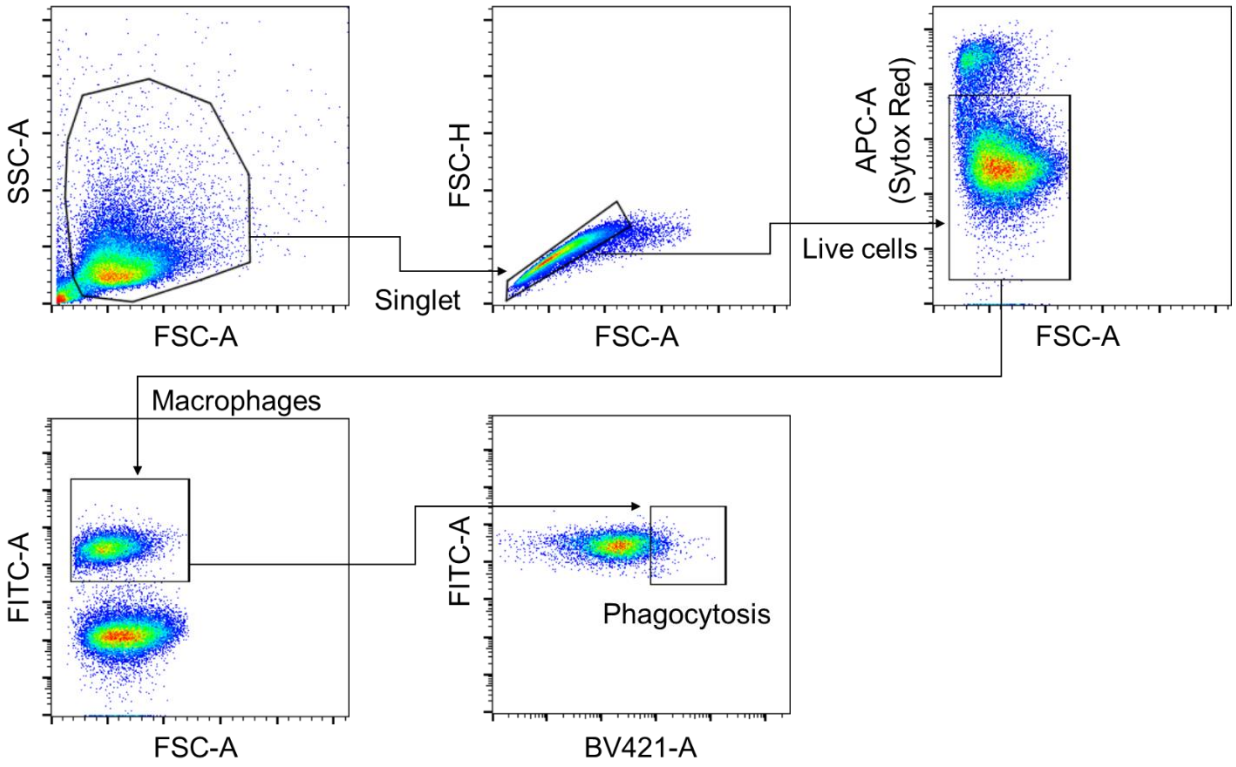


Macrophage phagocytosis assay, Fig. 4a, Supplementary Fig. 4d, 5d, 6d, 30.

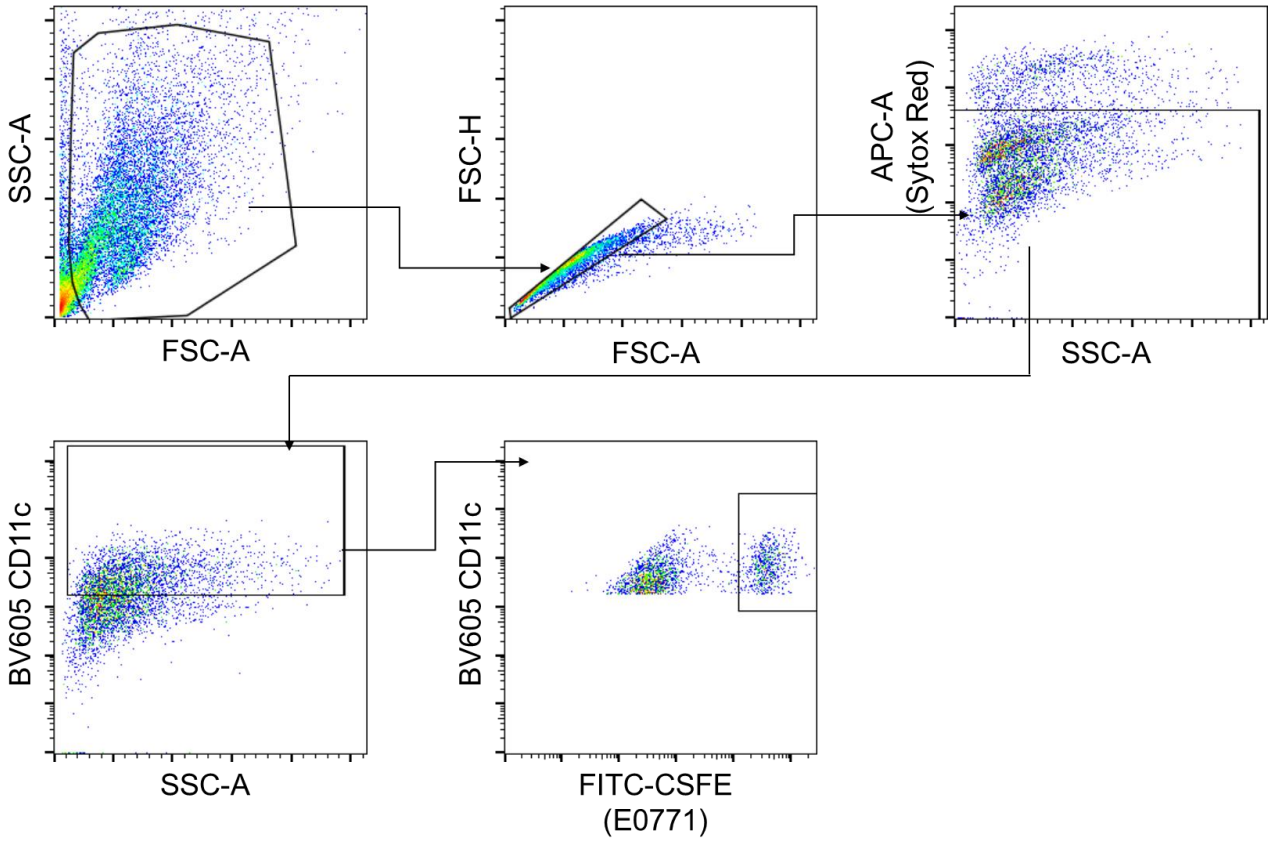


DC (dendritic cells) phagocytosis assay, Fig. 4a.

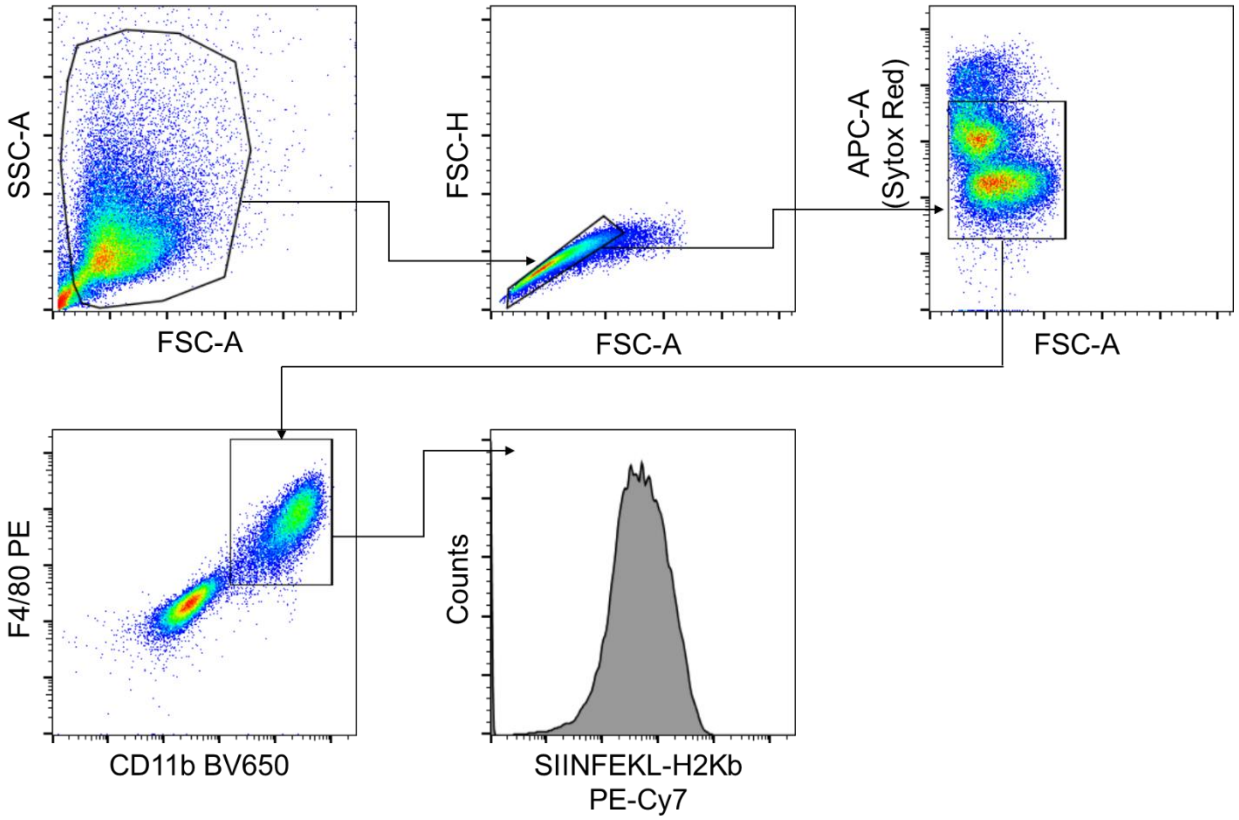


Macrophage antigen presentation, Fig. 4c and Supplementary Fig. 4e, 5e, 6e

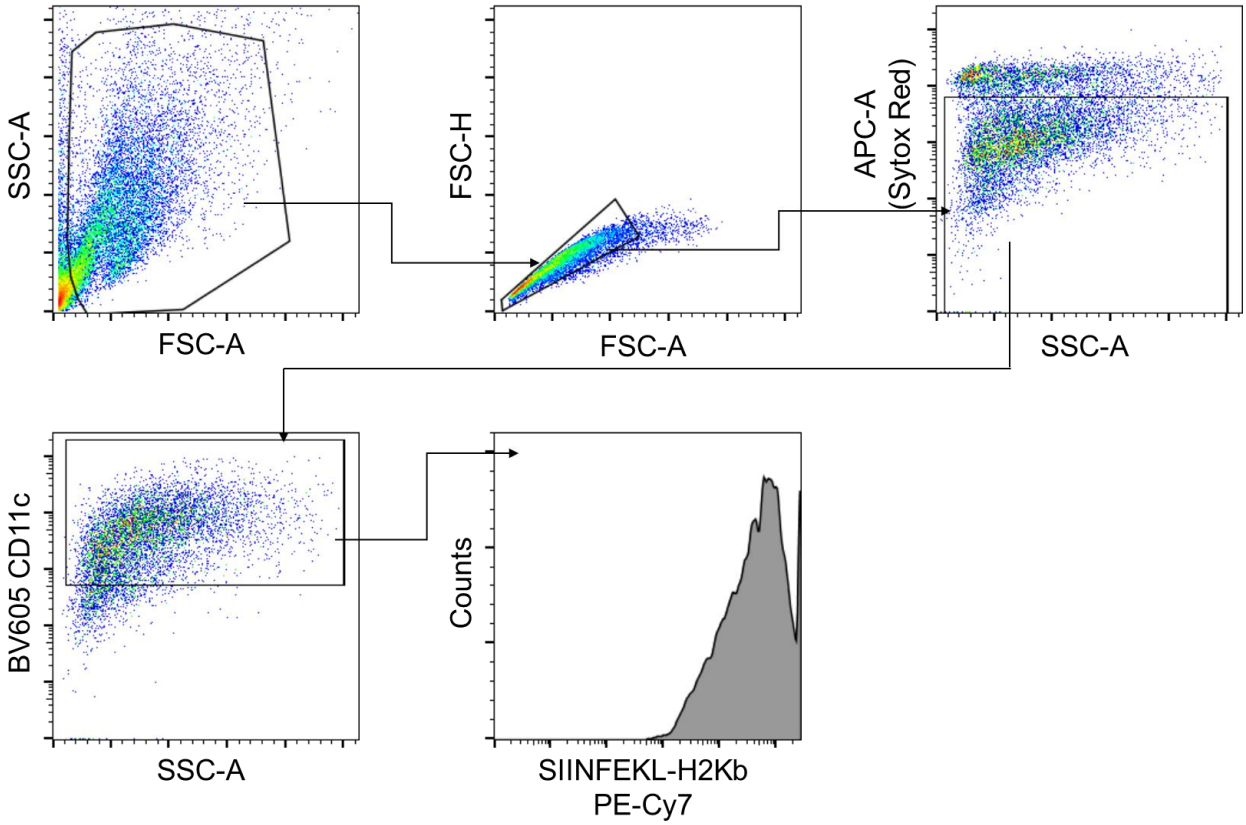


DC antigen presentation, Fig. 4c.

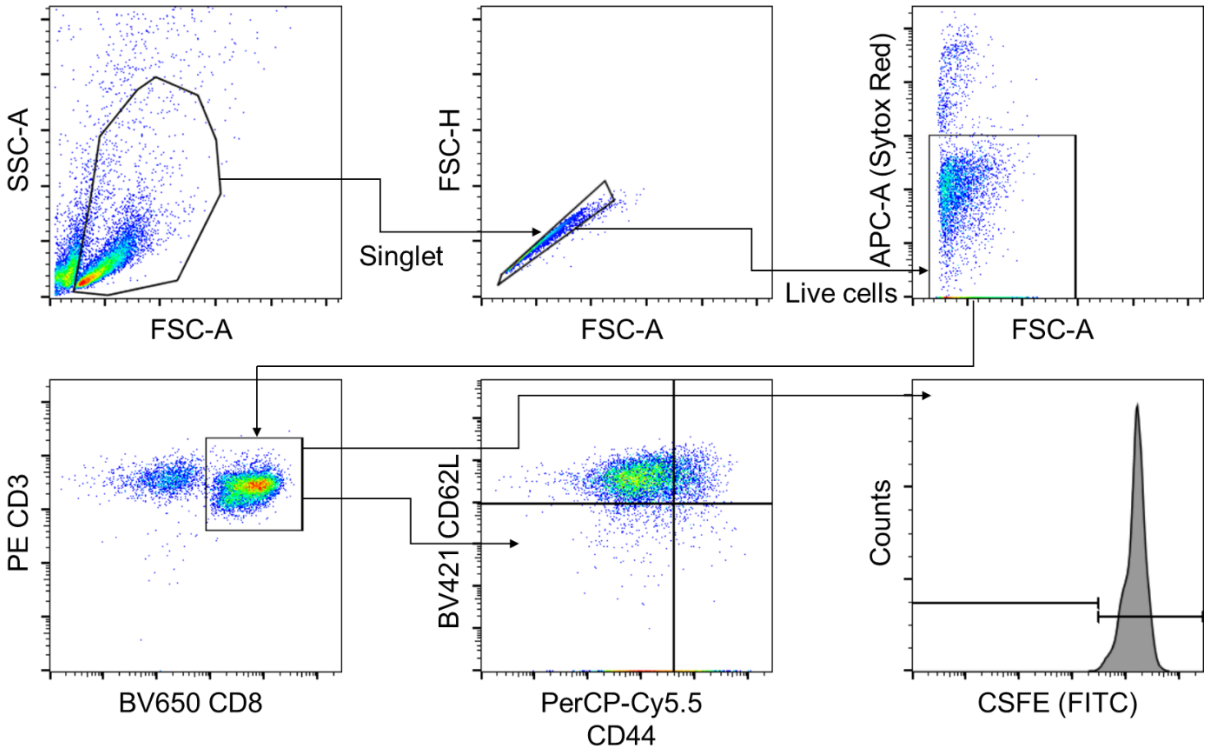


OT-I or OT-II proliferation and activation, Fig. 4f-h

**Tumor-infiltrating T cells**

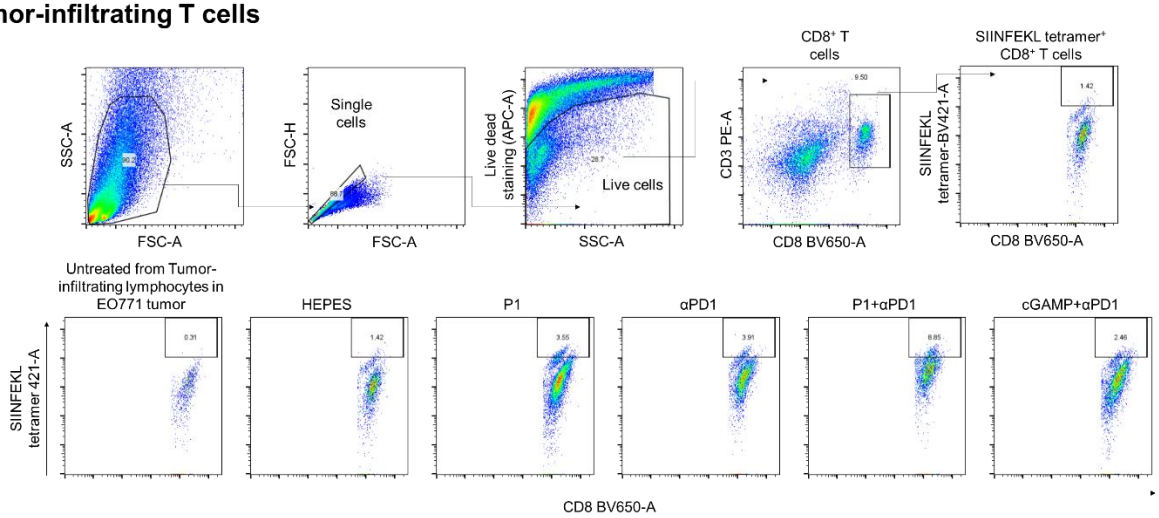


**Splenic T cells**

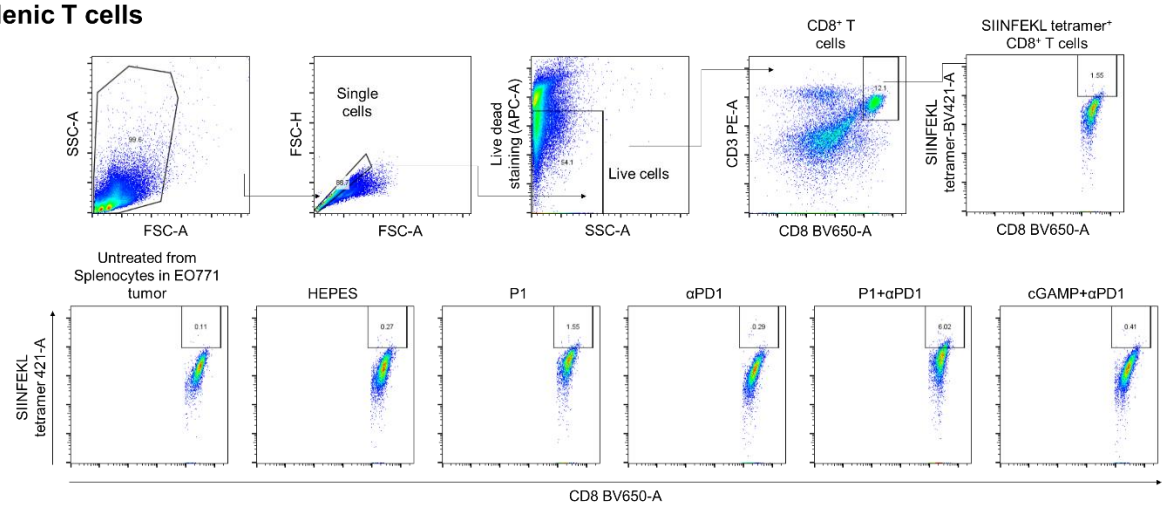


OVA tetramer staining, Fig. 5i,j

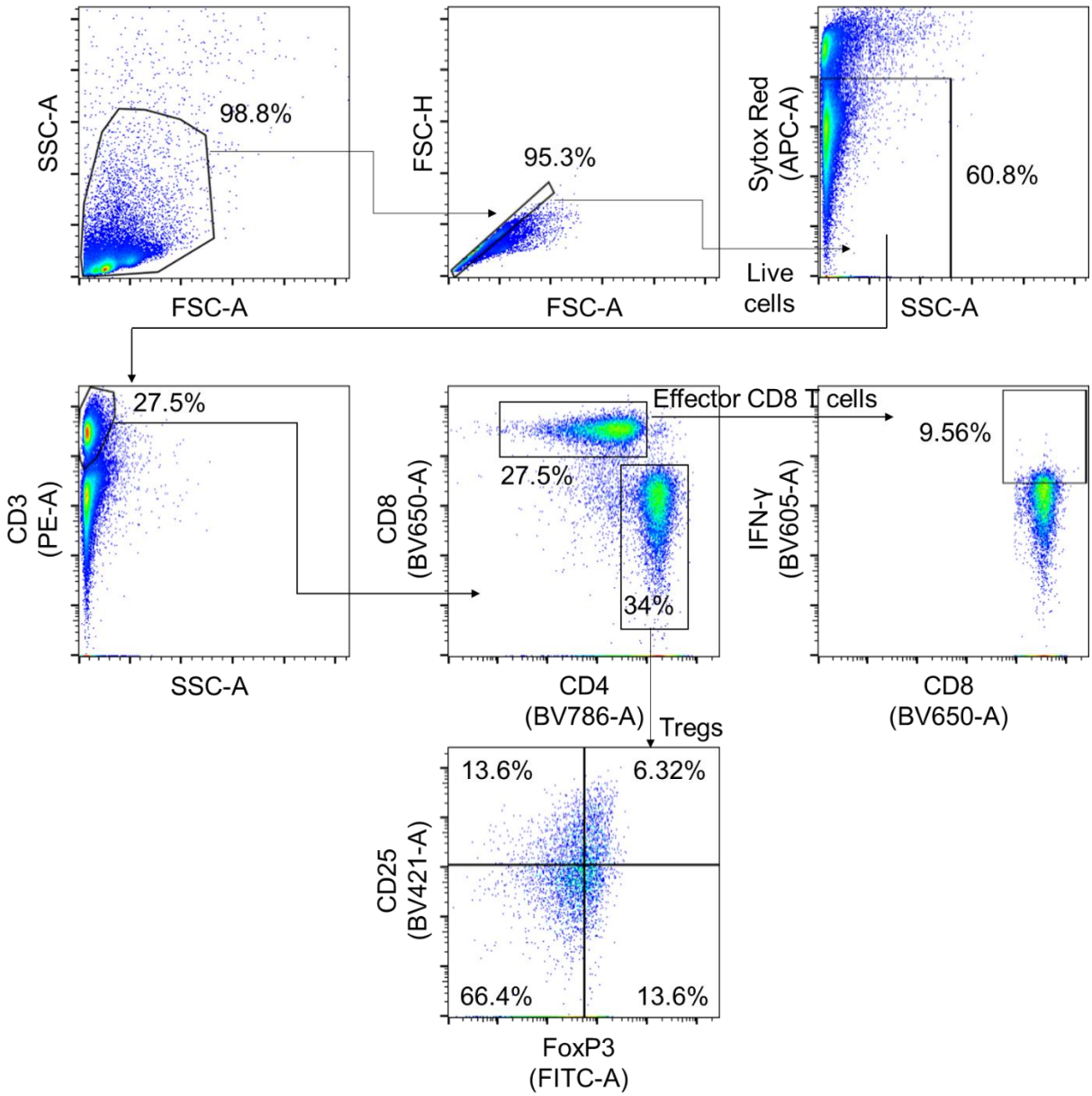


T cell gating in lymph nodes or spleen, Extended Fig. 3a

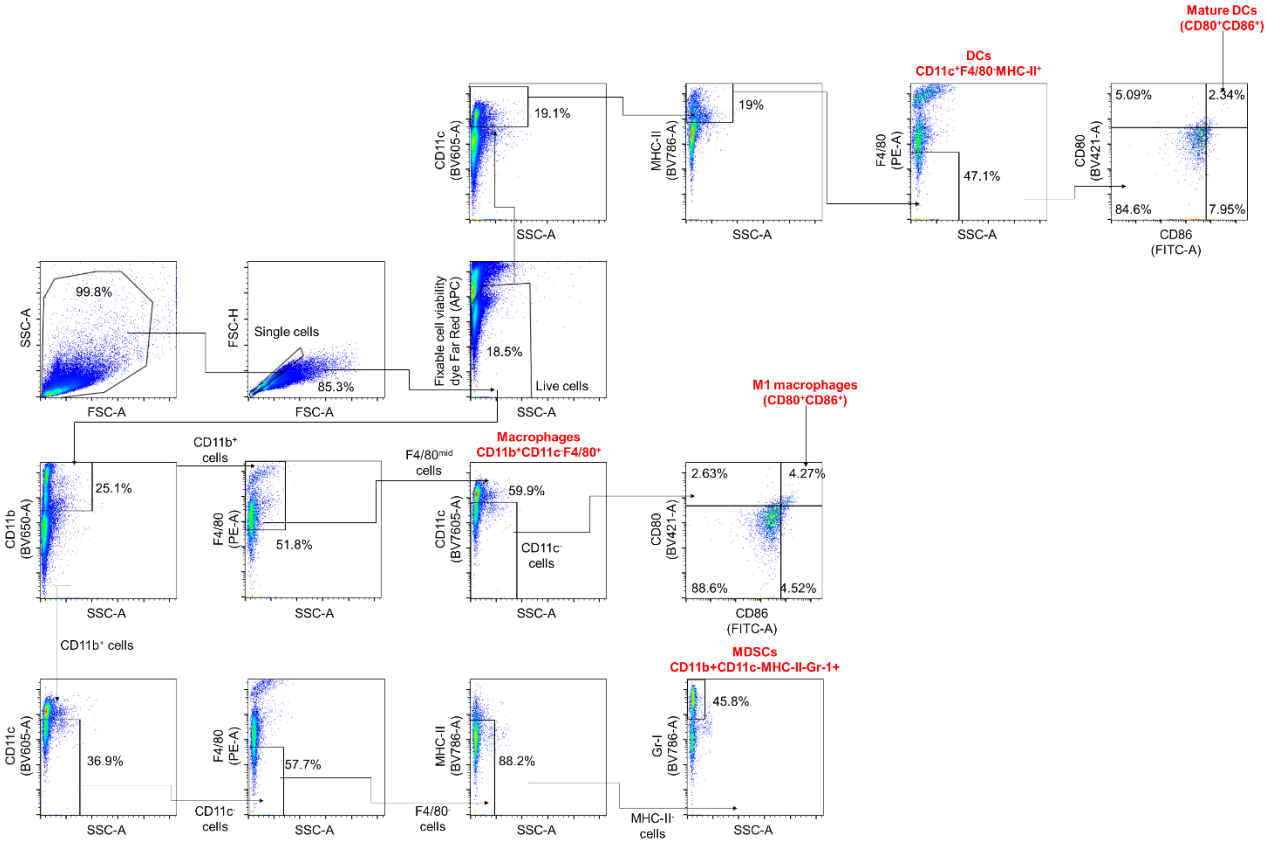


Myeloid cell gating in lymph nodes or spleen, Extended Fig. 3b

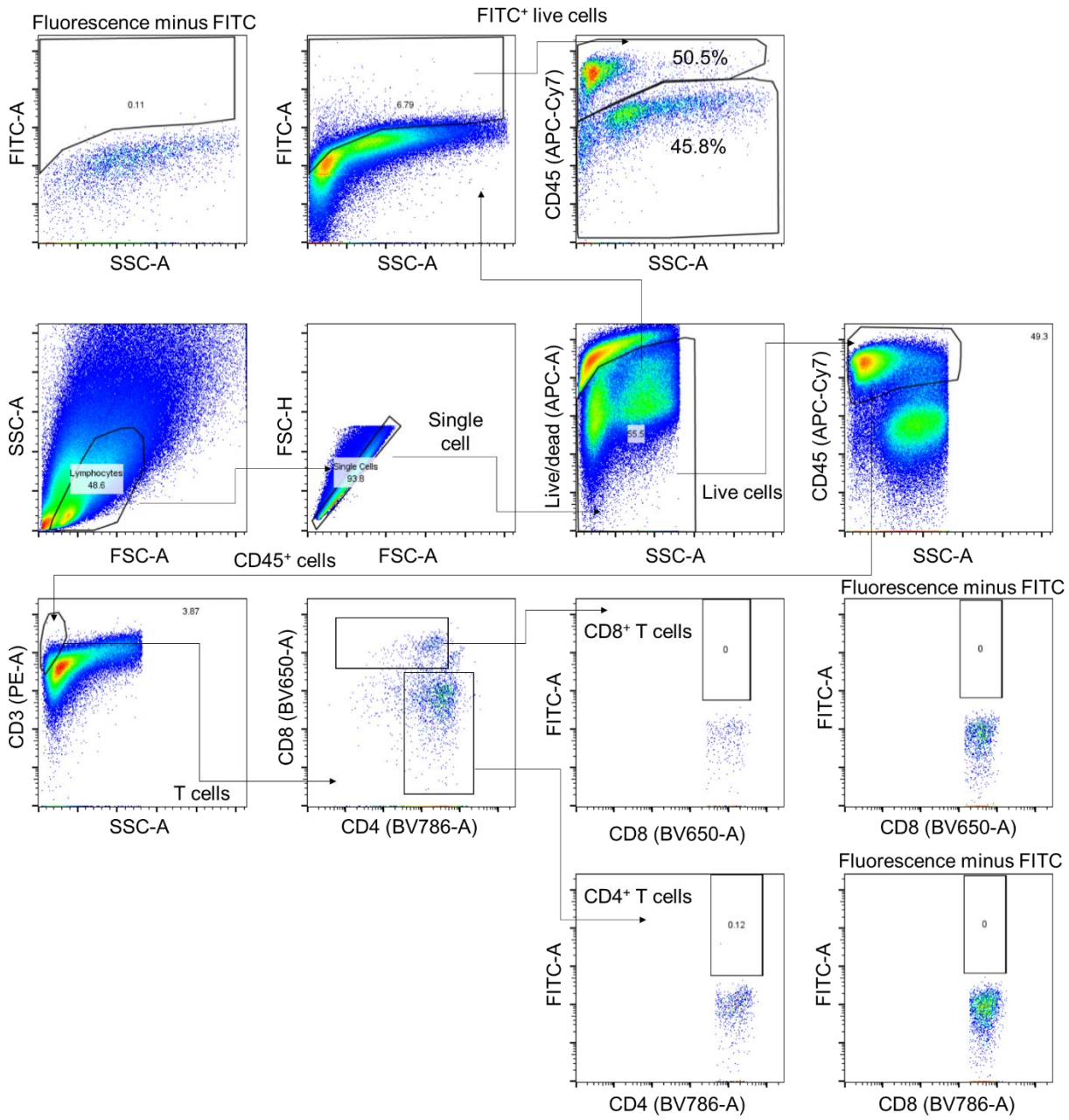


Gating strategies for FITC-P1 accumulation in CD45⁺ or CD45⁻ cells, and T cell subpopulations, Supplementary Fig. 7.

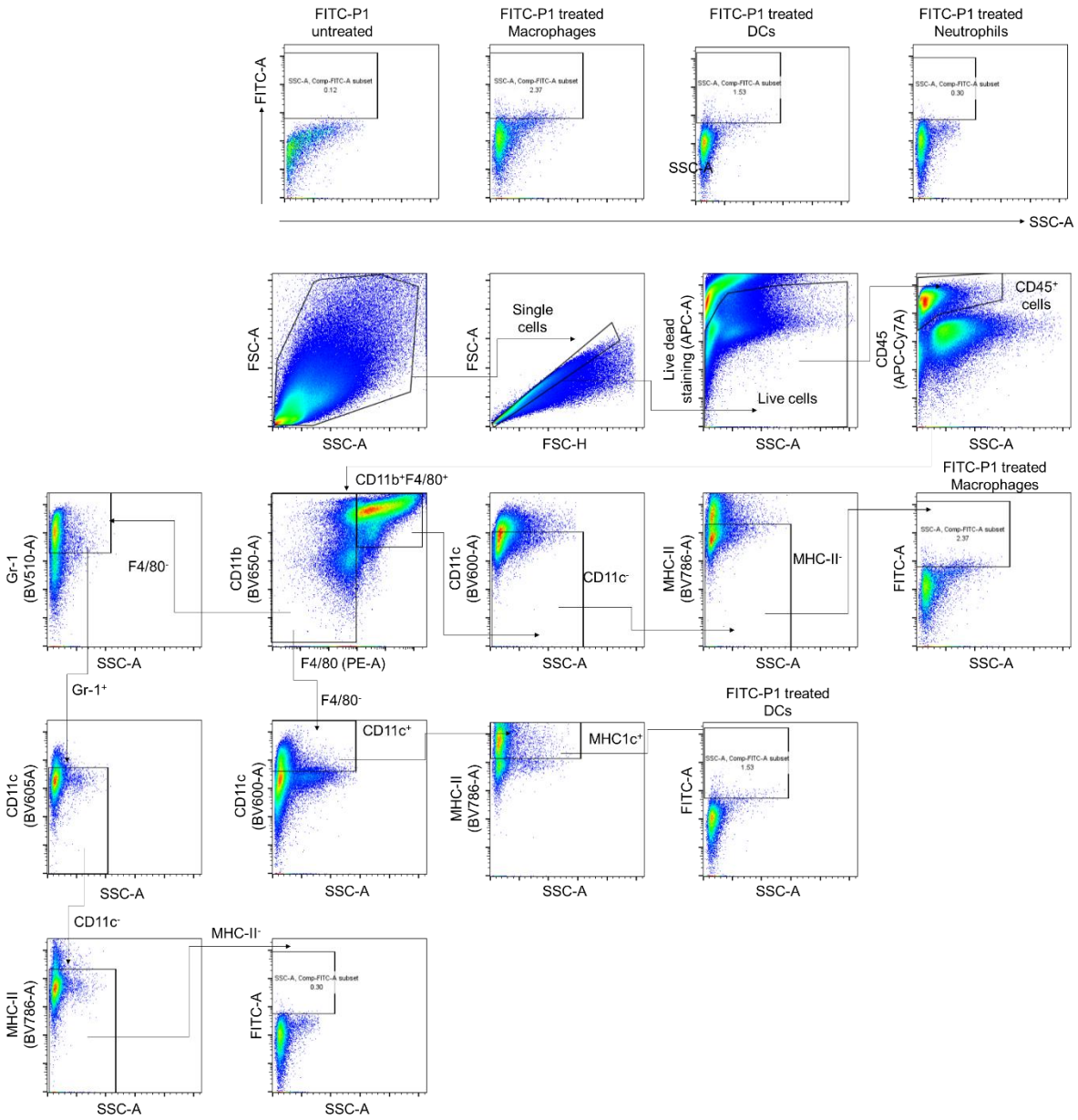


Gating strategies for FITC-P1 accumulation in myeloid cell subpopulations, Supplementary Fig. 7.

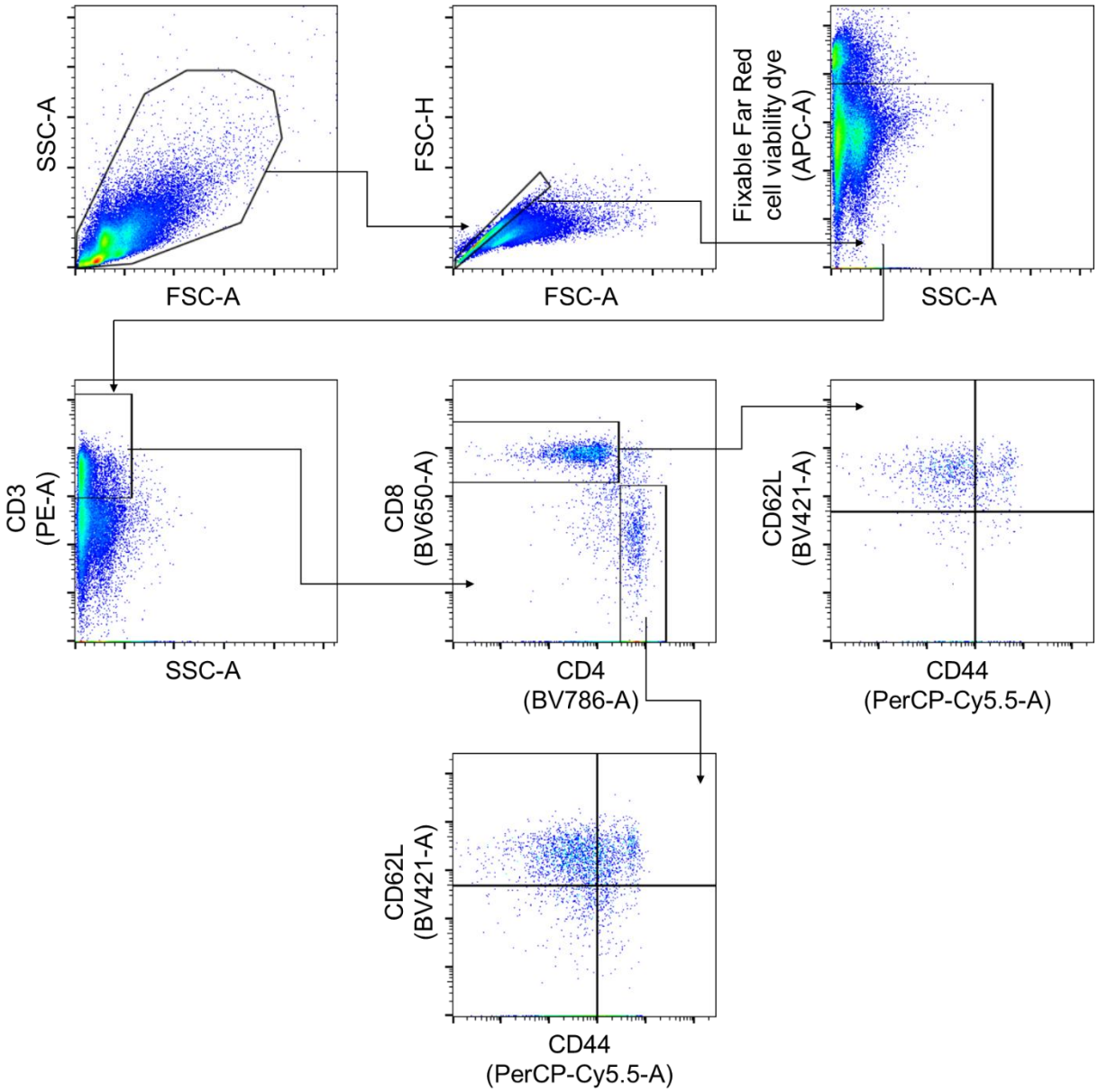


Splenic T cells *in vivo* for memory populations, Supplementary Fig. 16a, 34

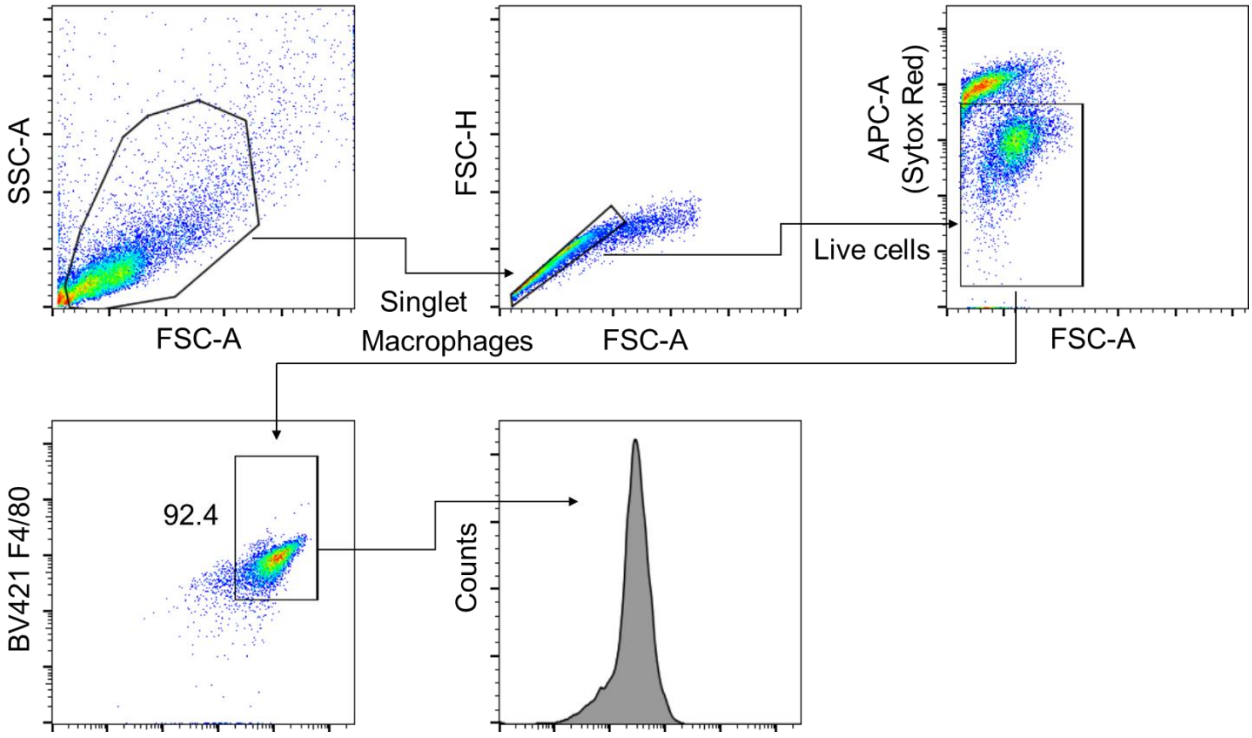


Membrane destabilization assay, Supplementary Fig. 20a.

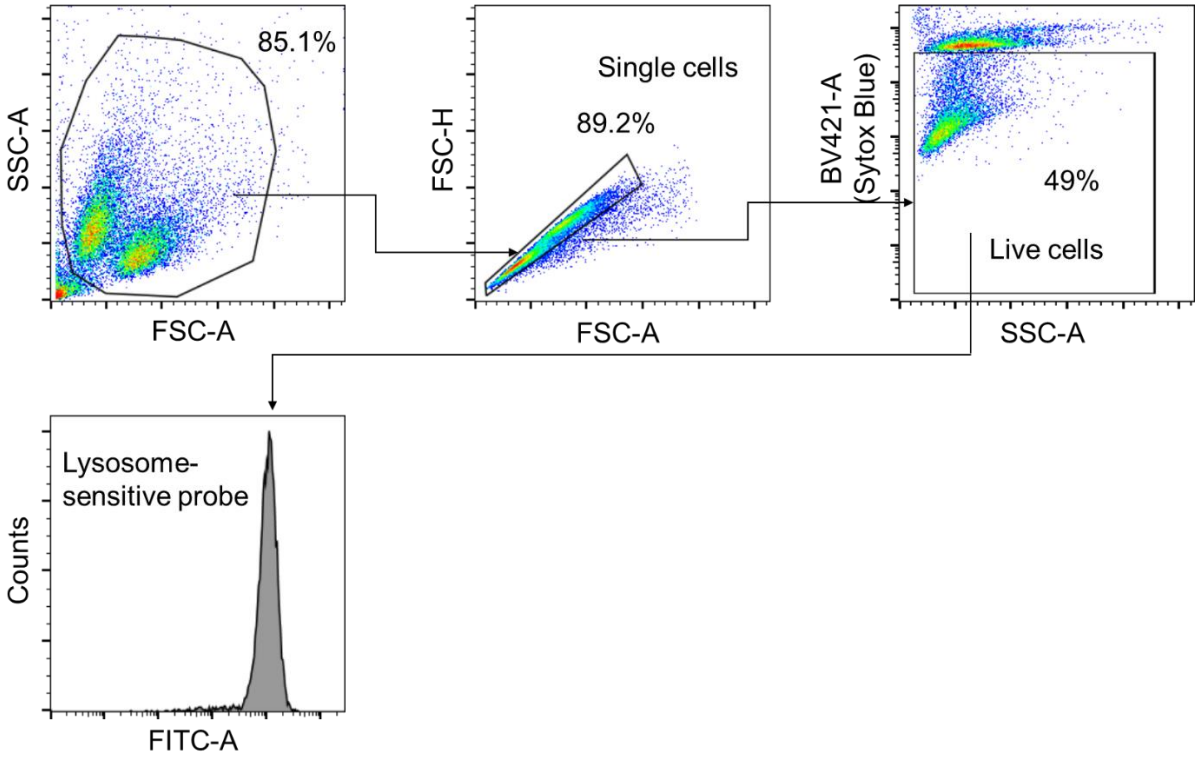


Intracellular lysosomal activity, Supplementary Fig. 20b.

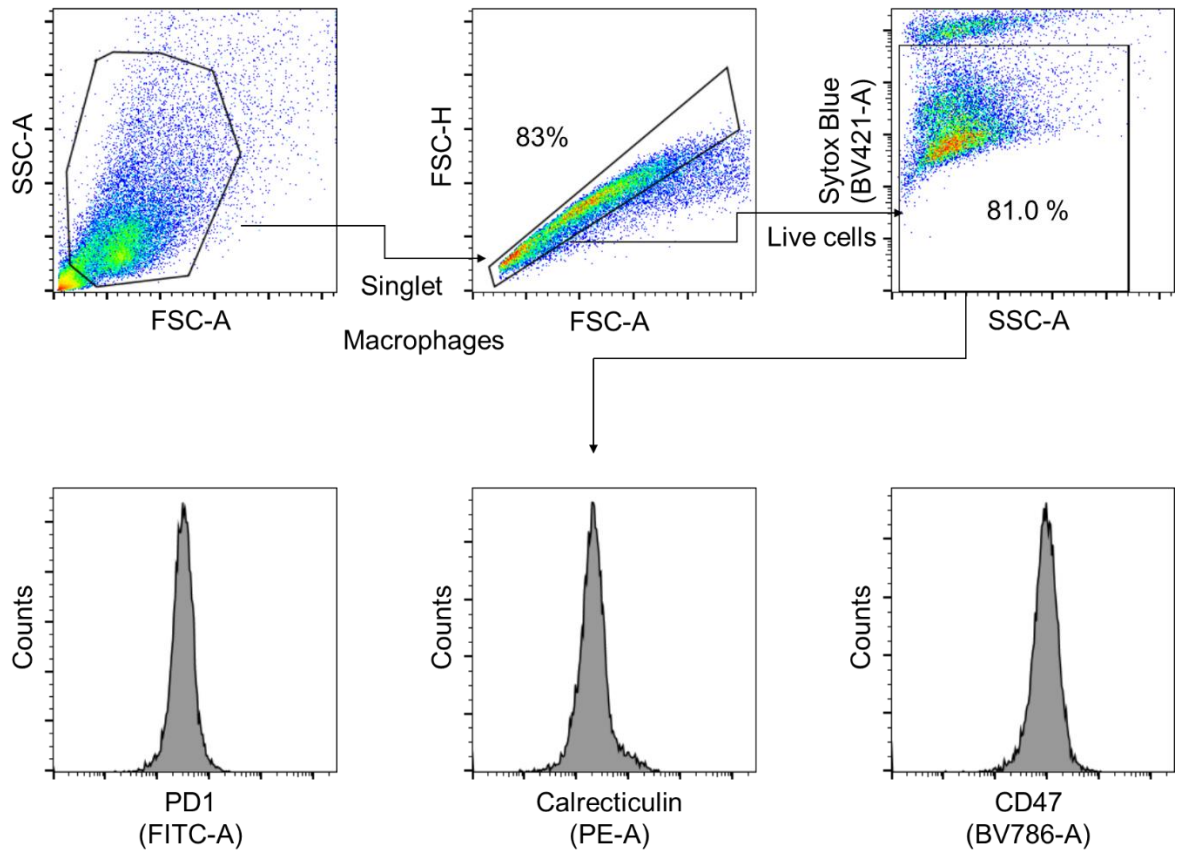


Expressions of PD1, Calrecticulin, CD47 in EO771 and 4T1, Supplementary Fig. 29.

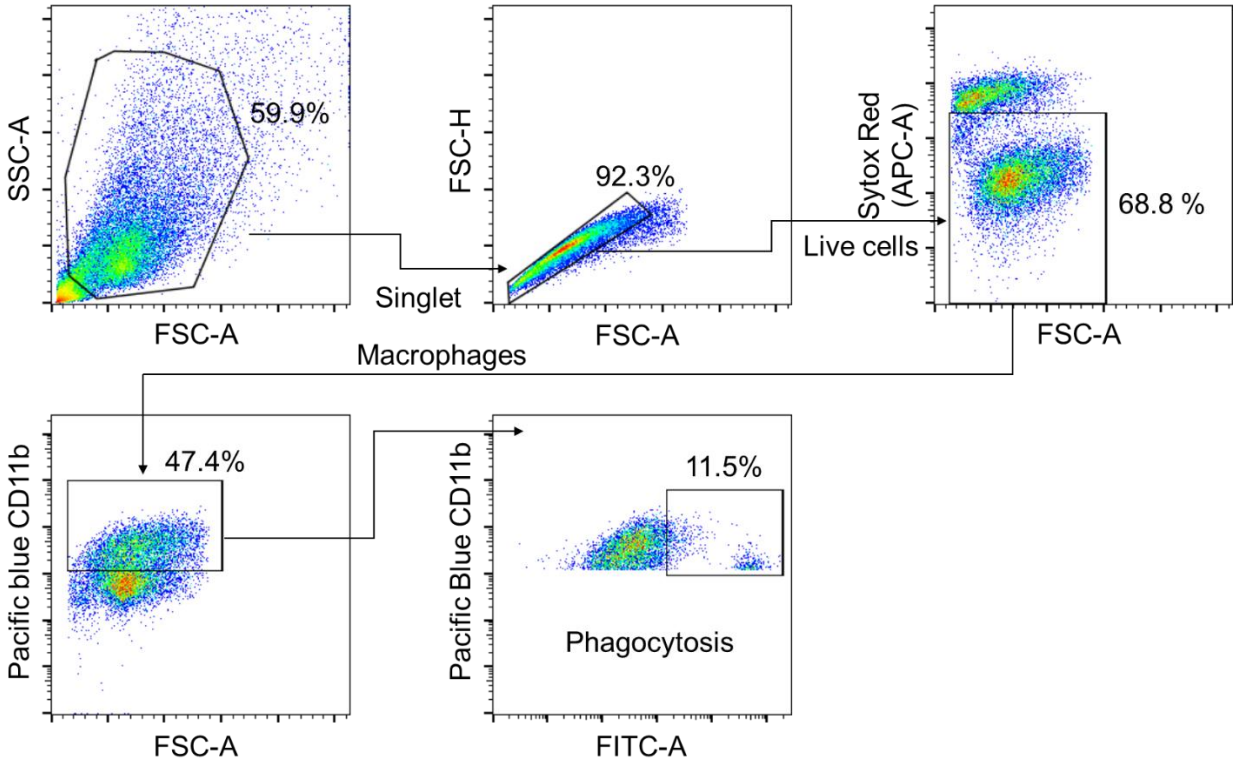


Phagocytosis assay using THP1-derived macrophages and SK-BR3, Supplementary Fig. 30.

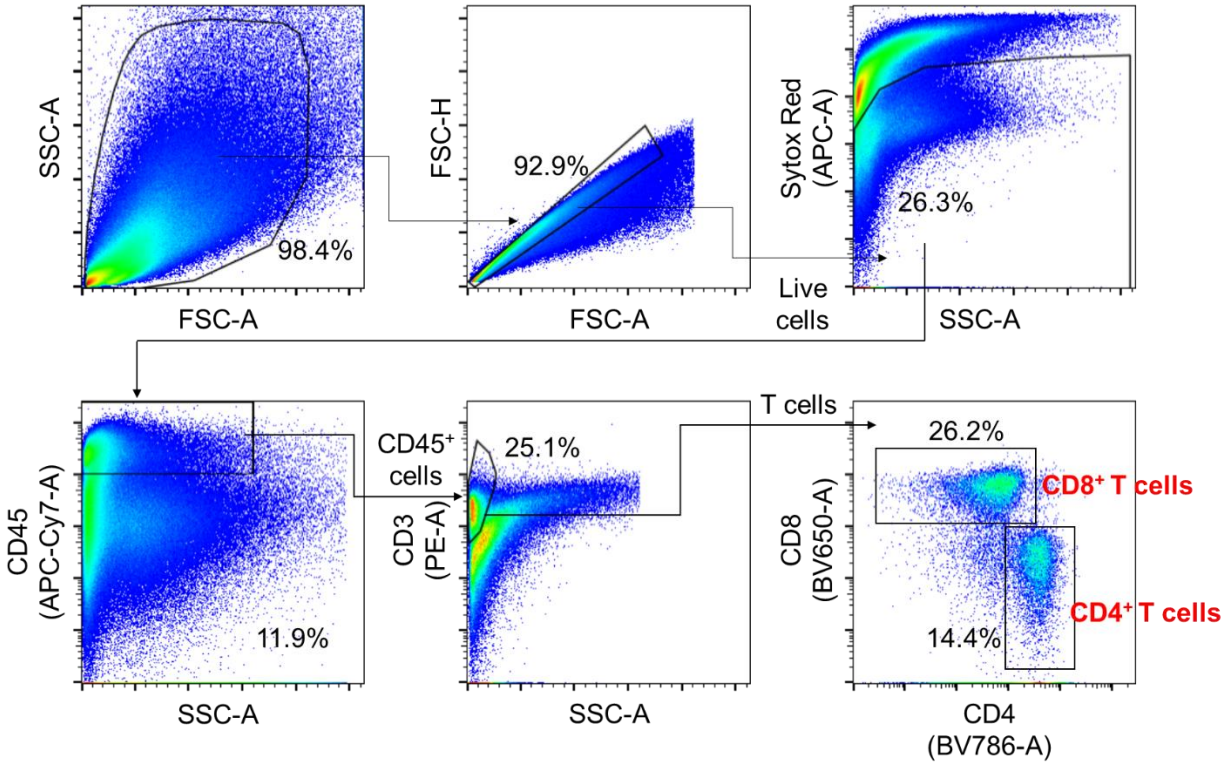


T cell gating without CD45 enrichment, Supplementary Fig. 33

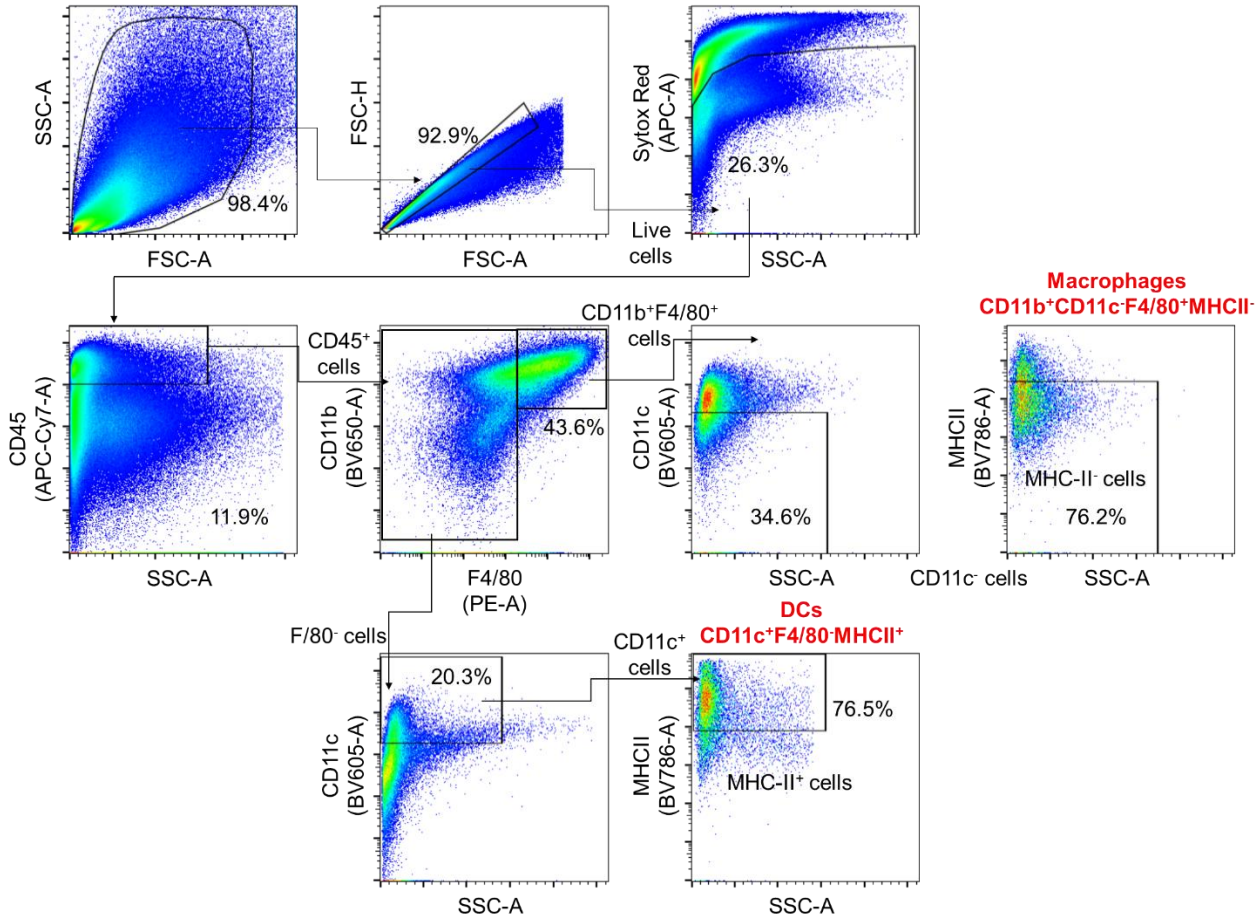


Myeloid cell gating without CD45 enrichment, Supplementary Fig. 33

## Uncropped western blot images

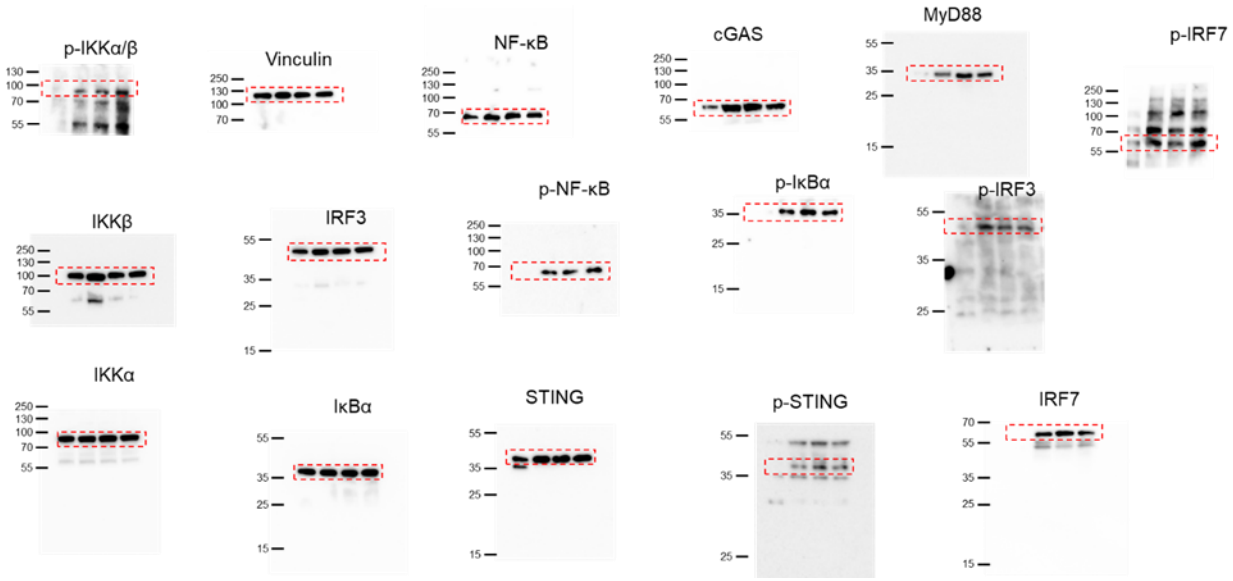


Uncropped western blot images of M2 BMDMs in Fig. 3c

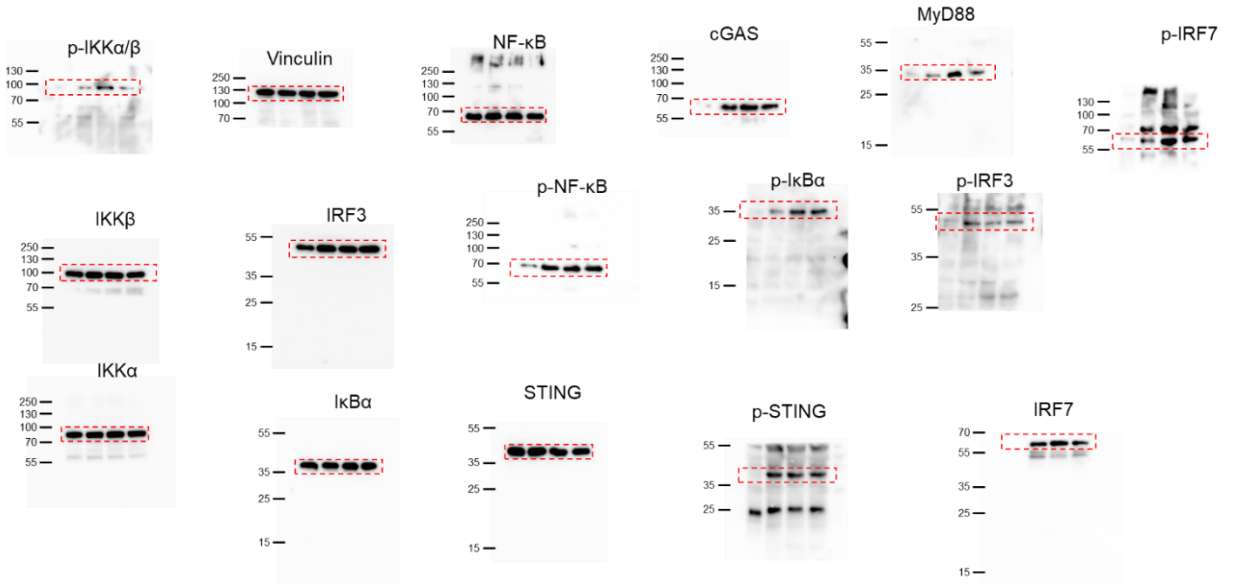


Uncropped western blot images of BMDCs in Fig. 3c

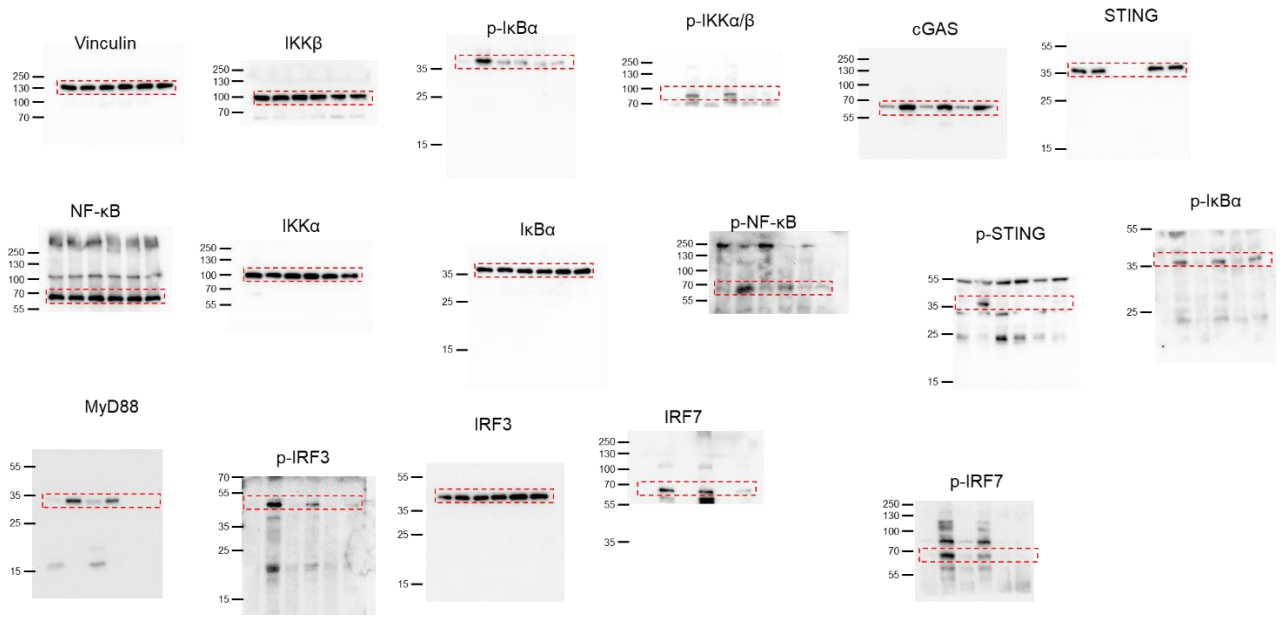


Uncropped western images of M2 BMDMs in Fig. 3g

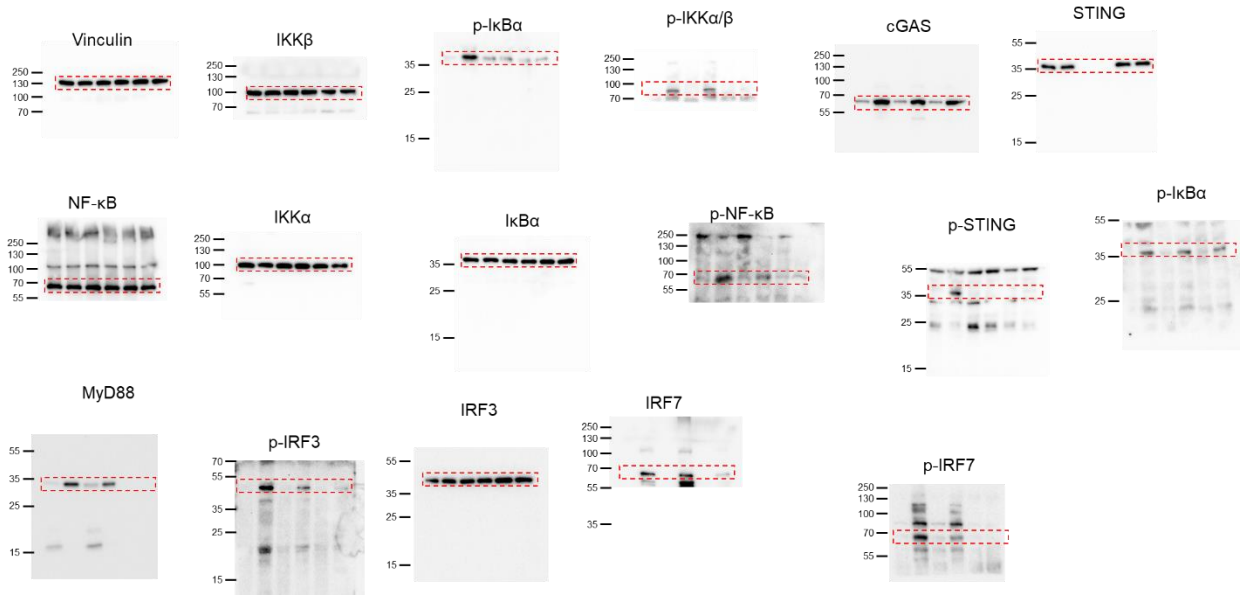


Uncropped western images of BMDCs in Fig. 3g

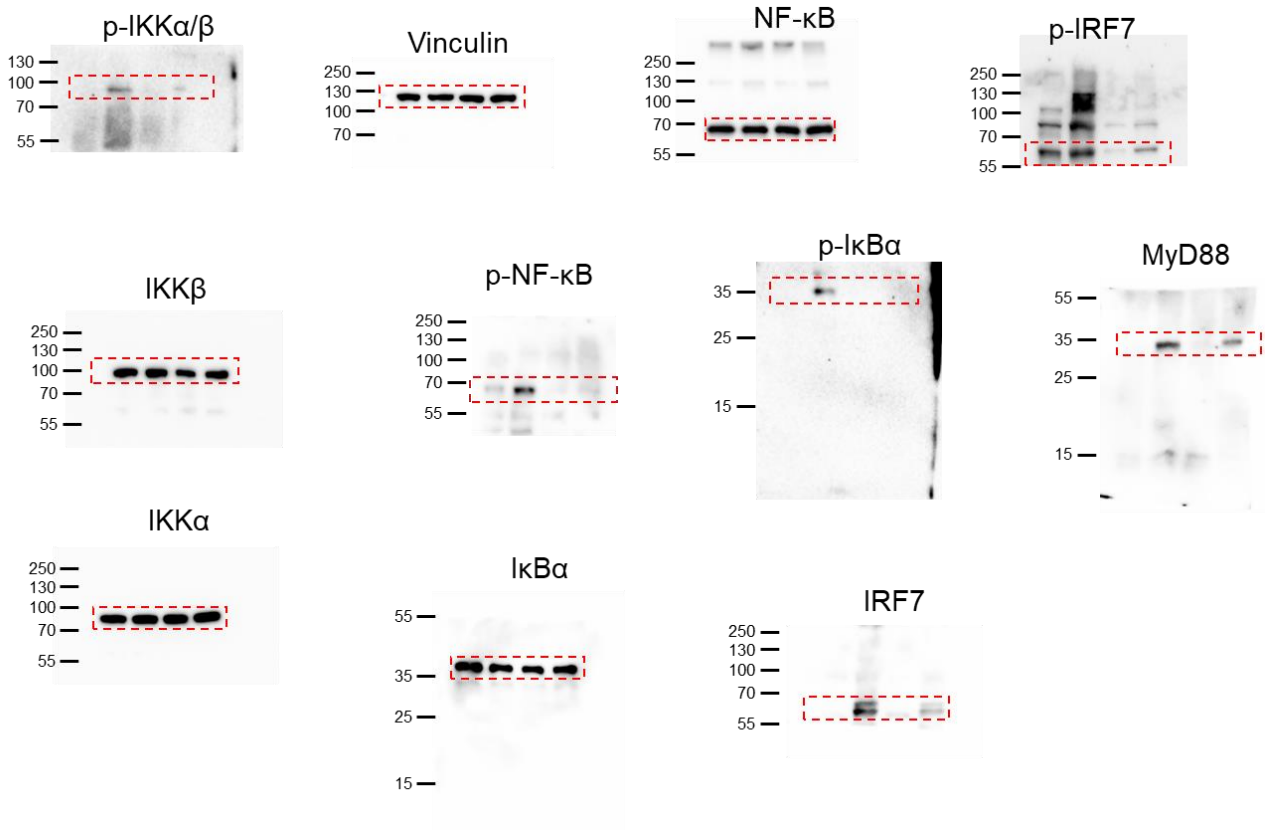


462

463 Uncropped western images of M2 BMDMs in Fig. 3i

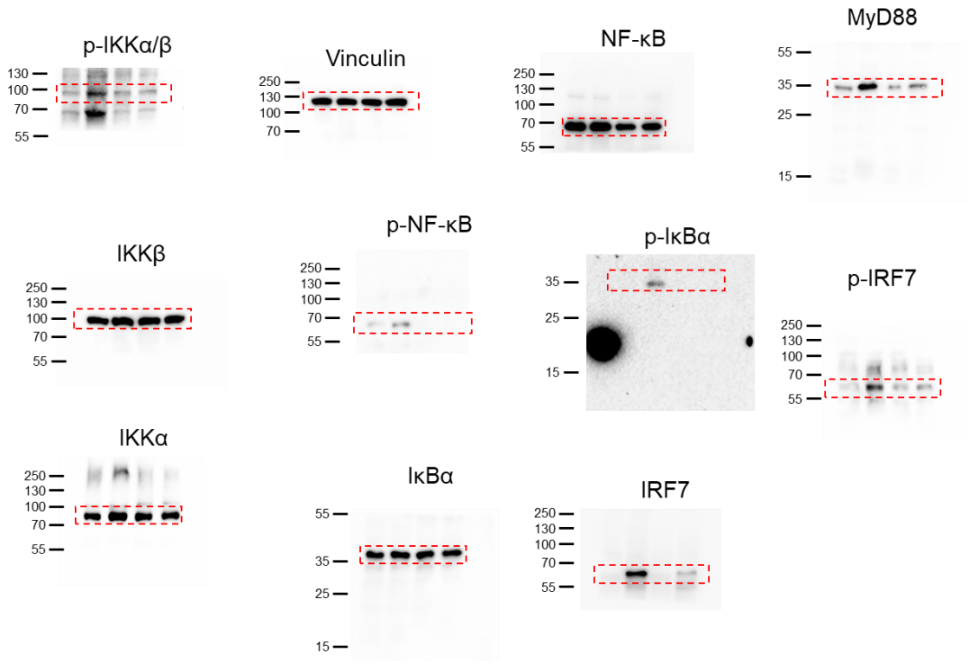


Uncropped western images of BMDCs in Fig. 3i

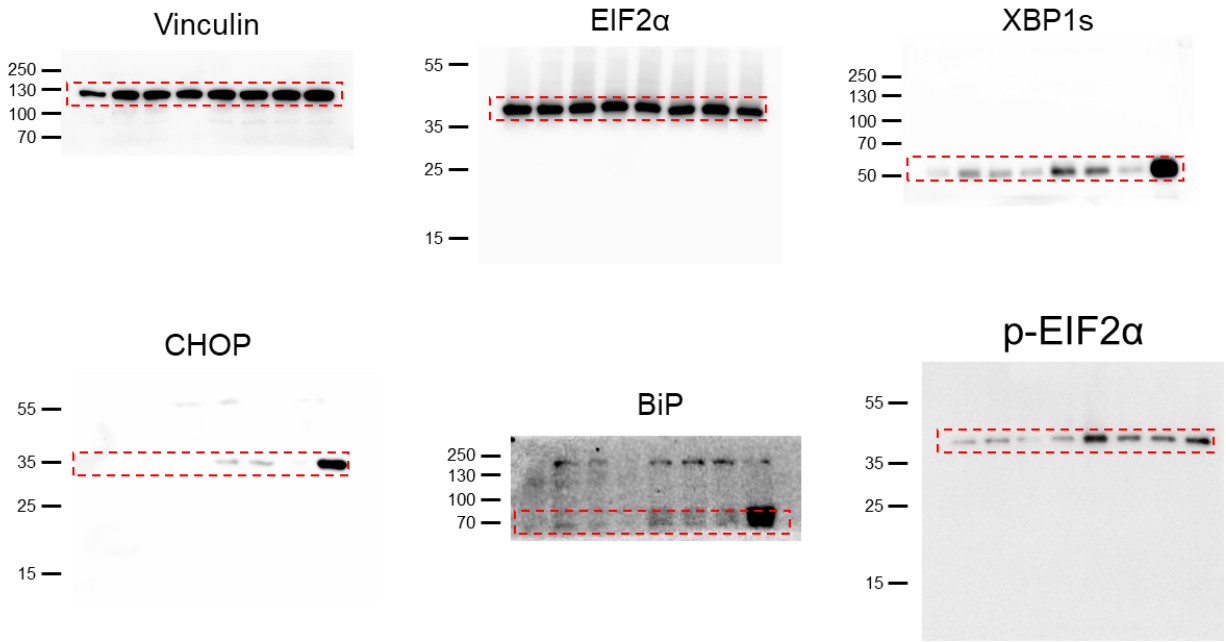


Uncropped western blot images in Extended Fig. 1b

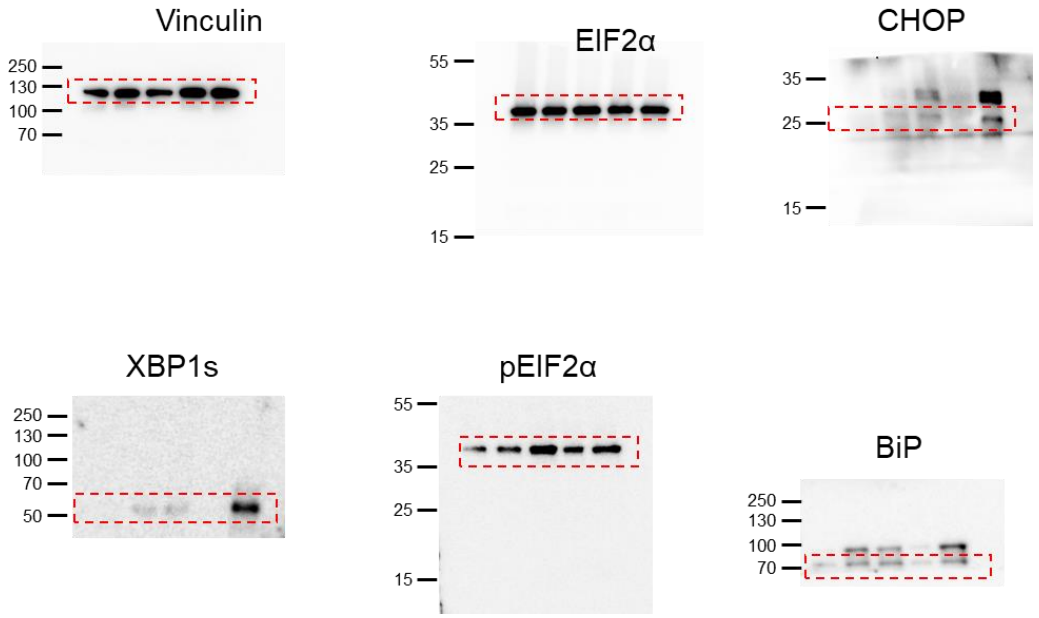


468

469 Uncropped western blot images in Extended Fig. 2b

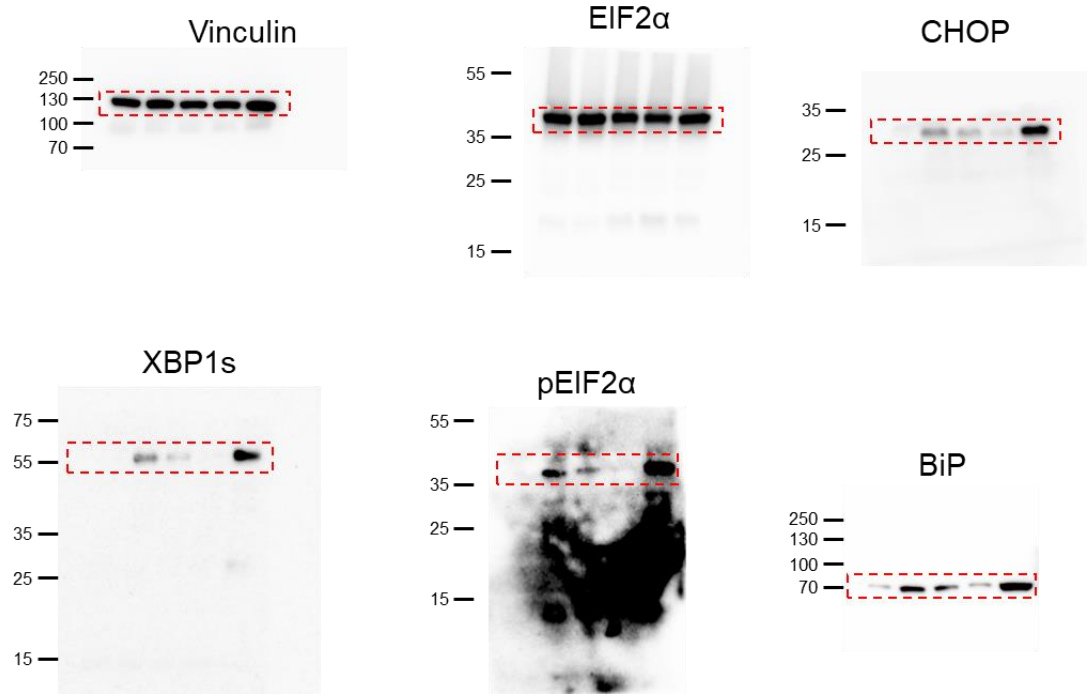


470

471 Uncropped western blot images in Extended Fig. 3b

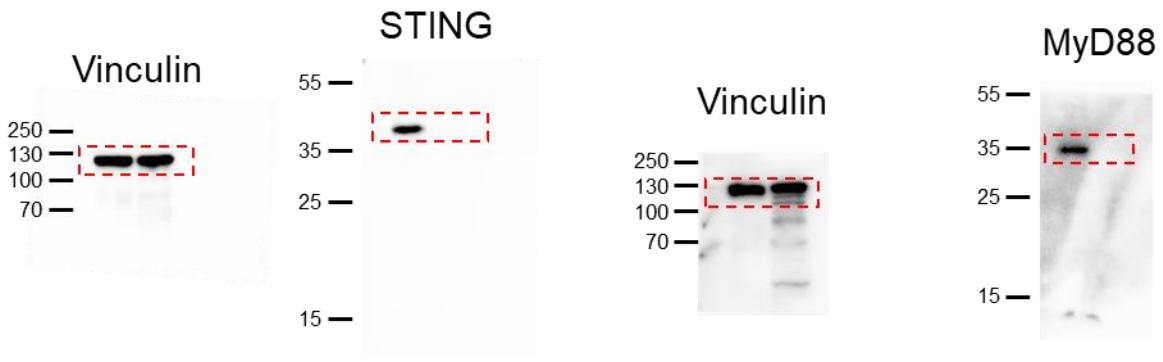


Uncropped western blot images in Extended Fig. 9a

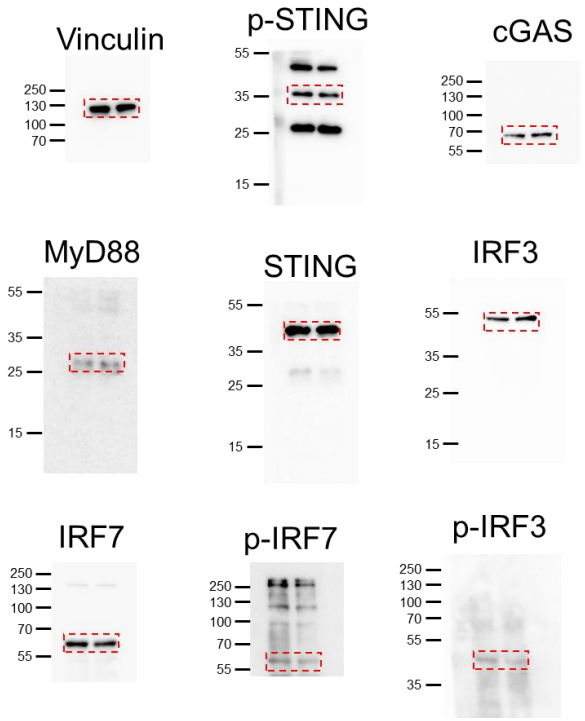


Uncropped western blot images in Supplementary Fig. 12a

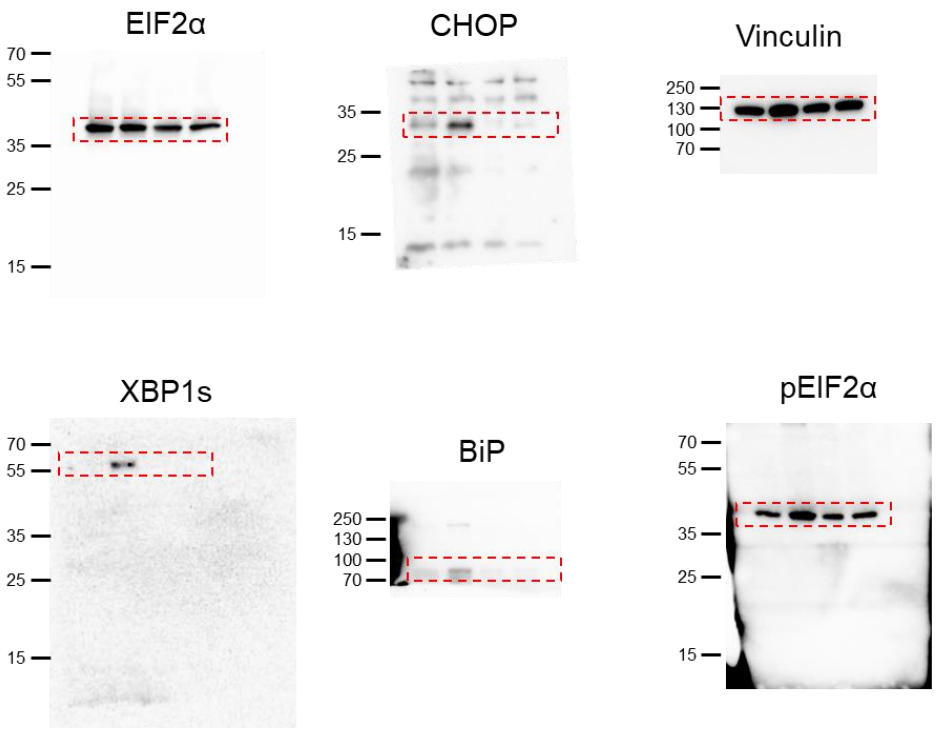


Uncropped western blot images in Supplementary Fig. 22b

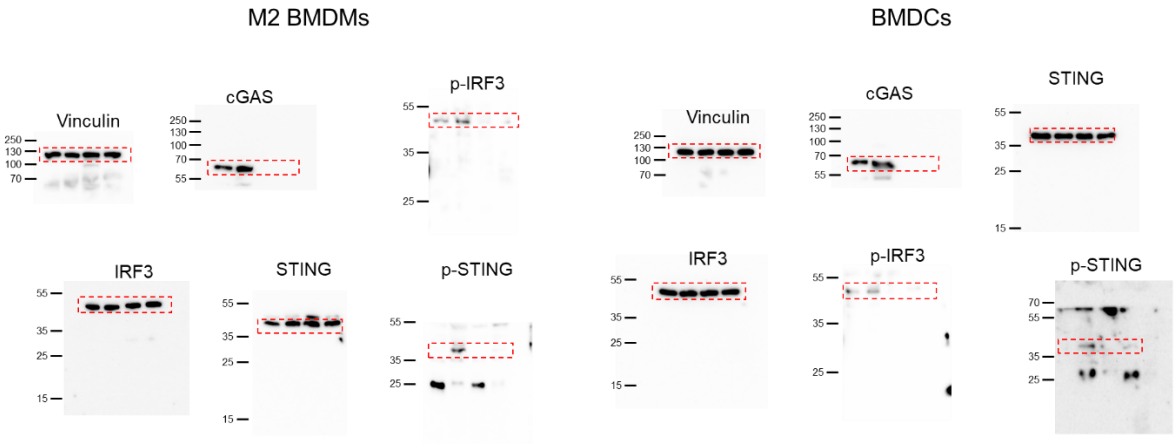


Uncropped western blot images in Supplementary Fig. 24

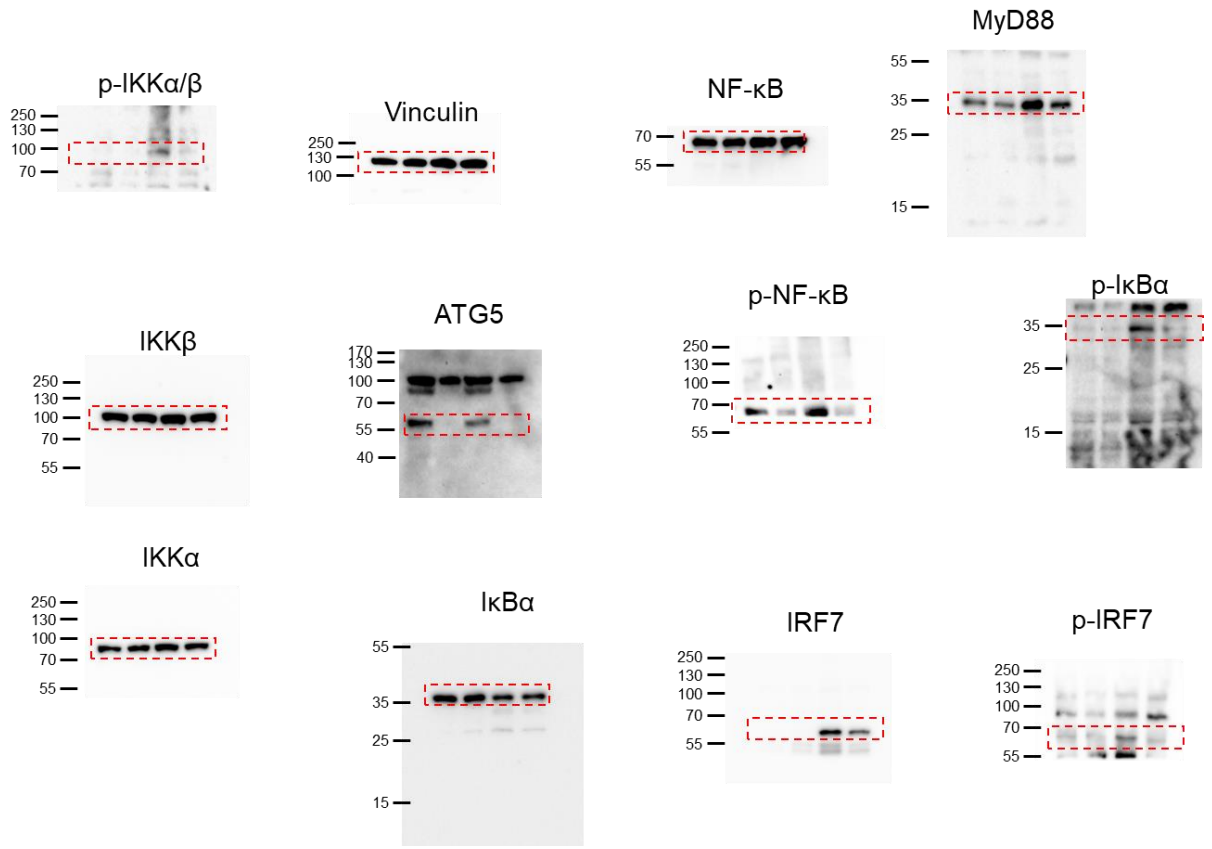


481

482 Uncropped western blot images in Supplementary Fig. 25b.

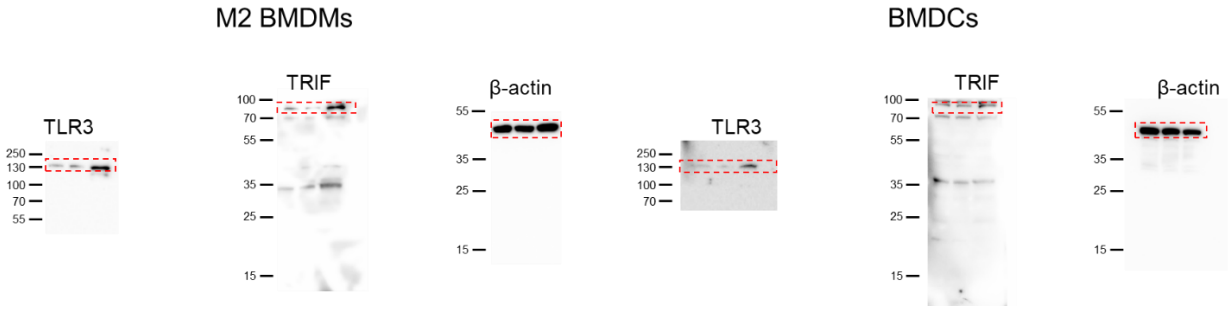


483

484 Uncropped western blot images in Supplementary Fig. 26.

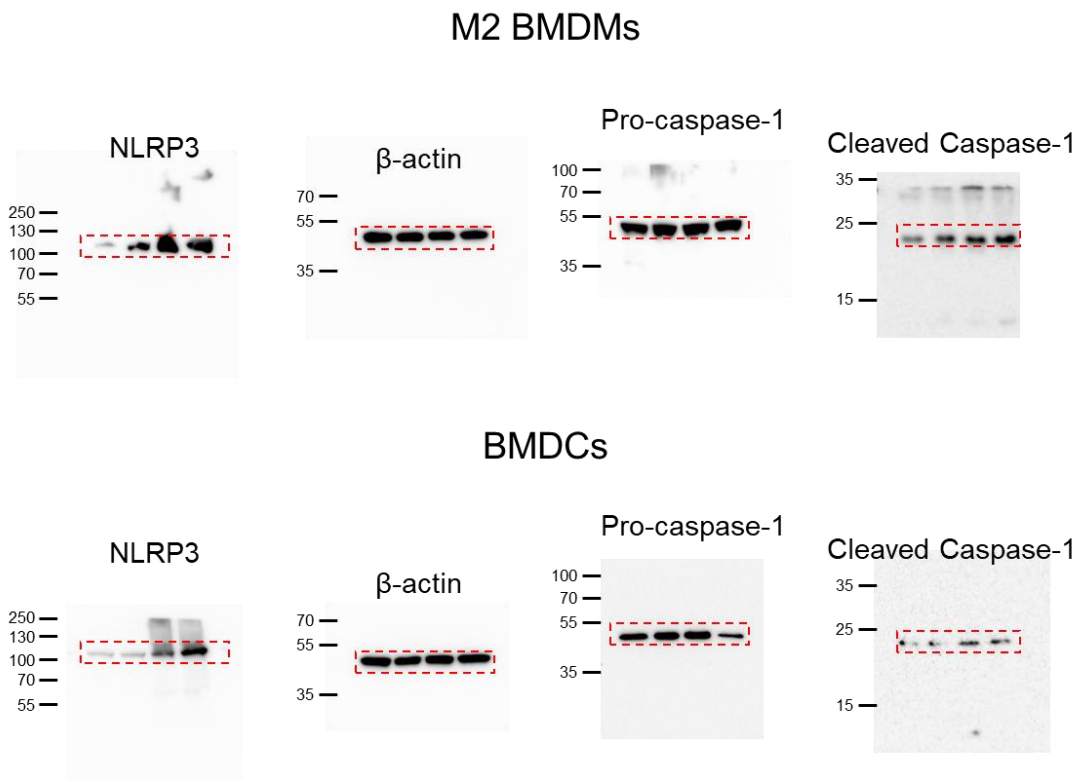


Uncropped western blot images in Supplementary Fig. 27a.

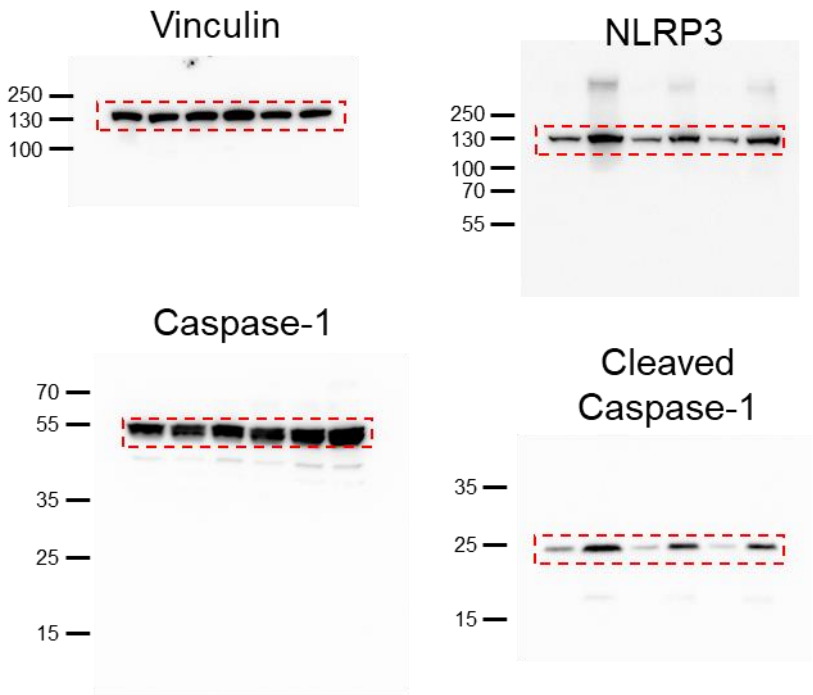


Uncropped western blot images in Supplementary Fig. 28a.

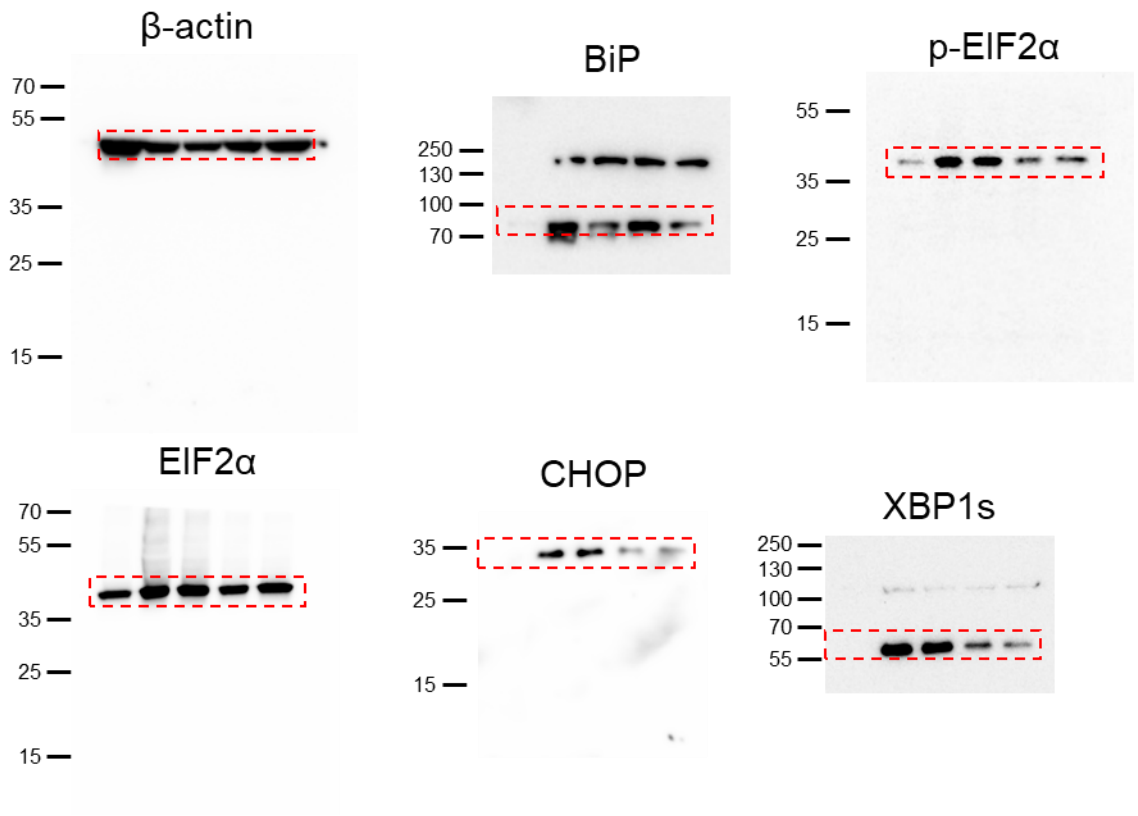


Uncropped western blot images in Supplementary Fig. 29a.

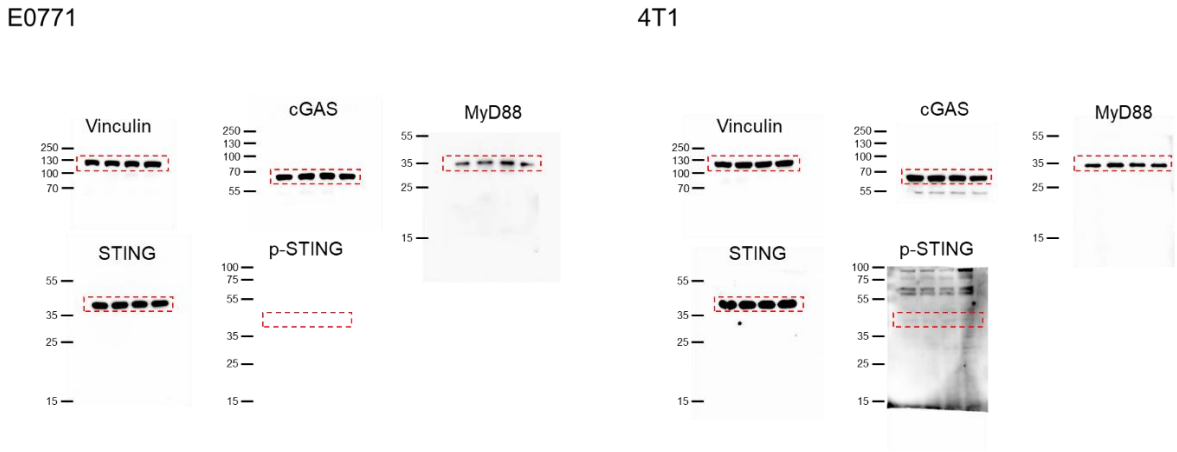


Uncropped western blot images in Supplementary Fig. 29c.

**Adjuvants used in this study**

2,'3'-cGAMP (Chemietek, USA)

CpG-ODN 1585 (Boc Sciences, USA)

LPS (Invitrogen, USA)

ADU-S100 (Chemietek, USA)

MSA2 (MedChemExpress, USA)

**Primers used for RT-qPCR**

Mouse *cd80* (Mm00711660_m1, Taqman® assay, ThermoFisher Scientific, USA)

Human *cd80* (Hs01045161_m1, Taqman® assay, ThermoFisher Scientific, USA)

Mouse *cd86* (Mm00444540_m1, Taqman® assay, ThermoFisher Scientific, USA)

Human *cd86* (Hs01567026_m1, Taqman® assay, ThermoFisher Scientific, USA)

Mouse *nos2* (Mm00440502_m1, Taqman® assay, ThermoFisher Scientific, USA)

Human *nos2* (Hs01075529_m1, Taqman® assay, ThermoFisher Scientific, USA)

Mouse *tnfa* (Mm00443258_m1, Taqman® assay, ThermoFisher Scientific, USA)

Human *tnfa* (Hs00174128_m1, Taqman® assay, ThermoFisher Scientific, USA)

Mouse *il1b* (Mm00434228_m1, Taqman® assay, ThermoFisher Scientific, USA)

Human *il1b* (Hs01555410_m1, Taqman® assay, ThermoFisher Scientific, USA)

Mouse *chil3* (Mm00657889_mH, Taqman® assay, ThermoFisher Scientific, USA)

Mouse *arg1* (Mm00475988_m1, Taqman® assay, ThermoFisher Scientific, USA)

Mouse *il10* (Mm01288386_m1, Taqman® assay, ThermoFisher Scientific, USA)

Human *il10* (Hs00961622_m1, Taqman® assay, ThermoFisher Scientific, USA)

Mouse *cd206* (Mm01329362_m1, Taqman® assay, ThermoFisher Scientific, USA)

Human *cd206* (Hs00267207_m1, Taqman® assay, ThermoFisher Scientific, USA)

Mouse *gapdh* (Mm99999915_g1, Taqman® assay, ThermoFisher Scientific, USA)

Human *gapdh* (Hs02786624_g1, Taqman® assay, ThermoFisher Scientific, USA)

Mouse *mtnd1* (Mm04225274_s1, Taqman® assay, ThermoFisher Scientific, USA)

Human *mtnd1* (Hs02596873_s1, Taqman® assay, ThermoFisher Scientific, USA)

Mouse *infa4* (Mm00833969-_s1, Taqman® assay, ThermoFisher Scientific, USA)

Mouse *ifnb1* (Mm00439552_s1, Taqman® assay, ThermoFisher Scientific, USA)

Mouse *xbp1s* (Mm03464496_m1, Taqman® assay, ThermoFisher Scientific, USA)

Mouse *xbp1u* (Mm00457357_m1, Taqman® assay, ThermoFisher Scientific, USA)

**Fluorophore-labelled antibodies or tetramer used for flow cytometry**

Anti-mouse CD16/32 antibody (Clone: 93, Catalog #:101301, Biolegend, USA)

BV650 anti-mouse CD11b antibody (Clone: M1/70, Catalog #: 101259, Biolegend, USA)

BV421 anti-mouse F4/80 CD11b antibody (Clone: BM8, Catalog #: 123132, Biolegend, USA)

Pacific Blue anti-mouse/human CD11b antibody (Clone: M1/70, Catalog #: 101224, Biolegend, USA)

BV605 anti-mouse CD11c antibody (Clone: N418, Catalog #: 117334, Biolegend, USA)

PE anti-mouse F4/80 antibody (Clone: QA17A29, Catalog #: 157304, Biolegend, USA)

BV421 anti-mouse CD80 antibody (Clone: 16-10A1, Catalog #: 104726, Biolegend, USA)

FITC anti-mouse CD86 antibody (Clone: PO3, Catalog #: 105110, Biolegend, USA)

APC/Cyanine7 anti-mouse CD86 antibody (GL-1, Catalog #l: 105030, Biolegend, USA)

PerCP Cy5.5 anti-mouse CD206 antibody (Clone: C068C2, Catalog #: 141716, Biolegend, USA)

PE-Cy7 anti-mouse SIINFEKL/H-2Kb antibody (Clone: 25-D1.16, Catalog #: 141608, Biolegend, USA)

APC anti-mouse SIINFEKL/H-2Kb antibody (Clone: 25-D1.16, Catalog #: 141606, Biolegend, USA)

BV421 anti-mouse CD62L antibody (Clone: MEL-14, Catalog #: 104436, Biolegend, USA)

PerCP Cy5.5 anti-mouse CD44 antibody (Clone: IM7, Catalog #: 103032, Biolegend, USA)

PE anti-mouse CD3 antibody (Clone: 17A2, Catalog #: 100206, Biolegend, USA)

BV650 anti-mouse CD8a antibody (Clone: 53-6.7, Catalog #: 100742, Biolegend, USA)

BV785 anti-mouse CD4 antibody (Clone: GK1.5, Catalog #: 100453, Biolegend, USA)

Alexa Fluor488 anti-mouse Foxp3 (Clone: 150D, Catalog #: 320012, Biolegend, USA)

BV605 anti-mouse IFN-γ antibody (Clone: 4S.B3, Catalog #: 505832, Biolegend, USA)

BV510 anti-mouse Ly-6G/Ly-6C (Gr-1) antibody (Clone: RB6-8C5, Catalog #:108438, Biolegend, USA)

BV421 anti-mouse CD25 antibody (Clone: 3C7, Catalog #: 101923, Biolegend, USA)

BV785 anti-mouse I-A/I-E antibody (Clone: M5/114.15.2, Catalog #: 107645, Biolegend, USA)

BV650 anti-mouse NK1.1. antibody (Clone: PK136, Catalog #:108736, Biolegend, USA)

BV421 anti-mouse NKp46 antibody (Clone: 29A.4, Catalog #: 137612, Biolegend, USA)

Tetramer/BV421-H2Kb OVA (SIINFEKL) (Catalog #: TB-5001-4, MBL International Corporation, USA)

**Antibodies used for western blotting and immunofluorescence staining**

CHOP (L63F7) Mouse mAb #2895 (Cell Signaling Technology, USA)

p-eIF2α (Ser51) (D9G8) XP® Rabbit mAb #3398 (Cell Signaling Technology, USA)

eIF2α (D7D3) XP® Rabbit mAb #5324 (Cell Signaling Technology, USA)

BiP (C50B12) Rabbit mAb #3177 (Cell Signaling Technology, USA)

XBP-1 (ERP22004) Rabbit mAb ab220783 (abcam, UK)

NF-κB p65 (D14E12) Rabbit mAb #8242 (Cell Signaling Technology, USA)

p-NF-κB p65 (Ser536) (93H1) Rabbit mAb #3033 (Cell Signaling Technology, USA)

IKKβ (D30C6) Rabbit mAb #8943 (Cell Signaling Technology, USA)

p-IKKα/β (Ser176/180) (16A6) Rabbit mAb #2697 (Cell Signaling Technology, USA)

IKKα (3G12) Mouse mAb #11930 (Cell Signaling Technology, USA)

IκBα (L35A5) Mouse mAb (Amino-terminal Antigen) #4814 (Cell Signaling Technology, USA)

p-IκBα (Ser32) (14D4) Rabbit mAb #2859 (Cell Signaling Technology, USA)

β-actin Rabbit pAb #4967 (Cell Signaling Technology, USA)

MyD88 Rabbit mAb #4283 (Cell Signaling Technology, USA)

IRF3 (D83B9) Rabbit mAb #4302 (Cell Signaling Technology, USA)

p-IRF3 (Ser396) (D6O1M) Rabbit mAb #29047 (Cell Signaling Technology, USA)

IRF7 (D8V1J) Rabbit mAb #72073 (Cell Signaling Technology, USA)

p-IRF7 (Ser437/438) (D6M2I) Rabbit mAb #24129 (Cell Signaling Technology, USA)

p-STING (Ser366) pAb PA5-105674 (ThermoFisher Scientific, USA)

STING (D2P2F) Rabbit mAb #13647 (Cell Signaling Technology, USA)

STING Rabbit pAb PA5-23381 (ThermoFisher Scientific, USA)

Vinculin Recombinant Rabbit mAb (42H89L44) 700062 (ThermoFisher Scientific, USA)

TFAM (Transcription Factor A, Mitochondrial) antibody Rabbit pAb H00007019-B01P (Abnova, USA)

Anti-dsDNA antibody Mouse mAb CBL186MI (MilliporeSigma™, USA)

Tom20 (D8T4N) Rabbit mAb #42406 (Cell Signaling Technology, USA)

Purified anti-mouse CD8a (Catalog No. 100702) (Biolegend, USA)

Anti-Iba1 antibody (ab5076) (abcam, UK)

Anti-F4/80 antibody [CI:A3-1] - Macrophage Marker (ab6640) (abcam, UK)

FITC-tagged Goat anti-rabbit secondary Ab (ThermoFisher Scientific, USA)

FITC-tagged Donkey anti-mouse secondary Ab (ThermoFisher Scientific, USA)

Alexa Fluor 647-tagged Goat anti-rabbit secondary Ab (ThermoFisher Scientific, USA)

Alexa Fluor 546-tagged Goat anti-rat secondary Ab (Biolegend, USA)

Purified anti-mouse CD8a Antibody (Biolegend, USA)

CD4 (RM4-5) Rat mAb (FITC Conjugate) #96127 (Cell Signaling Technology, USA)

CD11c Monoclonal Antibody (N418), eBioscience™ # 14-0114-82 (ThermoFisher Scientific, USA)

p-IRF7 (Ser471, Ser472) Polyclonal antibody # PA5-114592 (ThermoFisher Scientific USA)

CD11c Monoclonal Antibody (N418), Functional Grade, eBioscience™ # 16-0114-85 (ThermoFisher Scientific, USA)

Anti-TRIF antibody (ab13810) (abcam, UK)

Anti-TLR3 antibody (ab137722) (abcam, UK)

NLRP3 (D4D8T) Rabbit mAb #15101 (Cell Signaling Technology, USA)

Caspase-1 (E2Z1C) Rabbit mAb #24232 (Cell Signaling Technology, USA)

Cleaved Caspase-1 (Asp296) (E2G2I) Rabbit mAb #89332 (Cell Signaling Technology, USA)

Purified anti-mouse CD8b.2 Antibody #140402 (Biolegend, USA)

β-Actin (13E5) Rabbit mAb #4970 (Cell Signaling Technology, USA)

**Antibody list for *in vivo* study**

*InVivo*MAb anti-mouse PD1 (CD279) #BE0273 (BioXcell, USA)

*InVivo*MAb anti-mouse CD8α #BE0117 (BioXcell, USA)

*InVivo*MAb anti-mouse CSF1 #BE0204 (BioXcell, USA)

**ELISA kits**

Mouse TNF-α (ELISA MAX™ Deluxe Set Mouse TNF-α, Biolegend, USA)

Mouse IL-1β (ELISA MAX™ Deluxe Set Mouse IL-1β, Biolegend, USA)

IL-6 (ELISA MAX™ Deluxe Set Mouse IL-6, Biolegend, USA)

Mouse IFN-α (IFN alpha Mouse ELISA Kit (Invitrogen, USA)

Mouse IFN- β (Mouse IFN-beta DuoSet ELISA, R&D systems, USA)

Mouse IFN-γ (ELISA MAX™ Deluxe Set Mouse IFN-γ, Biolegend, USA)

Mouse IL-2 (ELISA MAX™ Deluxe Set Mouse IL-2, Biolegend, USA)

Mouse HMGB1 (Mouse HMGB1 ELISA kit LS-F11642-1, LSBio, USA)